Magnetocrystalline anisotropy nickel - vanadium alloys

Amighian, J.

MAGNETOCRYSTALLINE ANISOTROPY OF NICKEL - VANADIUM ALLOYS

by

J. Amighian, B.Sc.

Presented in Candidature for the Degree of

Doctor of Philosophy

March 1975

Abstract

Single crystals of 5N and 4N pure Ni and a series of NiV alloys up to 6.72 at % V were grown and cut into spheres and blocks for anisotropy, magnetization and resistivity measurements. Measurements of the first anisotropy constant of these crystals were made between 4.2 and 300K using a torque magnetometer. All the measurements were performed when the magnetic field of up to 11 kOe could rotate in a (001) plane. Corrections for the effect of the higher order constant K_3 on the torque curves were found to be necessary in the case of pure Ni and 0.98% alloy. Using a Faraday balance the magnetizations of the crystals of higher vanadium content were measured from 77K to room temperature. Values of M at 4.2K were measured to check the validity of the extrapolation of these results to OK. Using a D.C. method it was possible to measure the values of the resistivity of these samples from 4.2K to room temperature. In addition crystals of Ni Mo with 1 at % Mo and of NiV with 12.5 at % V were grown and their resistivities were measured from 4.2K to room temperature.

Using the results from anisotropy measurements it was possible to show that variationsof temperature or of concentration affect the first anisotropy constant in a similar manner. This is in good agreement with the results on Ni Mo of Hausmann and Wolf (1971).

The results from anisotropy and resistivity measurements were combined to check whether the hypothesis suggested by Hausmann (1970) were true. This was found not to be so even though the relationship was examined for a wide range of temperature.

Combining the results of anisotropy and resistivity measurements it has been found that there is further support for the suggestion by Fransе et al. (1973) of a link between temperature variation of anisotropy and the minority spin resistivity in accord with the work of Furey. There remains some doubt about the correctness of the method of distinguishing between majority and minority spin resistivities.

The temperature variation of K_1 and M was also examined and the value of n found in equation $K(T,C) = K(0,C)\left[M(T)/M(0) \right]^n$ in the case of NiV crystals is less than that for pure Ni and it decreases as the concentration is increased.

CONTENTS

Page

Page

Page

LIST OF FIGURES

Figure

Chapter Nine

Chapter Ten

LIST OF TABLES

CHAPTER ONE

Introduction

1.1 Ferromagnetism

Ferromagnetism is one of the important subjects in solid state physics and several models for describing its theory have been given, some of the most basic and important of them will be explained below.

1.1.1 The Weiss Model of Ferromagnetism

The first and in many ways the most illuminating was that of Weiss (1907). The task of a theory of ferromagnetism at that time was to explain (1) the existence of spontaneous magnetization below a certain temperature T_c called the Curie temperature, and (2) the passage from negligible total magnetization to saturation magnetization upon application of a small external field H. To account for this behaviour, Weiss put forward two hypotheses.

i) Below T_c a ferromagnet is composed of small spontaneously magnetized regions called domains. When the magnetic moments of these individual domains take different directions, the overall sample magnetization will be much smaller than if the sample were composed of a single domain. As a consequence, the passage to large sample magnetization can be produced by a relatively weak external field H, which need only align the already magnetized domains.

ii) Each domain is spontaneously magnetized because a very strong "molecular field" of origin unknown to Weiss, tends to align the individual atomic magnetic moments within the domains. These two hypotheses can give a general explanation of most of

the phenomena in ferromagnetism. Now if we consider the interaction which tends to align the atomic dipoles parallel as equivalent to an internal field H_m then by thermal agitation of the atoms we can misorient their directions and reduce the effect of H_m. The temperature at which the thermal agitation can destroy the spontaneous magnetization is called the ferromagnetic Curie temperature T_c.

For over a quarter of a century indirect experiments showed the usefulness of these theories. Today there is a great deal of evidence that both domains and molecular field really do exist, although their origin is still the subject of theoretical research.

A discussion of the theory of domains has been given by Kittel (1949). For common ferromagnetic materials estimations of the Weiss field obtained in this way yield values of $\sim 10^7$ oe, too large to be of simple dipole origin. The source of the effective field cannot therefore be due to simple magnetic interactions between atomic moments. An explanation in quantum mechanical terms was suggested by Heisenberg.

1.2 The Heisenberg Model of Ferromagnetism

Heisenberg's (1928) theory of ferromagnetism is based on the H_2 molecule and it was shown by this theory that the origin of the Weiss molecular field is the result of quantum exchange interactions.

As experimentally electrons have always antisymmetric wave functions (considering Pauli's exclusion principle) so the wave functions of the two electrons in hydrogen atoms are

$$\Psi_1 = A\left[\phi_a(1)\phi_b(2) + \phi_a(2)\phi_b(1)\right]\left[\chi_\alpha(1)\chi_\beta(2) - \chi_\alpha(2)\chi_\beta(1)\right] \tag{1.1}$$

$$\Psi_2 = B\left[\phi_a(1)\phi_b(2) - \phi_a(2)\phi_b(1)\right]\begin{vmatrix} \chi_\alpha(1) & \chi_\alpha(2) \\ \chi_\alpha(1)\chi_\beta(2) + \chi_\alpha(2)\chi_\beta(1) & \\ \chi_\beta(1) & \chi_\beta(2) \end{vmatrix} \tag{1.2}$$

where Ψ_1 is the wave function of the two electrons to have antiparallel spins and Ψ_2 for those whose spins are parallel, A and B are normalized factors, $\phi_a(1)$ is the one-electron radial wave function when electron 1 is in state (a) and similarly for $\phi_b(2)$ and $\phi_a(2)$ and $\phi_b(1)$, $\chi_\alpha(1)$ is the spin wave function for electron 1 if its magnetic moment μ_z is parallel to the magnetic field H, applied in z - direction, and $\chi_\beta(1)$ is when its magnetic moment is antiparallel, similarly for $\chi_\alpha(2)$ and $\chi_\beta(2)$.

Consider an interaction between these 2 - electrons, the Hamiltonian is given by

$$H_{12} = \frac{e^2}{r_{ab}} + \frac{e^2}{r_{12}} - \frac{e^2}{r_{1b}} - \frac{e^2}{r_{2a}} \tag{1.3}$$

where r_{ab} is the distance between nuclei, r_{12} between electrons, and r_{1b} and r_{2a} are distances between a given nucleus and the electron on the other atom. So the total energy of the system is

$$E = \int \Psi^* H_{12} \Psi \, d\tau \tag{1.4}$$

and so using Ψ_1 and Ψ_2 we get

$$E_1 = A^2(K_{12} + J_{12}) \tag{1.5}$$

$$E_2 = B^2(K_{12} - J_{12}) \tag{1.6}$$

where

$$K_{12} = \int \phi_a^*(1)\,\phi_b^*(2)\,H_{12}\,\phi_a(1)\,\phi_b(2)\,d\tau_1\,d\tau_2$$

$$J_{12} = \int \phi_a^*(1)\,\phi_b^*(2)\,H_{12}\,\phi_a(2)\,\phi_b(1)\,d\tau_1\,d\tau_2 \qquad (1.7)$$

K_{12} is the average coulomb interaction energy and J_{12} is called the exchange integral.

In the case of H_2 - molecule J_{12} is negative, $E_1 < E_2$ and so in the ground state, spins are antiparallel, $S = 0$, i.e. non magnetic. In order to have spins parallel, i.e. $\uparrow_2$ state, we should have $E_2 < E_1$, i.e. J_{12} should be positive thus giving ferromagnetism. Heisenberg (1928) showed that the energy E can be written as

$$E = \text{constant} - 2\,J_{12}\,\underline{S}_1 \cdot \underline{S}_2$$

The total energy thus contains an exchange term which corresponds to a direct coupling between two spins. In general for two atoms having spins S_i and S_j the exchange term is

$$W_{ij} = 2\,J_{ij}\,\underline{S}_i \cdot \underline{S}_j \qquad (1.8)$$

Slater (1930) has pointed out that in order to have J_{ij} positive, i.e. ferromagnetism, the ratio r_{ab}/r_o where r_o is the orbital radius, should be larger than 3 but not much larger. These ratios for some materials are given below:

Material	Ni	Fe	Co	Gd	Mn	Cr
r_{ab}/r_o	3.94	3.26	3.64	3.1	2.94	2.60

in which Mn and Cr are not ferromagnetic.

1.3 Band Model Theories of Ferromagnetism

In the Heisenberg theory the electrons responsible for ferromagnetism are localized at the lattice points, whereas

the electrons in metals or at least those from the outer shells of the atoms are not localized and a band theory approach might be expected to be more appropriate. Theories ascribing the ferromagnetic behaviour to mobile electrons or holes in unfilled bands were developed by Slater (1936) and Stoner (1938). The 4s and 3d bands overlap resulting in an incomplete filling of the 3d band. The exchange coupling causes alignment of the 3d - electron spins, but it is possible to explain the non-integral character of the resulting moment per atom. This provides good agreement with measurements for Ni, but less satisfactory for Fe and extension to cover 4f electrons in rare earthsyields unsatisfactory results. An alternative approach is the Vonsovky (1946) model in which the 3d electrons are localized at the lattice points and the Heisenberg exchange interactions between the 3d shells of neighbouringatoms aligns the spins of the 3d shells. This will produce an internal field which interacts with the 4s - conduction electrons. The result of this interaction gives more conduction electrons to have spins parallel than antiparallel to the spin direction of the 3d electrons. i.e. the conduction electrons become polarized. The moment due to this polarization will add to that due to the 3d electrons again explaining the non-integral moment per atom. There are indications that this model may apply to metallic Fe. Zener (1951) realized that the 3d exchange coupling could be indirect via the conduction electrons, which would again become polarized. This theory has been considerably developed by Rudermann, Kittel, Kasuya and Yosida and

applied to the heavy rare earths.

Considerable development of these energy band theories of ferromagnetism has taken place in recent years. By the use of the A.P.W. method and computer programmes calculations of the shapes of the energy bands of ferromagnetic metals have been made which agree well with experiment, Mattheis (1964) and Connolly (1967). This work is described very clearly by Slater (1968) and by Slater et al (1969). In all these theories the exchange coupling is an isotropic one so that they give no account of the anistropic magnetic properties found in single crystals.

1.4 Ferromagnetic Crystalline Phenomena

The theories which have been briefly outlined provide a satisfactory general explanation of the phenomena of ferromagnetism, but two important exceptions to this exist of which there are, as yet, no completely satisfactory quantitative explanations, namely magnetocrystalline anisotropy and magnetostriction. Keffer (1966) has collected and discussed most of the theories in this field and other related phenomena.

1.4.1 Magneto crystalline Anisotropy

The anisotropy energy or the magnetocrystalline energy of a ferromagnetic crystal acts in such a way that the magnetization tends to be directed along certain definite crystallographic axis which are called easy directions, whereas the directions along which it is most difficult to magnetize the crystal are called hard directions. The anisotropy energy

is defined as the work required to make the magnetization be along a certain direction compared to an easy direction. Using the restrictions imposed by cubic symmetry it is possible to show that the anisotropy energy may be represented by an empirical expression of the form,

$$E_A(\alpha) = K_1(S)+K_2P+K_3(S^2)+K_4SP+K_5S^3+K_6P^2+\ldots\ldots \quad (1.9)$$

where

$S = \alpha_1^2\alpha_2^2+\alpha_2^2\alpha_3^2+\alpha_1^2\alpha_3^2$ and $p= \alpha_1^2\alpha_2^2\alpha_3^2$ and $\alpha_1, \alpha_2, \alpha_3$ are the direction cosines of the magnetization with respect to the crystal axes and K_1, K_2....etc. are the first and second... anisotropy constants of cubic crystal.

E_A for hexagonal crystals can be expressed using polar co-ordinates as derived by Mason (1954) and Bozorth (1954) as a series of the form,

$$E_A = K_1 \sin^2\theta + K_2 \sin^4\theta + K_3 \sin^6\theta + K_4 \sin^6\theta \cos^6\phi + \cdots (1.10)$$

where θ and ϕ are the angles between magnetization and the hexagonal c - axis and between the projection of the magnetization on the basal plane and an a - axis respectively. These expressions are purely empirical and the anisotropy constants should be measured by experiment. In this work the experiments are restricted to the (001) plane of face-centred cubic crystals of Ni and NiV , so in this plane equation (1) reduces to

$$E_A(\alpha) = K_1 \sin^2\theta \cos^2\theta + K_3 \sin^4\theta \cos^4\theta + \ldots\ldots\ldots \quad (1.11)$$

since

$\alpha_1 = \cos\theta$ and $\alpha_2 = \sin\theta$, $\alpha_3 = 0$, $S(001) = \sin^2\theta\cos^2\theta$, $P(001) = 0$

θ is the angle between magnetization and $\langle 100 \rangle$ direction.

1.4.2 Magnetostriction

This phenomenon, in which the dimensions of a ferromagnetic sample will change if its magnetization varies, is allied to magnetocrystalline anisotropy; in a system exhibiting the latter the total lattice energy is reduced by the development of a magnetization related strain. Linear magnetostriction, λ, is defined as the change of length per unit length, $\frac{\delta l}{l}$ and the direction of measurement must be specified. A variety of techniques have been developed for the measurement of the strain including mechanical, optical and electrical methods. Resistive strain gauges are frequently found to be a convenient means of measurement. In the case in which magnetization saturates λ is called saturation magnetostriction, λ_s, and its values in different crystallographic directions are shown by $\lambda_{(100)}$ and $\lambda_{(111)}$ etc. For a cubic crystal an adequate expression for the magnetostrictive strain measured in a direction whose direction cosines relative to the cubic axes are $\beta_1, \beta_2, \beta_3$, is in the form,

$$\frac{\delta l}{l} = \frac{3}{2}\lambda_{100}\left(\alpha_1^2\beta_1^2 + \alpha_2^2\beta_2^2 + \alpha_3^2\beta_3^2 - \frac{1}{3}\right) + 3\lambda_{111}\left(\alpha_1\alpha_2\beta_1\beta_2 + \alpha_2\alpha_3\beta_2\beta_3 + \alpha_3\alpha_1\beta_3\beta_1\right) \qquad (1.12)$$

in which $\alpha_1, \alpha_2, \alpha_3$ are as defined in the previous section. This equation is usually convenient for the analysis of experimental measurements, Chikazumi (1964). A useful survey of the theory of magnetostriction in other types of crystals is given by Callen and Callen (1965).

CHAPTER 2

A Review of Magnetocrystalline Anisotropy

2.1 The Origin of Magnetocrystalline Anisotropy

The origin of the anisotropy is believed to be the result of the combined effects of the spin - orbit interaction and the incomplete quenching of the orbital angular momentum. In other words, the magnetization of the crystal sees the crystal lattice through the agency of the orbital motion of the electrons.

Van Vleck (1937) considered the anisotropy to originate from an indirect coupling between nearest neighbour spins i and j. Then he expanded the effective coupling energy into a dipole - dipole term

$$\mathcal{H}_D = \sum_{i>j} D_{ij} \left[\underline{S}_i \cdot \underline{S}_j - 3 r_{ij}^{-2} \, (\underline{S}_i \cdot \underline{r}_{ij}) \, (\underline{S}_j \cdot \underline{r}_{ij}) \right] \quad (2.1)$$

plus a quadrupole - quadrupole term

$$\mathcal{H}_Q = \sum_{i>j} Q_{ij} \, r_{ij}^{-4} \, (\underline{S}_i \cdot \underline{r}_{ij})^2 \, (\underline{S}_j \cdot \underline{r}_{ij})^2 \quad (2.2)$$

where D_{ij} and Q_{ij} are temperature independent coupling constants and r_{ij} connects nearest neighbours.

This spin - orbit coupling has the effect of making the spin vectors, responsible for the ferromagnetism, sensitive to the anisotropic electrostatic forces that exist within the lattice. This occurs because the spin interacts with the orbital motion and the orbital motion is controlled by the lattice due to electrostatic fields and overlapping orbital wave functions of neighbouring atoms, that is:

$$(\text{spin})_i \text{---} (\text{orbit})_i \text{---} (\text{crystalline field}) \text{---} (\text{orbit})_j \text{---} (\text{spin})_j$$

It is also worthwhile to mention that in a dipole - dipole model anisotropy exists only when the second approximation of perturbation theory is used, otherwise the effect is too small to be worth consideration, and the quadrupole - quadrupole model is generally possible only if the spin quantum numbers of the atoms are greater than $1/2$. In both models a Weiss molecular field was used to represent exchange interaction.

Another approach was tried by Brooks (1940) using the "collective electron" or "Itinerant" model of Stoner and Slater instead of the Heisenberg localized electron model as tried by Van Vleck. He represented the exchange energy as a Weiss internal field and the spin - orbit coupling as a perturbation. He then put these ideas on a quantative basis by considering the form of the d - bands in cubic crystals, in which the overlapping of the d shells is small and so a Bloch approximation of tight binding was reasonably acceptable. These basic calculations of Brooks have been used in recent years to calculate and interpret the anisotropy energy of Ni and Fe , Furey (1967) and Franse (1969). The wave functions used to describe the state of a 3d - electron in this model were

$$\Psi_n(\vec{r},\vec{K}) = N^{-1/2}\sum_{\ell} \exp(ia\vec{\ell}\cdot\vec{K})\,\phi_n(\vec{r} - a\vec{\ell}) \qquad (2.3)$$

where a is the lattice constant, ℓ is a vector which represents lattice points, and N the total number of atoms. ϕ_n's are the atomic wave functions and are solutions of the eigen value equation

$$\left[p^2/2m + U(r)\right]\phi(r) = E\phi(r) \quad \text{where } U(r) \qquad (2.4)$$

is the atomic potential. These solutions which correspond to 5 - fold degenerate 3d level of the isolated atom are

$$\phi_1(r) = (15/4\pi)^{1/2} \frac{xy}{r^2} f(r), \quad \phi_2(r) = (15/4\pi)^{1/2} \frac{yz}{r^2} f(r),$$

$$\phi_3(r) = \left(\frac{15}{4\pi}\right)^{1/2} \frac{2x}{r^2} f(r), \quad \phi_4(r) = (15/16\pi)^{1/2} \left(\frac{x^2-y^2}{r^2}\right) f(r),$$

$$\phi_5(r) = (15/16\pi)^{1/2} \left(\frac{3z^2 - r^2}{r^2}\right) f(r)$$

where $f(r)$ is the normalized radial function of the isolated atom. Brooks, by assuming that for nickel the bands constructed from ϕ_1, ϕ_2 and ϕ_3 orbitals are well apart from ϕ_4, ϕ_5 bands, could calculate the anisotropy energy from ϕ_1, ϕ_2 and ϕ_3 orbitals. He then, by using fourth order perturbation theory for a number of K points of the Brillouin Zone and summation of the spin - orbit energy correction over all occupied states, found the right order of magnitude and the right sign for K_1 of Ni , but because states over a large region of the zone contributed to the anisotropy energy he could not find a strong temperature dependence for K_1.

Even though in Brooks' model anisotropy of the right magnitude and sign for iron and nickel appears in the 4th approximation, there is no sharp change in anisotropy as the lattice passes from face - to body-centred cubic in Fe - Ni alloys. Also the temperature dependence of the anisotropy is not described at all by this model. Fletcher (1954) has developed Brooks' ideas and corrected some minor errors in his treatment. Using his own data, Fletcher (1952), for the energy distribution of d electrons in ferromagnetic nickel he found a value of 5×10^7 erg cm^{-3} for K_1 at 0 K. This was two orders of magnitude greater than the earlier estimate

of Brooks, 10^5 - 10^6 erg cm^{-3}, which had agreed well with the available experimental data.

Carr (1957) by using a virial theorm and perturbation theory explained the anisotropy energy in terms of Coulomb energy alone. He found one of the basic mechanisms for anisotropy arises from the interaction between the charge distribution about a lattice site and the crystalline potential of the lattice, which is different from Van Vleck's mechanism. He was not able to make numerical estimates of the size of the anisotropy constants, but using Hartree functions he showed that they should be of the correct order of magnitude to agree with experimental results. Slonczewski (1962) has pointed out that in the calculations of Brooks and Fletcher an integration is made of the spin - orbit energy over the occupied states of the Brillouin Zones, but that changes in occupation of the states due to the spin - orbit perturbation are neglected He showed that this omission was very important and that after making allowances for it the results of Fletcher would be reduced by a factor of about 200 which would lead to much better agreement with experimental results.

Furey (1967) has calculated the anisotropy energy for nickel, using improved energy bands, in which he has considered the hybridization between 3d - bands and the conduction bands following Hodges et al (1966). The main principle of his work is that only special points in the Brillouin zone contribute strongly to the magnetic anisotropy and these lie in regions of the zone where there would be degenerate bands without the spin - orbit interaction. These points are situated on Γ - X and Γ - L directions of the first zone.

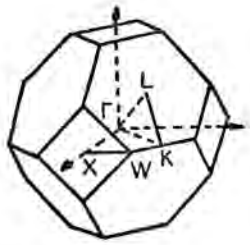

Fig.(2.1) First Brillouin Zone of fcc Ni showing Γ -x and Γ - L directions (after Furey 1967).

Mori 1969 also has used energy band shapes obtained by Yamashita et al (1963) to calculate the anisotropy energy of nickel and iron. A big discrepancy with Furey in the case of nickel is that the contributions of degenerate states to the anisotropy energy are less important, even though experimental evidence at low temperature (Franse, 1971) supports the work of Furey.

Recently Kondorskii et al (1973), by using band structures and Fermi surface shapes, have given a development of the theory of magnetic anisotropy of nickel, the values for K_1 obtained from this theory are in good agreement with the experimental results for the liquid helium temperature range. They used the same basic approach as that used by Furey.

CHAPTER 3

A Review of Temperature dependence of Magnetic Anisotropy

3.1 Temperature Dependence of Magnetocrystalline Anisotropy

The theory of the temperature dependence of magnetocrystalline anisotropy of cubic crystals has had a very complicated history. The first attempt at a theoretical model was due to Aukulov (1936) who suggested a classical treatment of single spin anisotropy, assuming that each spin has an intrinsic direction dependent energy which arises by interaction with the internal magnetic field of atoms Using simple classical arguments he showed

$$\frac{K_1(T)}{K_1(0)} \simeq 1\text{-}10\left(\frac{M(0) - M(T)}{M(0)}\right) \simeq 1\text{-}10\,\delta m(T) \qquad (3.1)$$
$$\simeq \left[1-\delta m(T)\right]^{10} \simeq \left[m(T)\right]^{10}$$

where m(T) is the reduced magnetization $\frac{M(T)}{M(0)}$ and $\delta m(T) = 1 - m(T)$.

This result applies only at temperatures sufficiently low that $\delta m(T) \ll 1$. This was the first and simplest derivation of the tenth power law.

After that a series of experimental tests, e.g. Bozorth (1937) and Brukhatov et al (1937), was done giving results which ranged from complete agreement to outright contradiction. Amongst all these confusions several important extensions of the theorem were achieved. Van Vleck (1937) employed a molecular field treatment of the exchange interaction in a Hamiltonian which contained pseudo - dipolar and pseudo - quadrupolar terms representing spin-orbit and crystal field

interactions. The pseudo - dipolar term gives a second power law while the pseudo - quadrupolar term leads to a sixth power law shifting to a fifth power with increasing temperature. Both disagree with Akulov's tenth power theorem. The reason why Van Vleck obtained too weak a temperature dependence was that in considering the temperature dependence of the anisotropy to be caused by statistical deviation of S_i and S_j from maximum alignment he employed a molecular field model thereby neglecting the correlation in the alignment of neighbouring spins. Zener (1954) by generalizing the Akulov tenth power law to a $\ell(\ell+1)/2$ power law revived interest in the subject. Zener assumed that,. (i) the temperature dependence of magnetocrystalline anisotropy arises solely from the local deviation in the direction of magnetization and (ii) the local deviation in an elementary region is the resultant of a very large number of independent deviations. The effect of these local deviations, which could be represented by a random walk function, upon the magnetic anisotropy was most conveniently expressed by representing the magnetic energy as a series of surface harmonics. He arrived at a power law relationship for the coefficient C associated with the ℓ^{th} order harmonic as

$$\frac{C_\ell(T)}{C_\ell(0)} = \left[\frac{M_S(T)}{M_S(0)}\right]^{\ell(\ell+1)/2} \qquad (3.2)$$

He compared the right hand side of this equation with the ratio $\frac{K(T)}{K(0)}$ obtained from experimental measurements for iron and found a good agreement with $\ell = 4$ for K_1 and $\ell = 6$

for K_2. In the case of nickel the anisotropy decreases much more rapidly and so Zener's classical assumptions would not seem to be applicable. Keffer (1955) took a middle path between the Zener and Van Vleck theories and by choosing quadrupole - quadrupole coupling of Van Vleck found that at low temperature pseudo - quadrupolar interaction would give a tenth power law, changing rapidly to the Van Vleck sixth power on increasing the temperature. He was the first to point out that this change over corresponded to a change in the degree of correlation between neighbouring spins: for high correlation a tenth power law would be expected, but low correlation would form a sixth power. He also rederived the Zener $\ell(\ell+1)/2$ generalization, using the classical single - ion mechanism and molecular field theory. Brenner (1957) by choosing a conventional Boltzmann distribution instead of Zener's random walk function found a reasonably good agreement with the measured temperature dependence of the first anisotropy constant for nickel for $T/\theta > 0.3$, where θ is the Curie temperature. He also pointed out that the intrinsic shape of the anisotropy energy surface might well change with temperature due to changes in spin - orbit coupling with increased lattice vibration and thermal expansion. Carr (1958) by using a Langevin function adjusted to fit the measured magnetization curve derived Zener's tenth power law for iron. He also, by using Zener's results and with the postulate that the intrinsic anisotropy varies with thermal expansion, found good agreement with experimental results for cobalt. For nickel he assumed that, since the structure had cubic symmetry,

a tenth power law would be obeyed as was found to be so for iron, but by analogy with cobalt he included an empirical factor to allow for lattice expansion giving the expression

$$K_1(T) = K_1(0,0)\left(1-1.74\ \frac{T}{T_c}\right)\left(\frac{M(T)}{M(0)}\right)^{10} \qquad (3.3)$$

In which $K_1(0,0)$ is the first anisotropy constant of nickel for zero temperature and zero strain and T_c is the Curie temperature. Van Vleck (1959) by presenting a spin Hamiltonian or effective potential of the type $V = a(S_x^4 + S_y^4 + S_z^4) + c$ has discussed the cubic anisotropy. The constant c is included to make V average to zero when all Zeeman components are weighted equally. The matrix elements of V have the structure of a spherical harmonic of cubic symmetry and degree $n = 4$, so V is called "octopolar potential". He has then used this theory in the limit of high neighbouring correlation and found a tenth power law, which again was not applicable to the case of nickel. Keffer and Oguchi (1960) have reevaluated Van Vleck's second order perturbation theory of dipolar - type anisotropy in cubic ferromagnets. Then by giving a physical picture of the origin of dipolar - type in the form of precession of spin vectors about the axis of quantization and because of strong correlation between directions of them at low temperature, they could obtain a tenth power law. Callen & Callen (1960) have also given a pictorial description of the decrease of the first anisotropy constant of cubic materials with increasing temperature. The physical origin of this decrease is because of wide angular deviation of the individual spins from

their average directions as the temperature increased. As in fig. (3.1) at higher temperatures the individual spins sample the anisotropy over a wider angle, and the average energy becomes more nearly isotropic. In fig. (3.1) the energy at A′ is greater than the zero temperature value at

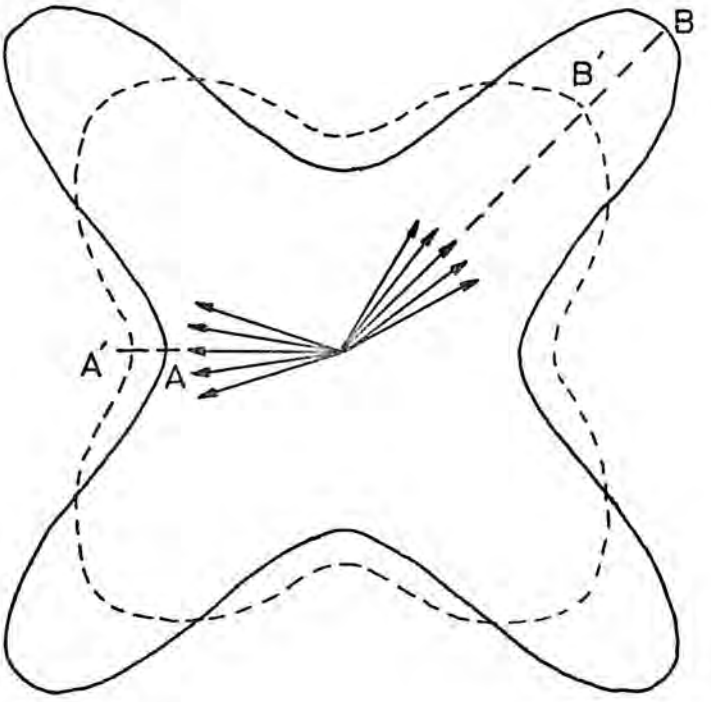

Fig. (3.1) Temperature dependence of anisotropy energy

A (Easy Direction), whereas the energy in the hard direction is greater at zero temperature (B) than at temperature T, (B′). In another paper Callen and Callen (1966) by a quantum mechanical treatment obtained Zener's $l(l+1)/2$ law at low temperatures. Also by using a Boltzmann distribution function for the deviations of the spins from the mean directions they extended this theory to arbitrary temperatures.

Aubert (1968) assumed that the major contribution to the anisotropy of the magnetization, in the special case of nickel, will arise from an orbital contribution rather than a spin

contribution. The main effect of spin - orbit interaction was considered to be to introduce anisotropy in the orbital contribution to energy and magnetization. He then by considering an effective field H_S collinear to M_S has represented the interaction of the spin system on the quenched orbital moments through spin - orbit interaction. For simple crystal directions where M_S and M_L, which are the spin and orbital contributions to the magnetization respectively, are collinear he assumed that:

$$M_L = a H_S + b H_S^3 + \qquad (3.4)$$

and the corresponding energy would be

$$W = -\frac{1}{2} a H_S^2 - \frac{1}{4} b H_S^4 + \qquad (3.5)$$

Due to cubic symmetry, a is a constant and b has a value that may depend on the direction of H_S and leads to anisotropy of M_L. Aubert has shown that to first order

$$H_S = -4 \left(\frac{\Delta W}{\Delta M} \right) \qquad (3.6)$$

in which $\Delta W = -\frac{1}{4} B H_S^4$ and $\Delta M = B H_S^3$ are the differences in energy and magnetization respectively between $\langle 111 \rangle$ and $\langle 100 \rangle$ directions and B is the difference in b in the two directions. He has then, by using equation (3.6) and experimental results, found that H_S will vary as tenth power of M , total magnetization ($M_L + M_S$), and so ΔM varies as fortieth power of M which is a reasonable approximation to the experimental results over a limited range of low temperatures. Mori (1969) has

calculated the low temperature values of K_1 and K_2 for iron and nickel using band structures due to Yamashita et al (1966). He applied perturbation theory to calculate the contributions for those points in the Brillioun Zone where the orbital angular momentum is quenched and showed that where this is not so the contributions were very small. To calculate the temperature dependence he determined splitting between plus and minus spin bands to agree with the experimental results on the temperature variation of the spontaneous magnetization and then recalculated K_1 and K_2 making allowance for the Fermi distribution. The results were very satisfactory for iron, but did not agree so well in the case of nickel. Hausmann (1970) has given a general derivation of tenth power law for the anisotropy constant K_1 of cubic ferro - and ferri-magnets, using spin wave and ferromagnetic resonance theory. He then found for low temperatures that:

$$K_1(T) = K_{1V}\left[1 - 10\,\frac{M(0) - M(T)}{M(0)}\right] \qquad (3.7)$$

where K_{1V}, the anisotropy constant in a state of vacuum of magnons, does not depend on the temperature. Yang et al (1973) have extended previous work (Yang 1971) on hexagonal crystals to cubic crystals and applied the results to a consideration of the temperature variation of K_1 for iron and nickel. They found it necessary to establish coefficients in an expression by comparison with experimental results and to this extent the work is empirical. Very good fitting with the measured results was however achieved.

3.2 Empirical Formulae Representing Temperature Dependence of Magnetic Anisotropy of Nickel

As mentioned in the previous section the M^{10} - Law was not applicable to the case of nickel and usually some empirical formulae without any theoretical background have been used to represent the temperature dependence of the anisotropy of nickel. In table (3.1) some of these formulae have been given. As can be seen from this table a variety of expressions have been proposed to describe the variation of K(T) with temperature and magnetization. Some of these are entirely empirical, such as that due to Brukhatov, while others attempt to include theoretical predictions usually in the form of a m^x power law factor. The exponential expressions include an arbitrary temperature which is not related to any simple parameter of the material and varies between 100K and 169K depending on the investigator. It is not clear why these temperatures should be used and no satisfactory theoretical model has been advanced to account for them. The power n involved also varies between 1.5 and 2.0 again without any clear reason. Other workers have introduced an m^x law combined usually with a dependence on the ratio of temperature to the Curie temperature. Here again there are numerical differences in the values of x chosen and in the way in which T/Tc is introduced. The work of Yang is unique in its replacement of these forms by one using hyperbolic Bessel functions and is of a semi-theoretical nature.

It is not at present obvious that these relations are all approximations to one more adequate expression. Each has its

range of validity as a means of representing measured values, but only limited insight into the processes involved may be obtained.

Author	Year	Formula, m = M(T)/M(0)	Description
Brukhatov	1937	$K_1(T) = K_1(0) \exp -(T/T_o)^n$ where $K_1(0) = -4 \times 10^{-5}$ erg cm^{-3}, n = 2 and T_o = 169 K.	Based on the results of measurements of torque curves in (100) plane between 78K and room temperature.
Carr	1958	$K_1(T) = K_1(0,0)\ (1.74\ \frac{T}{T_c})\ (m)^{10}$	see previous section
Iwata et al	(1965,1967)	$K_1(T) = K_1(0)\ (1.- 1.3\ \frac{T}{T_c})(m)^{25(1+1.4\ \frac{T}{T_c})}$ $K_2(T) = K_2(0)(m)^{36(1 + 0.6\ \frac{T}{T_c})}$	Where T_c in these two formulae are the Curie temperature.
Hofmann et al	1970	$K_1(T) = K_1(0) \exp - (\frac{T}{T_o})^n$ where n = 1.6, T_o = 146K and $K_1(0) = - 10.4 \times 10^5$ erg cm^{-3}	Based on the results of torque measurements at temperatures between 4.2K and 90K in (001) plane of a nickel single crystal sphere (99.9%)

Table 3.1 Empirical Formulae Representing Temperature Dependence of Magnetic Anisotropy of Nickel.

Author	Year	Formula	Description
Hofmann et al	1970	$K_1(T)=K_1(0)\exp-(\frac{T}{T_o})^n$ where $n=1.6$, $T_o=142^oK$, $K_1(0)=-12.25\times10^5 ergs/cm^3$	Using the results on nickel single crystal (99.999%) by Franse (1969) and Krause et al (1969)
Hausmann et al	1971	$K_{1V}(T)=K_1(0)\exp-(T/T_o)^n$ where $K_{1V}(T)=K(T)\left[M(0)/M(T)\right]^{10}$ and $n=1.5$, $T_o=100^oK$	Based on the results of Hofmann and Kaul et al (1969). K_{1V} is the first magnetic anisotropy constant of nickel in the magnon vacuum state.
Hofmann	To be published	$K_1(T)=K_1(0)\exp-(T/T_o)^n$ with $n=1.5$, $T=100^oK$	Used for temperature and concentration dependence of K_1 in Ni Mo alloys.
Yang et al	1973	$\frac{K_1(T,H)}{K_1(0,0)} = -6.14\ \hat{I}_{5/2}(T,H)+ 3.36\ \hat{I}_{9/2}(T,H)+4.88\ m^2(T,H) -1.10\left[\hat{I}_{5/2}(T,H)\right]^2$	In which $\hat{I}_{5/2}, I_{9/2}$ are the hyberbolic Bessel functions of order 2 and 4 respectively and m is the reduced magnet-ization. This formula has been obtained by fitting the experiment-al data for nickel into a theoretical formula derived by Yang (1971) for hexa-gonal crystals.

Table 3.1 (Continued)

CHAPTER 4

Mean Free Path and Anisotropy

4.1 M.f.p. of conduction electrons and K_1 of Ni

As mentioned in the previous chapter none of the theories could give a power law which agreed with the experimental results in the case of nickel. The purpose of this chapter is to describe some of the possible interpretations of this anomalous temperature dependence of the first anisotropy constant of nickel and its deviation from the tenth power law. This anomaly can be caused by:

(1) magnon-magnon interaction.

(2) thermal expansion of the lattice.

(3) assuming that the anisotropy energy of a crystal is due to the indirect anisotropic exchange.

It has been found that (1) and (2) have a very small effect on the temperature dependence of the first anisotropy constant at low temperature. This can be seen when the M^{10}-Law is valid for insulators e.g. haematite, cobalt ferrite etc.

In the case (3) as it has been shown by Mattis (1965) that, the isotropic indirect exchange depends on the mean free path of the conduction electrons; the same mechanism should be applicable to anisotropic exchange. As the mean free path of the conduction electrons depends strongly on temperature, thus this mechanism may be useful to describe the anomaly of nickel. The following qualitative arguments are given to support this hypothesis.

1 - The mean free path of the conduction electrons can be reduced by the addition of impurity atoms. A similar reduction

can also be seen in the magnetic anisotropy constant K_1 of nickel when impurity atoms are added to nickel, Franse et al (1968, 1973).

2 - The mean free path of conduction electrons will be changed by ordering processes in alloys. This has been experimentally found by Hausmann et al (1971), when they measured the electrical resistivity and the first anisotropy constant of Ni_3Fe monocrystalline spheres after several heat treatments. The results of these measurements upon the electrical resistivity and the first anisotropy constant showed that both resistivity and anisotropy change strongly during the same stage of the ordering process. Similar effects had been previously observed by Bozorth et al (1953) using the same material.

3 - Hausmann (1970) has suggested that the dependence of K_1 on concentration in a dilute binary alloy can be represented by an expression of the form

$$K_1^{\underline{Ni}\ Me} = K_1^{Ni}(1 - \alpha_{Me}\, C_{Me}) \qquad (4.1)$$

where C_{Me} is the small concentration of the alloying metal and α_{Me} is a constant characteristic of the metal. A similar relation holds for the effect on resistivity with

$$\rho^{\underline{Ni}\ Me} = \rho^{Ni}(1 + \beta_{Me}\, C_{Me}) \qquad (4.2)$$

where β_{Me} is another constant. Using measurements on Ni Fe and Ni Co alloys he has shown that $\alpha \simeq \beta$, suggesting a similar mechanism for both effects.

4 - On the basis of this similarity Hausmann has also calculated the temperature coefficient of anisotropy from measured values

of the temperature coefficient of resistivity and found reasonable agreement with the measured value.

It should be pointed out that the results discussed in 3) and 4) above are based on measurements at room temperature only and might not have any general validity.

Hausmann and Wolf (1971) wrote equation (3.7) for nickel, assuming that the deviation from the tenth power law can be caused by temperature dependence of K_{1V}, as follows

$$K_1(T) = K_{1V}(T) \left[\frac{M(T)}{M(0)} \right]^{10} \qquad T \ll \theta \qquad (4.3)$$

where θ is the Curie temperature. Then by applying the hypothesis previously described, they related K_{1V} to the mean free path of the conduction electrons, for small concentrations $C_i \ll 1$ and low temperatures $T \ll \theta$, as follows,

$$K_{1V}(T, C_i) \approx K_{1V} \left[\lambda^{-1} (T, C_i) \right] \qquad (4.4)$$

where λ is the mean free path of the conduction electrons. Strictly this is not the same mean free path as that which determines the resistivity as pointed out by Hausmann et al (1971) but the difficulty can be circumvented if Matthiessen's rule is obeyed and the effect of variation of temperature and concentration represented by separate terms,

$$\lambda^{-1}_{\underline{Ni}\ Me} (T, C_i) = \lambda^{-1}_{Ni} (T) + \lambda^{-1}_{Me} (Ci) \qquad (4.5)$$

They then by using empirical results for K(T) and M(T) from Hofmann (private communication) and Kaul et al (1969) found the following experimental formula for pure nickel.

$$K_{1V}^{Ni}(T) = K_1(0)\ e^{-\left(\frac{T}{To}\right)^{3/2}} \qquad (4.6)$$

To interpret equation (4.6) they used the hypothetical equation (4.4) and so the following exponential form of equation was written in a similar form to (4.6).

$$K_{1V}(\lambda^{-1}) = K_1(0)e^{-\gamma/\lambda} \qquad (4.7)$$

It is obvious that γ should be a concentration and temperature independent length. Using equations (4.5) and (4.7) the following expression for an alloy was obtained, in which the temperature and concentration parts of $K_{1V}^{\underline{Ni}\ Me}$ are now separated.

$$K_{1V}^{\underline{Ni}\ Me}(T, C_i) = K_{1V}^{Ni}(T)\ e^{-\gamma/\lambda_{Me}(C_i)} \qquad (4.8)$$

where $K_{1V}^{Ni}(T) = K_{1V}^{Ni}(0)\, e^{-\gamma/\lambda_{Ni}(T)}$. As λ_{Me}^{-1} is proportional to the concentration of the alloying atoms so:

$$\lambda_{Me}^{-1}(C_i) \approx \frac{\alpha}{\gamma} C_i \qquad (4.9)$$

In which the constant proportionality $\frac{\alpha}{\gamma}$ has been chosen for convenience. Using equation (4.3) $K_1^{Ni\ Me}(T, C_i)$ can be written as follows,

$$K_1^{\underline{Ni}\ Me}(T,C_i) = K_1^{Ni}(T)\left\{\frac{M^{\underline{Ni}\ Me}(T,C_i)M^{Ni}(0)}{M^{\underline{Ni}\ Me}(0,C_i)M^{Ni}(T)}\right\}^{10} \exp -\sum_i \alpha_i C_i \qquad (4.10)$$

and for low temperatures and small concentrations this approximates to

$$K_1^{\underline{Ni}\ Me}(T,C_i) = K_1^{Ni}(T)\ \exp\left(-\sum_i \alpha_i C_i\right) \qquad (4.11)$$

Where a binary alloy is involved the summation is of course unnecessary.

Hausmann and Wolf (1971) from the experimental results on Ni Mo alloys found an exponential form of variation in a good agreement with (4.11). This factorization of K_1 into purity dependent and temperature dependent terms would also appear to be reasonable from the experimental results on nickel samples of different purity Hofmann et al (1970). Kortekaas et al (1972) by using nickel samples containing from .1 to 1 atomic percent of Cu, Co and Fe showed that a relation in the form of (4.11) would give a correct representation of the effect of impurities at 4.2°K and 77°K. From their results they calculated values of α for the three alloys. They also investigated a ternary alloy (Ni + 0.45% Cu + 0.45% Co) and found that the effect of Cu and Co impurities were additive as in Equation 4.11 contrary to expectations from a rigid band model.

Franse et al (1973) have used the idea of the mean free path of the conduction electrons to check the relation between α_i and residual resistivity. According to Furey (1967) the anisotropy energy of nickel is very sensitive to the shape and the occupation of the 3d minority bands near the Fermi level. Farrell and Greig (1968) have split the residual resistivity up into $\rho_o(\uparrow)$ and $\rho_o(\downarrow)$. In this paper for most of the alloys $\rho_o(\uparrow)$ is determined to a large extent by the enhanced scattering probability of the minority spin conduction electrons due to the high density of vacant d - states in the spin $\uparrow$ minority d - band. They describe how the values of the minority electron resistivity $\rho_o(\uparrow)$ can be calculated from resistivity measurements at low and room temperatures on a dilute alloy and

the pure metal. They define a parameter Δ which represents the deviation from Matthiessen's rule as

$$\Delta = (\rho_m - \rho_o)_{\text{alloy}} - (\rho_m - \rho_o)_{\text{pure metal}} \qquad (4.12)$$

where ρ_m is the measured value at room temperature and ρ_o is the residual, low temperature, resistivity. They then show that simultaneous solution of the following two equations will give $\rho_o(\uparrow)$ and $\rho_o(\downarrow)$, the minority and majority resistivities respectively

$$\rho_o = \frac{\rho_o(\uparrow)\,\rho_o(\downarrow)}{\rho_o(\uparrow) + \rho_o(\downarrow)} \quad \& \quad \frac{\Delta}{\rho_o} = \frac{\left\{\rho_o(\uparrow) - \rho_o(\downarrow)\right\}^2}{4\,\rho_o(\uparrow)\,\rho_o(\downarrow)} \qquad (4.13)$$

this treatment assumes that at room temperature the deviations are dominated by spin mixing.

Following the suggestions by Furey and Farrell et al, Fransе et al have compared α_i values from anisotropy measurement with the $\rho_o(\uparrow)$ values from resistivity measurements and have found that α increases in the series Pd, Cu, Co, Fe and Cr and that $\rho_o(\uparrow)$ also increases, though not in exact proportion, except for the case of Cu where the value of $\rho_o(\uparrow)$ is anomalously high. They then conclude that a relation between the s - d scattering of the minority spin electrons and the anisotropy energy cannot give a perfect correlation between α_i and $\rho_o(\uparrow)$ values. In the case of Ni Pd and Ni Cu they have mentioned that S - S scattering is probably not negligible. In addition the anisotropy energy and the S - d scattering of minority electrons may not be fully determined by the same energy states. They conclude that the similarity in the temperature and concentration dependences of α_i and $\rho_o(\uparrow)$

values could arise from a diminishing sharpness of band shape and Fermi level, due to scattering on impurities or thermal excitation.

CHAPTER 5

Growth, cutting, polishing and orientation of crystals

5.1 Specimen Preparation

Single crystals of nickel and nickel - vanadium alloys (Pearson et al, 1951) were grown by the Bridgeman technique, Rothery (1961), Hanson (1958). The cutting and polishing of the crystals into the form of spheres and their orientation by x-ray methods will be described in the following sections.

5.1.1 Bridgeman Method

Nickel rods of 99.99% purity were purchased from Metals Research Limited and vanadium turnings of 99.8% purity were purchased from Koch - Light Laboratories Limited. Before using nickel rods it was found better to give them a wash in concentrated nitric acid followed by one in alcohol and air drying. Also vanadium turnings were washed in very dilute nitric acid and then in alcohol followed by drying in air.

The crucibles in which melting took place were of high purity recrystallized alumina (Al_2O_3) from Thermal Syndicate Limited. They were of internal diameter 12.7 mm, wall thickness 1 mm, and length 190.51 mm. The base of the crucible tapered at an angle of 60°. Inside of the crucibles were all washed by acetone and dried by air.

After loading the crucible with appropriate weighed quantities of the metals it was then placed in a silica support inside a water - cooled melting chamber made of pyrex glass shown in Fig.(5.1). A flow of high purity argon gas was maintained around the crucible during the whole crystal growth

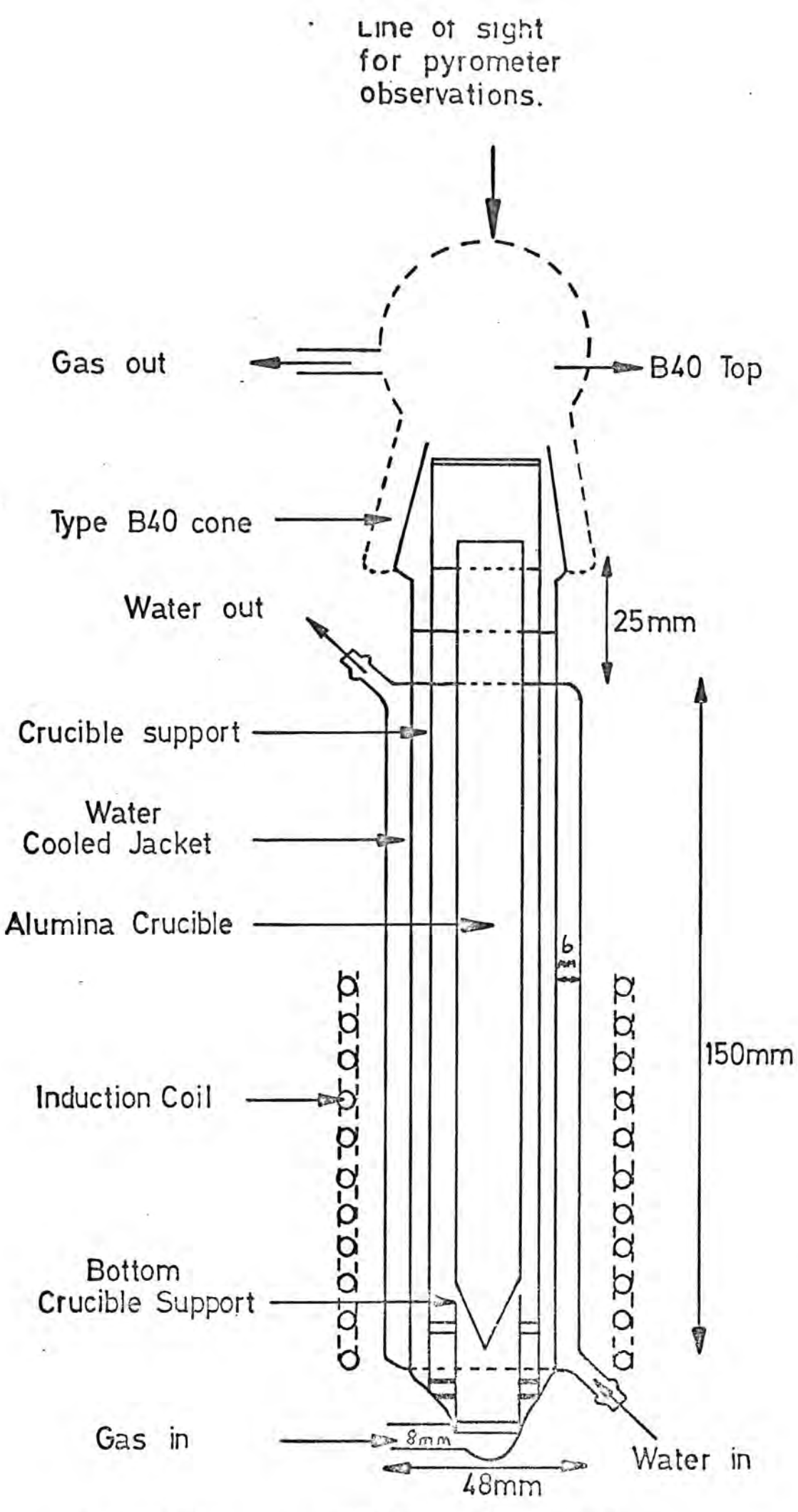

FIG. (5·1) MELTING CHAMBER

process. The argon was dried by passing first through concentrated sulphuric acid and then over phosporous pentoxide. Gas was allowed to flow for one hour before starting to melt. The whole assembly of crucible in melting chamber was capable of being moved vertically inside the output coil of an induction furnace. To make use of the Bridgeman method a motor driven cooling system was designed which was able to lower the melting chamber at two different speeds, one with 4.6 cm/hour and the other with 1.14 cm/hour. The bottom of the melting chamber was kept on a platform. The platform was attached to a rod which had 16 threads per centimetre on which was threaded a pulley driven from an electric motor. This system served to drive the platform down. An induction furnace from Stanelco Limited with the frequency of 400 kHz and power output 12-15 kW was used for heating and melting, Simpson (1960).

For checking the temperature an optical pyrometer was used. Fig. (5.1) shows details of the melting chamber which has been made of borosilicate glass (pyrex) and contains a recrystallized alumina crucible and silica crucible holder through the top of which light can emerge for optical temperature measurements, Walker et al. (1949). Melting of the charge was achieved by increasing the power output of the generator until the temperature inside the crucible was observed to be at least 1500°C. This temperature was maintained for about half an hour to ensure homogeneity. The motor was then switched on and lowering of the crucible from the hot zone took about 12 hours on the slow speed (1.14 cm/hour). The generator was then switched off and the argon gas

FIG.(5·2)

CUTTING A SPHERE BY ELECTRO-SPARK EROSION.

CUTTING A RECTANGULAR BLOCK FROM AN INGOT

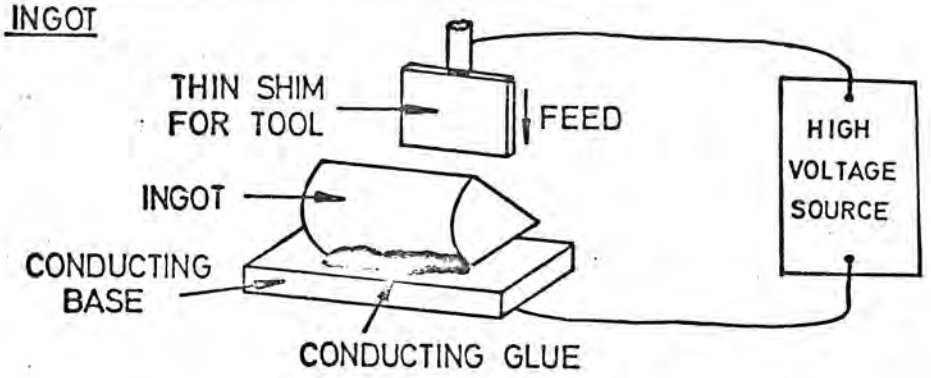

TURNING A CYLINDER FROM A RECTANGULAR BLOCK

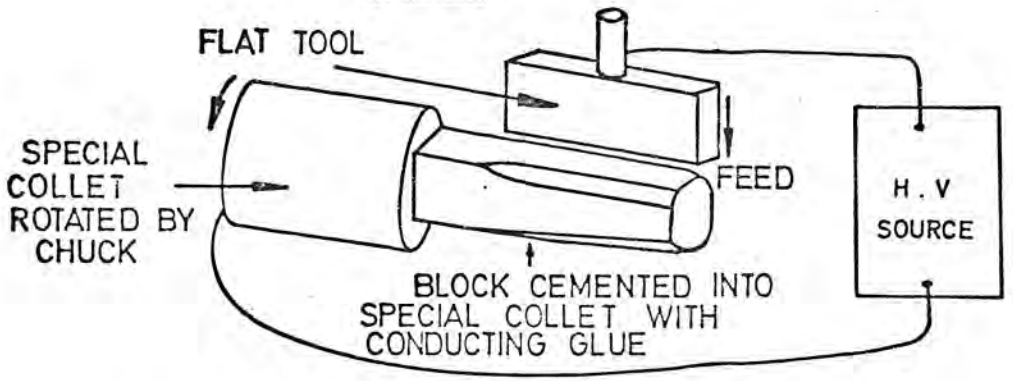

TURNING A SPHERE FROM A CYLINDER

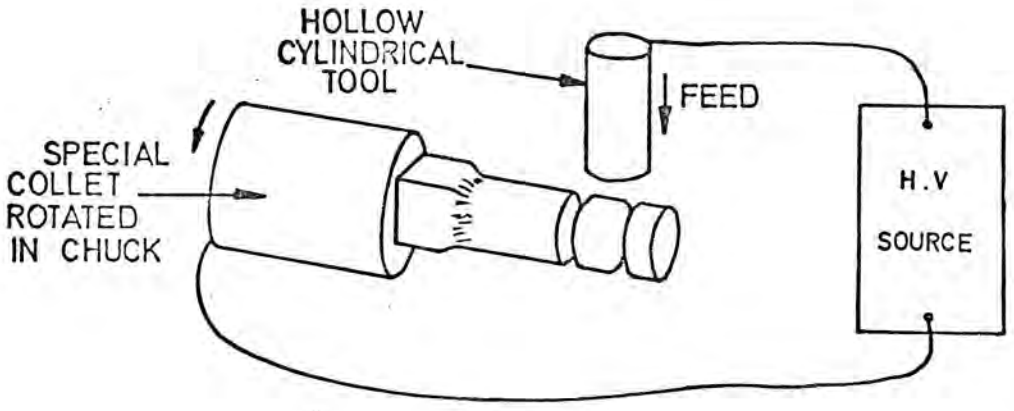

flow continued for some hours before opening the melting chamber to remove the crucible.

5.1.2. Czochralski Method

Two samples, 1% V and 5% V , were prepared by Mr. T.B. Brown. Cavandish Laboratories, Cambridge University, using the Czochralski technique. The equipment was similar to that which was used for the growth of dislocation free copper crystals. The length and the diameter of the crystals were approximately 25 mm and 8 mm respectively.

5.1.3. Cutting & Polishing

After breaking the crucible to remove the ingot a conventional method of mechanical polishing was carried out by using successively finer grades of emery paper (0/0, 2/0, 3/0, 4/0) followed by diamond paste on a rotating wheel with grades (6/3, 3/2, 1/1/4) micron. It was found that for seeing the grain boundaries, even though other methods were used (Popkova et al, 1974), it was better to etch the crystal in hot nitric acid for about five to ten minutes.

For cutting the crystals an electrical discharge machine (E.D.M.) from Metals Research was used. By this machine and using different types of tools, either a thin phosphor-bronze shim or continuously moving soft tinned copper wire of .457 mm diameter for cutting a rectangular block from an ingot, a copper flat tool for turning a cylinder from this rectangular block and a copper hollow cylinder tool for turning a sphere from a cylinder. Fig. (5.2) shows the basic technique for cutting spheres.

When the sphere was obtained it was usually found to be not quite spherical and sphericity could be improved by using a technique for mechanical polishing, (Gray et al, 1969) in which two rods of copper, whose diameters were nearly equal to three quarters that of the sphere were drilled to form pipes. One pipe was rotated in a lathe whereas the other pipe was worked by hand and the specimen held between them. The second pipe could move the specimen in a random manner and a diamond paste was applied for polishing. Grades of diamond pastes were (6/3, 3/2, 1/1/4) micron succesively. After using the finest diamond paste and checking the sphericity by a micrometer to $\pm$ .004 mm the sphere was ready for electropolishing.

For this the sample, which acted as anode was held by a pair of stainless steel tweezers. The ends of the tweezers were protected by a non-conducting adhesive (Durofix) except for the contact points for holding the sample. The cathode was a stainless steel sheet and the electrolyte was 100 cc methanol with 1 cc perchloric acid disolved in it, which was kept in dry ice (solid CO_2), Hopkins et al (1965). The current passing through the circuit was about 10 mA. The specimen was gripped in the tweezers and held in the electrolyte for about twenty seconds. It was then removed, placed in a dish and picked up again in the tweezers, gripping along a different diameter. The process was repeated about twenty times in an attempt to obtain as uniform a polish as possible. X-ray back reflection photographs easily showed whether the electropolishing was complete or not.

By using a travelling microscope and focusing the light at the edge of the spheres it was possible to measure their

diameters. Table (5.1) shows the results of measurements.

TABLE (5.1)

Values for diameters of spheres and percentage of vanadium from analysis (All alloys were made using Ni(99.99%)

Sample	Ni(99.999%)	Ni(99.99%)	.98 at % V	2.71 at % V
Diameter mm	4.208 ± .003	4.47 ± .004	3.654 ± .003	5.66 ± .004

Sample	3.92 at % V	5.14 at % V	6.72 at % V
Diameter mm	4.97 ± 004	4.8 ± .003	4.39 ± .004

5.2 Orientation of Single Crystals

The orientation of single crystals was performed by a Laue back reflection method. For taking the photographs a polaroid XR-7 system was used which was very useful for reducing the time required for orientation of the sample. The specimen was mounted, using Durofix glue, on the top of a small brass rod, which was clamped on top of a goniometer. The length and diameter of the brass rod was chosen in such a way, firstly would keep the specimen in the x-ray beam, when rotation was required, and secondly would be easy for mounting and dismounting the sample by using durofix glue. The first photograph usually showed a random orientation. Then as the specimen - film distance was chosen to be three

centimetres a Wolf net reference was used to study the random orientation. Then by rotations in the goniometer the second photograph was taken which was nearer to the desired crystallographic direction. This was done for several other photographs by appropriate rotations on the goniometer till the desired direction was found. It was necessary to rotate the crystal on the goniometer through 180^{o} to check that the crystal was a single one.

After orientating the sample a technique was designed for transferring the sample with the same orientation to a sample holder which fitted into the apparatus for torque measurements. The sample holder was mounted in a special bracket that could slide along the track on which the goniometer was mounted on the x-ray generator. It was brought into contact with the sample and Durofix glue applied. When this had set the previous bond between the sample and the goniometer was removed by dissolving with acetone. This allowed only a very small disorientation to take place and a further check was made by mounting the sample holder in the goniometer and taking another Laue back reflection photograph. When using samples mounted to rotate about the $\langle 100 \rangle$ direction any appreciable misorientation could be readily detected by the appearance of other components than those proportional to sin 4θ and sin 8θ in the torque curves. It is worthwhile to mention that a suitable x-ray tube for nickel and Ni - V alloys crystals was a Cu - tube which worked with about 800 W (25 kV and 32 mA) and the time exposure for the polaroid system was about 4 minutes. Some exposures were made using Kodak Crystalex and Kodirex films and here the exposure time was about 10 minutes.

5.3 Specimens Used For Resistivity Measurements

After cutting the ingots grown by the Bridgeman method to give rods suitable for the production of spheres there remained a number of off-cuts of non-rectangular cross-section. By using a diamond wheel the surfaces of these off-cuts were made nearly parallel and further mechanical polishing using diamond paste down to 1/4 μ made them very nearly parallel. These rods were then suitable for resistivity measurements.

5.3.1 Annealing

The samples which were cut and polished for resistivity measurements were then annealed in order to remove any damage or defect from cutting and polishing. For this purpose a muffle furnace through which a fused silica tube could pass was chosen. The samples were kept inside an alumina boat which was placed inside this tube. Before starting to heat the specimen pure argon gas which was dried by passing through concentrated sulphuric acid was allowed to pass through the silica tube for half an hour. Then the furnace was heated to 900°C and held at this temperature for about two hours and subsequently cooled at a rate which did not exceed 100°C per hour. For some of the samples the difference between resistivities at 0°C before and after annealing has been given in table (5.2).

TABLE (5.2)

Effect of annealing on Ni & Ni V alloy resistivities at 0°C.

SAMPLE	ρ(ohm-cm) BEFORE ANNEALING	f(ohm-cm) AFTER ANNEALING
PURE Ni(99.99%)	6.12×10^{-6}	5.83×10^{-6}
2.71 at % V	17.37×10^{-6}	16.58×10^{-6}
3.92 at % V	24.76×10^{-6}	21.79×10^{-6}
6.72 at % V	37.3×10^{-6}	36.16×10^{-6}

5.3.2 Four-Point Probe Methods and Related Measurements

It was found that copper electrodes were suitable for Ni and Ni-V alloys. These electrodes were spot welded to the broad face of each sample using a Hirst spot-welding machine. It was found that a high voltage and a short time of welding could give the best result. In the preparation of each sample an attempt was made to have as large a separation between the ends of the specimen, the current probes, and the voltage probes as possible. In Fig. (5.3) the disposition of the leads are shown and the corresponding dimensions for each sample are shown in table (5.3) as measured by a travelling microscope.

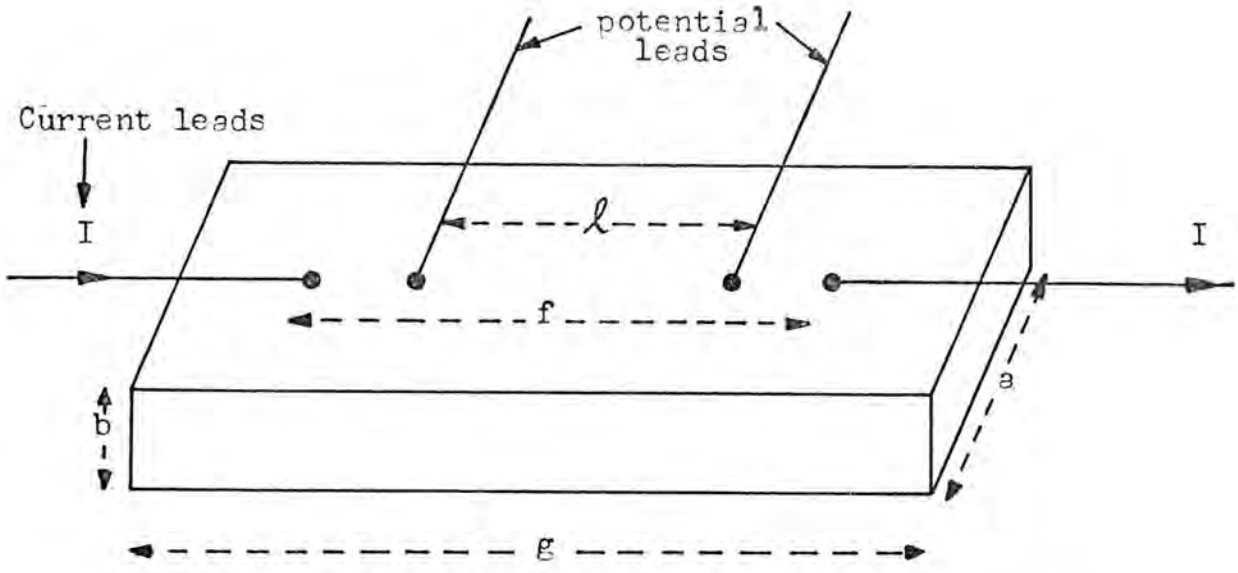

Fig.(5.3) The disposition of the leads

TABLE (5.3)

Dimensions of the rectangular samples

Sample	a mm	b mm	g mm	ℓ mm	f mm
Ni(99.99)	2.094 ± .016	1.103 ± .003	14.78	8.25	13.01
0.98 at % V	2.534 ± .015	1.187 ± .018	20.15	10.05	15.93
2.71 at % V	1.858 ± .011	0.859 ± .007	17.06	9.66	14.02
3.92 At % V	2.213 ± .010	1.070 ± .013	14.08	7.74	12.20
5.14 at % V	2.073 ± .007	1.123 ± .002	17.09	6.58	13.14
6.72 at % V	2.223 ± .007	1.448 ± .008	15.48	8.61	12.72
Ni(99.999)	1.683 ± .015	0.860 ± .007	13.06	6.35	10.83
12.5 at % V	2.904 ± .010	1.416 ± .005	35.01	13.76	25.43
1.02 at %Mo	3.336 ± .005	1.312 ± .009	31.50	15.28	25.18
			± .01		

5.3.3 Ni Mo Alloy

A NiMo alloy with 1 at % Mo was grown, using the Bridgeman technique. This was then cut into blocks for resistivity measurements and annealed as described in section(5.3). The Ni used was as stated in section (5.1.1) whereas the Mo was of 99.9% purity from Mullard (Blackburn) Ltd. The analysis of this sample was performed at Newcastle University. The dimensions of this sample are also given in table (5.3).

5.4 Analysis of Samples

Electron probe microanalysis of the samples was carried out on off-cuts at Newcastle University. Measurements at different points on the samples showed no appreciable difference in composition, thus proving the adequacy of the precautions taken to ensure good homogeneity. The vanadium concentrations in pure Ni (99.99) were those which have been mentioned in table (5.3).

5.5 (99.999%)Purity Ni

During the course of the work it was realized that it would be valuable to have measurements on 5N purity Ni crystals for comparison with the work of Franse (1969). A supply of 5N purity nickel was bought from Johnson MattheyLtd and by the Bridgeman technique a single crystal was grown and this was then cut, using the spark machine, into a sphere and a block for magnetocrystalline anisotropy and resistivity measurements respectively. The dimensions of the sphere and block have been given in tables (5.1) and (5.3) respectively. The block was annealed as described in section (5.3.1)

CHAPTER 6

Methods for Determining the Magnetocrystalline Anisotropy Energy

Experimental measurements of the magnetocrystalline anisotropy constants may be made by a variety of methods. The following are the principal methods that have been used.

6.1 Ferromagnetic Resonance

In this method the motion of the ferromagnetically coupled elementary magnetic moments in a magnetic field is studied. The equation of motion gives a precession frequency $w = g/\mu_B H_e/K$. Using a convenient sample in which the demagnetizing factors can easily be calculated and mounting it in a resonant cavity which can be placed in a magnetic field in such a way that the steady magnetic field and the radio frequency magnetic field are perpendicular it is possible to obtain conditions of resonance between the precession frequency and radio frequency. This resonance frequency, w_r, will be obtained by a fixed microwave frequency and altering the D.C. magnetic field until the precession frequency is equal to that of the microwaves. In an anisotropic crystal the resonance frequency depends on the direction in which the magnetic field is applied, the expressions for w_r involving functions of the anisotropy constants. From a series of measurements with fields in different crystallographic directions these expressions may be solved to yield values of K_1 and K_2. Such relations were first derived by Kittel (1949) and are described by Morrish (1965). A review for hexagonal

crystals has been given by Welford (1974). Results obtained by this method have not always been in agreement with those obtained by torque magnetometry. Franse (1969) has used this method to evaluate anisotropy constants of Ni and some Fe alloy crystals. The expressions which he used for the resonance frequencies in different crystallographic directions included terms ommitted by previous workers and led to values of K_1, K_2 and K_3 which are in good agreement with torque measurements. For example he obtained a value for K_1 at 77°K for pure nickel of $(-84 \pm 3) \times 10^{+4}$ ergs cm^{-3} compared with $(-84.2 \pm 1) \times 10^{+4}$ erg cm^{-3} from torque measurements. However it should be noticed that the accuracy of the ferromagnetic resonance results is less than that of torque measurements especially if a large sample is used and also it is not possible to obtain and make a detailed study of higher order constant contributions to the magnetocrystalline anisotropy.

6.2 Magnetization Curves

In this method the work required to saturate the magnetization M of the sample in different crystallographic directions is compared. This work for a change of M from zero to saturation M_S is equal

$$W = \int_0^{M_S} H_e \, dM \qquad (6.1)$$

which is the area between the magnetization curve and the M axis. Here H_e is the effective field acting on the sample. By using a symmetrical sample and enough available field to achieve saturation despite the effects of demagnetizing fields then the difference between W'S for different crystallo-

graphic directions is just the difference of the anisotropy energy E_a for these directions. By determining E_a in three crystallographic directions it is possible to calculate the values of K_1 and K_2 for a cubic crystal. This method compared with other methods has some disadvantages e.g. it requires laborious plotting of magnetization curves and the application of a demagnetizing correction. Details are given by Zijlstra(1967).

6.3 Inelastic Neutron Scattering

By using mono-energetic neutrons for bombarding a crystal, spin waves can be excited with the wave vector $\underline{q}$ and the amount of energy that they absorb is equal to:

$$\hbar w(\underline{q}) = \hbar^2(\underline{k}_1^2 - \underline{k}_2^2)$$

in which $\underline{k}_1$ and $\underline{k}_2$ are the wave vectors of the incident and scattered neutrons respectively and can be measured by using a crystal spectrometer. By measuring maxima in intensity of the scattered neutrons the magnon dispersion relation can be plotted, from which the value of $\hbar w(0) = \mathcal{E}(0)$ obtained by extrapolation to $\underline{q} = 0$ can be evaluated. This value of $\mathcal{E}(0)$ can be expressed in terms of magnetocrystalline anisotropy constants and so is useful to measure these constants. This can be done by applying fields along different crystallographic directions. Hausmann (1970) obtained the following expression which relates $\mathcal{E}(0)$ to the first anisotropy constant, field H, magnetization M and $S = \alpha_1^2\alpha_2^2 + \alpha_1^2\alpha_3^2 + \alpha_2^2\alpha_3^2$ as described in chapter one.

$$\mathcal{E}(0) = g\mu_B \left[H - 10 \frac{K_1}{M} \left(S - \frac{1}{5}\right) \right] \qquad (6.3)$$

It should be noticed that $\mathcal{E}(0)$ in his case was found from ferromagnetic resonance and not by this method, but for presenting this expression in terms of K_1 the method of measurement is not important.

6.4 Torque Magnetometry

The mechanism and basic principle of this method is as follows. The torque produced in a crystal with internal magnetization M, by an external applied field H is given by $\underline{L} = \underline{M} \times \underline{H}$. If the crystal is anisotropic this will be balanced by a mechanical torque coupling the overall moment system to the crystal lattice and is given by $L_A = \frac{-\partial E_A}{\partial \theta}$. To achieve equilibrium of a crystal in a magnetic field a counter-torque equal and opposite to this must be applied. Using equation (1.11) the following expression for L_A in the (001) plane is obtained

$$L_A = - \sin 2\theta \cos 2\theta (K_1 + \tfrac{1}{2} K_3 \sin^2 2\theta + \ldots.) \qquad (6.4)$$

This equation is used as a basis for analysis of torque curves. For the other crystallographic planes there are other expressions, Brailsford (1966). Franse (1969) has given the expressions for (110) and (111) planes as follows:

$$L_A(110) = \tfrac{1}{4} \sin 2\theta (1 + 3 \cos 2\theta) \left[K_1 + (\tfrac{1}{2} K_2 + 2K_3) \sin^2 \theta + \ldots\ldots \right] \qquad (6.5)$$

$$L_A(111) = \left[-P + q^2/2 \left(\mu_o MH + R \right) \right] \sin 6\theta + \ldots \qquad (6.6)$$

in which $P = \frac{1}{18} K_2 + \frac{1}{972} K_4 + \ldots$, $q = K_1 + \frac{1}{6} K_2 + \frac{1}{2} K_3 + \ldots$,

$$R = -K_1 + \frac{1}{9} K_2 (1 + \frac{1}{2} \cos 6\theta) - \frac{1}{18} K_3 (5 + 4 \cos 6\theta) + \ldots,$$

Corresponding expressions may be obtained for crystals of different symmetry.

The shape of the sample in this method is important, it must have at least cylindrical symmetry. For crystals where the amount of anisotropy energy and the magnetization are not very high, a sample in the shape of a sphere is quite convenient. In the case of hexagonal crystals such as rare earths for which the magnetocrystalline anisotropy and the magnetization are quite high the effect of demagnetizing fields would be large for a sphere and so samples in the shape of a disc which has a lower demagnetizing field should be used. These samples should be located accurately between the poles of an electromagnet to avoid the effect of field inhomogeneity. Then the amount of torque which is exerted on the sample, fixed in a magnetic field, can be measured by applying a counter - torque to restrain the crystal from turning when the field is rotated.

The following ways have been used for producing this counter - torque.

1 - A suspension wire in which a torsional strain is produced may be employed. Care must be taken to avoid instability and damping systems are often employed. Several investigators have used flexible cages, in spite of the fact that this reduces the sensitivity of the system, instead of wire. By using strain gauges, Tajima (1971) or a variable transformer, Aldenkamp et al (1960), or a variable capacitor, Alberts et al (1971), it is possible to measure the distortion of the cage.

2 - A current carrying coil lying in a magnetic field may be used to produce a counter torque. Some investigators have used a separate coil lying in the field of a permanent magnet and rigidly connected to the sample. This system may be combined with a simple servo system and made to balance automatically e.g. Penoyer (1959), Corner et al (1962). Alternatively the coil may lie close to the sample and the torque be produced by the interactions of the current in the coil and the magnetic field that is also being applied to the sample e.g. Rhyne & Clark (1967).

6.5 Choice of the Method of Determining Anisotropy Constants

One of the most convenient methods for measuring anisotropy constants is by the torque magnetometer. The system can be made to record torque curves automatically thus permitting rapid and reliable measurements to be made. A torque magnetometer of adequate sensitivity, but requiring some modifications, was available in the laboratory so this was used for the present measurements and the system is fully described in the following chapter .

CHAPTER 7

The Apparatus

For the present work it was necessary to measure the magnetocrystalline anisotropy, magnetization and electrical resistivity of the samples; for each a distinct apparatus was used as follows.

7.1 Torque Magnetometer

One of the most convenient methods of measuring the anisotropy constants is by using a torque magnetometer in which a single crystal of the material under investigation is suspended in a magnetic field, the torque due to the magnetic field being measured. The direction of the magnetic field may be varied and a simple servo system enables the sample to be held in a fixed position, i.e. prevented from rotating. This "null" position can be maintained by a current which is fed to the coil of a moving coil galvonometer to which the specimen has been rigidly attached. The resulting counter - torque due to this current would be sufficient to hold the specimen back in the null position. The necessary feed-back can be provided by the use of a mirror attached to the specimen mounting and by shining a beam of light onto the mirror from a fixed lamp, the reflected beam illuminating a pair of photo-transistors, the difference signal from which is amplified and fed back to the counter-torque coil. Suitable calibration of the counter-torque coil supplies a measurement of the torque produced on the specimen.

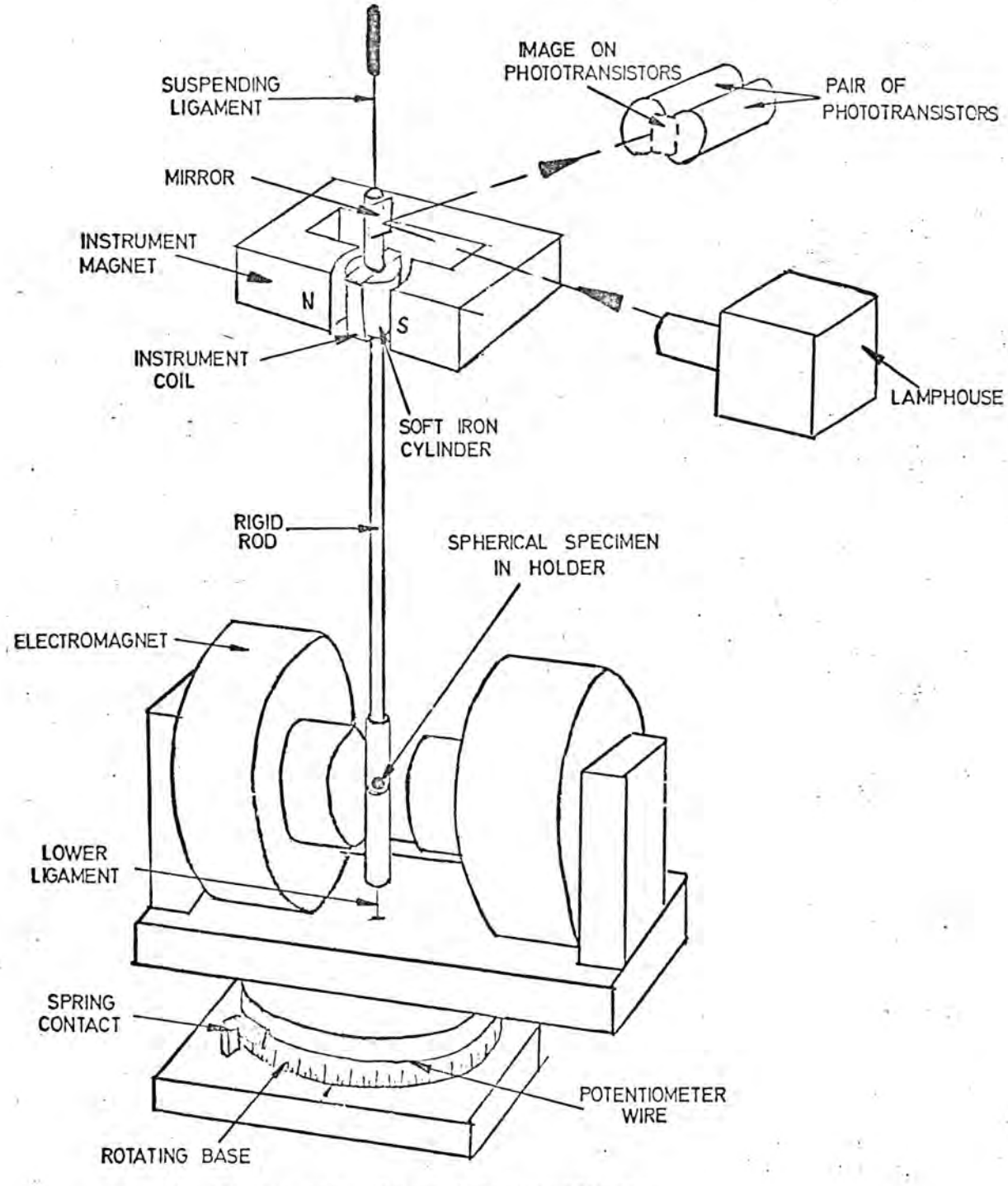

FIG.(7·1) GENERAL VIEW OF TORQUE MAGNETOMETER
(Outer Sheath and Dewars Not Shown)

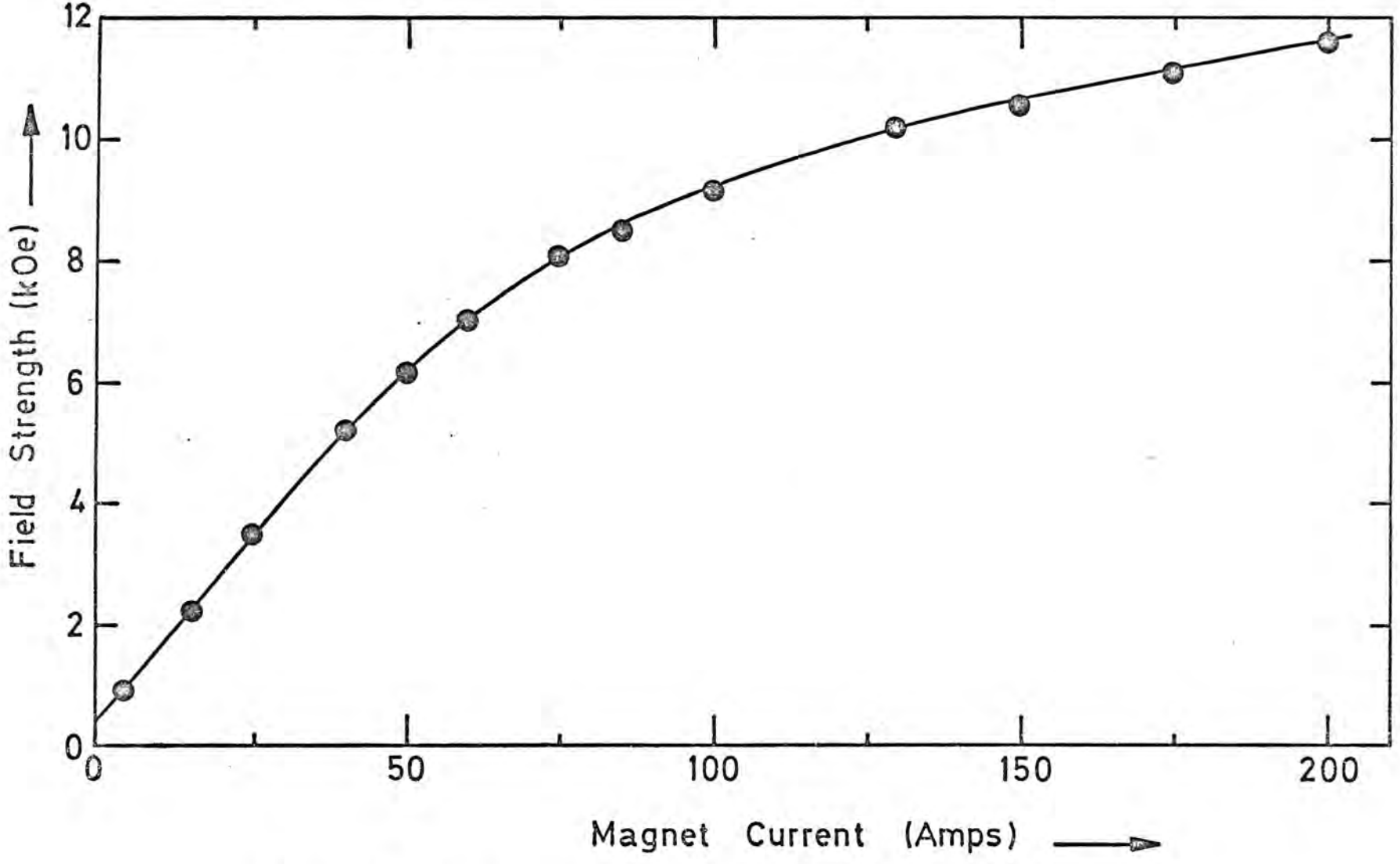

FIG. (7·2) Magnet Calibration Curve.

The torque magnetometer used for the present work was constructed originally by Roe (1961) and several modifications have been made by Bly (1967) and Welford (1974). For the present work some extra modifications were made especially for using liquid helium, the original design being suitable only for measurements down to 77K. Fig. (7.1) shows a general view of the torque magnetometer.

7.1.1 The Electromagnet

This was first constructed by Roe (1961) and is of conventional design. The coils are carried on the pole pieces and are water cooled, the cooling water flowing in a closed system containing a pump and heat exchanger. The maximum field obtainable with a gap of 5.07 centimetres and a power dissipation of 40 kW, 11.6 kOe. Magnetic field was measured using a fluxmeter and a calibration curve of current versus field was plotted. Fig. (7.2). For most of the measurements a current of 80 amps. was enough to give a sufficient field, 8 kOe, to saturate the specimens used. The field was uniform to within $\pm$ 1/2% over a volume of 3 cm^3 at the centre of the pole gap. The electromagnet could run on a railway track and could rotate on a calibrated base, rotation being limited to 200° because of the current cables and cooling water hoses attached to it. An accuracy about $\pm$ 1/2° in rotation could be achieved. Fig. (7.2) shows the calibration of the magnet after a slight increase in the separation of the pole pieces to allow for a double dewar system.

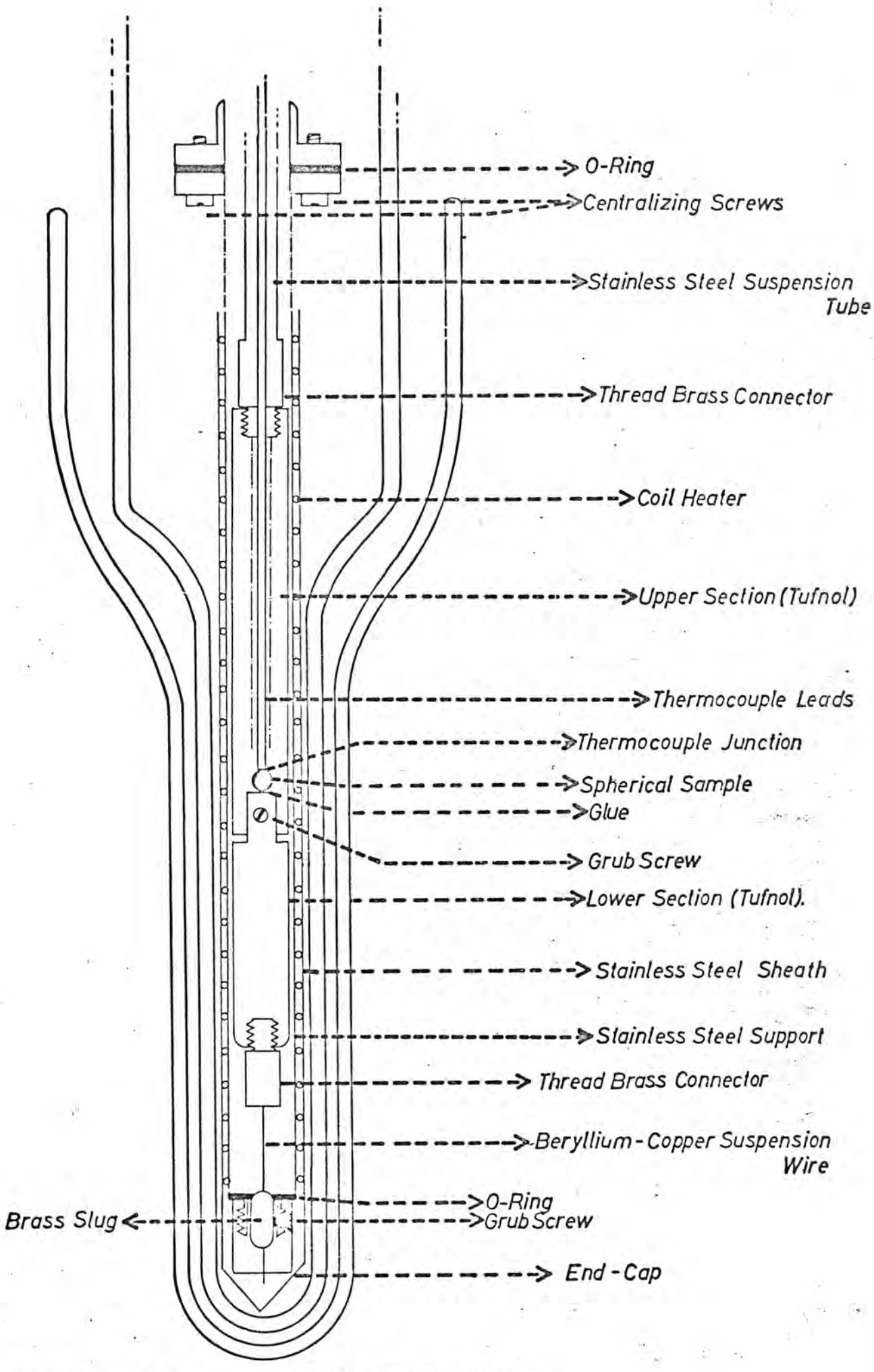

CROSS SECTION OF THE SPECIMEN HOLDER

FIG (7 · 3)

7.1.2 Liquid Helium Modification

As mentioned previously the original apparatus was not suitable for liquid He measurements and the following modifications were found to be necessary

1 - a slight increase in the separation of the pole pieces in order to locate the new nitrogen and helium dewars between them.

2 - the construction of an adapter through which passed a demountable liquid helium syphon to allow the attachment of the new helium dewar to the old part of the apparatus.

3 - the building of a new vacuum system in order to flush the system with helium gas before commencing measurements.

4 - the addition of a new helium gas pipe to get rid of the gas boiling from liquid helium during operation.

7.1.3 Specimen Holder

The specimen holder forms the lower part of the rigid rod in Fig. (7.1) and more details of it can be seen in Fig. (7.3). The material used for the specimen holder is 3/8" diameter tufnol rod. The upper portion is screwed at the top to a stainless steel tube with outer diameter 0.125" and 63 cm of length. The lower part of the specimen holder can be inserted into the upper part and a brass grub screw passing through in a groove cut in the bottom side of the upper section can hold it quite firmly. The lower suspension ligament is soldered into a brass fitting at the lower end of the specimen holder and its other end soldered into a brass slug which can be attached to a vacuum jacket tube. The thermo-couple leads pass down inside the specimen holder and the junction

has a thermal contact with the sample which is cemented to the top of the lower part of the sample holder.

It is worthwhile to mention that all these parts including the stainless steel tube have been covered by a stainless steel vacuum jacket tube on which a heater wire is wound and could be used to give different temperatures by passing a current through it. The lower end of this tube to which the brass slug is attached is covered by an end-cap with an o-ring seal so that the tube may be evacuated and the top part of it can be fastened by 3 screws to a rigid brass flange with o-ring seal through which the stainless steel suspension tube passes. These 3 screws have a very important role for centralizing the specimen between the electromagnet poles using a special gauge for this purpose.

7.1.4 Calibration of the Magnetometer

Even though both electromagnet and magnetometer were carefully calibrated by Welford (1974), it was found necessary to recalibrate them again because of two reasons:

1 - due to the change of the separation of the pole pieces of electromagnet which was made to allow the insertion of a new dewar system capable of reaching a temperature of 4.2 K.

2 - because of changing the optical system and the positioning of the counter-torque coil. The recalibration was done by using a flux meter and a current carrying coil of known dimensions. A coil of N = 12 turns of .11 mm diameter copper wire was wound on a cylindrical Tufnol former of cross sectional area A and then was attached to a holder by 2 screws. The coil holder then was attached to the upper part of the sample holder in place of the lower section. The size of

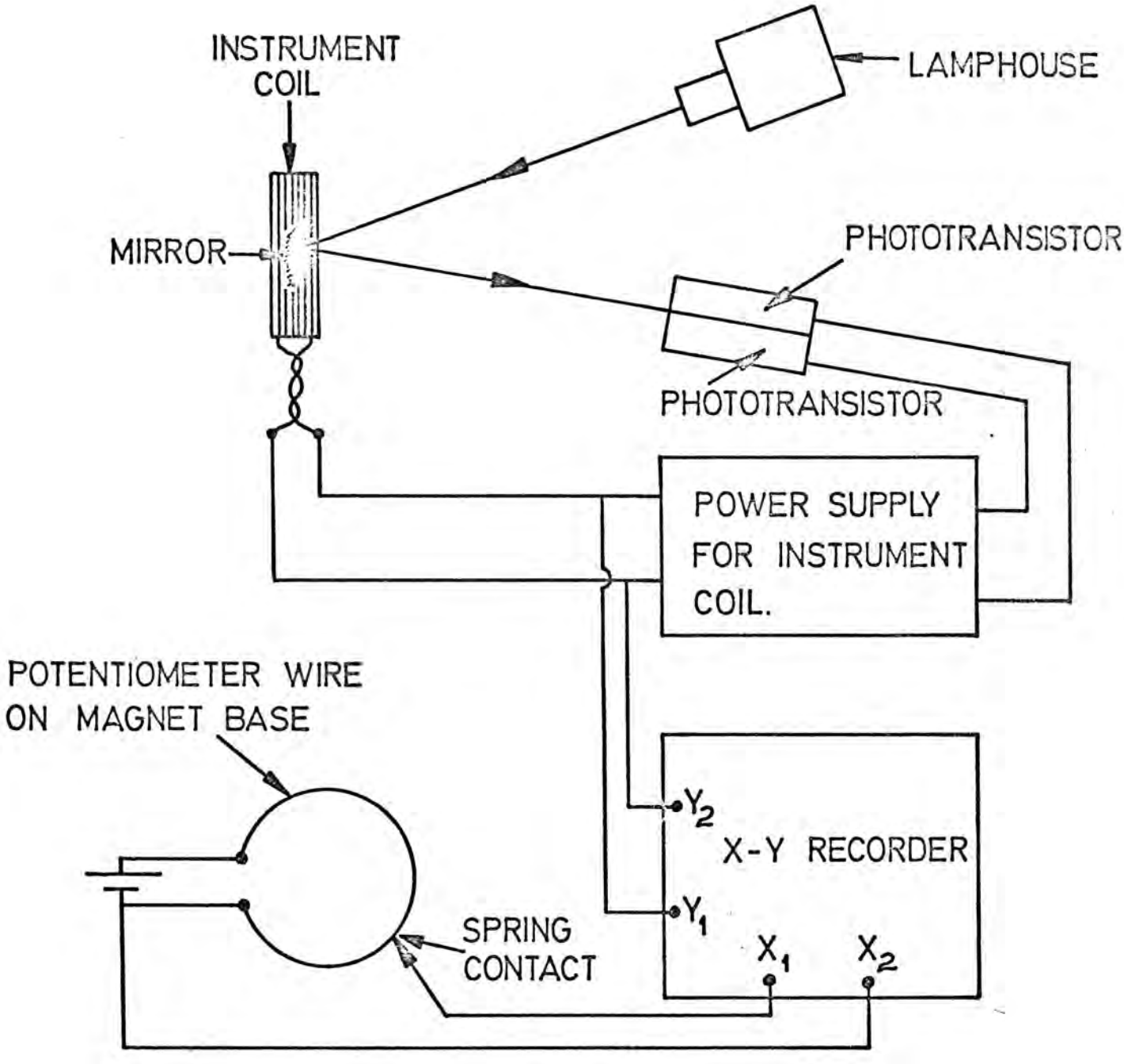

FIG. (7·4)

SIMPLE SERVO SYSTEM FOR AUTOMATIC BALANCING AND TORQUE RECORDING.

the coil diameter and coil holder was so chosen that the coil could hang as near the centre of the electromagnet as possible. The suspended system was made to hang vertically by attaching a suitable weight at the lower end.

Currents I between 0.4 and 0.7 amps were passed through the coil and were measured using a standard resistance and a digital voltmeter. Torque curves were then plotted on the x - y recorder for 2 different currents through the electromagnet. The corresponding fields were at the same time measured by a flux meter.

The amplitude of the torque curve V obtained with a field B was measured on the recorder trace. Thus BAIN = kV and the constant k could be evaluated. The mean value from 15 determinations was $k = 7.32 \pm 0.02$ erg/mvolt .
Fig. (7.4) shows a simple servo system for automatic balancing and torque recording.

7.2 Choice of Method for Restivity Measurements.

As it was necessary to have absolute values of electrical resistivity for definite temperatures a D-C method was employed. A constant current of about .5 amps from a power supply was passed through a one ohm standard resistance and the specimen. The voltages across the potential leads on the specimen and the standard resistance were measured by using a digital voltmeter. For eliminating the effects of polarity a reversing switch was used. As in some experiments it was convenient to use more than one sample and also at the same time it was necessary to measure a thermocouple voltage, a rotary change over switch was employed. It was also necessary to heat up

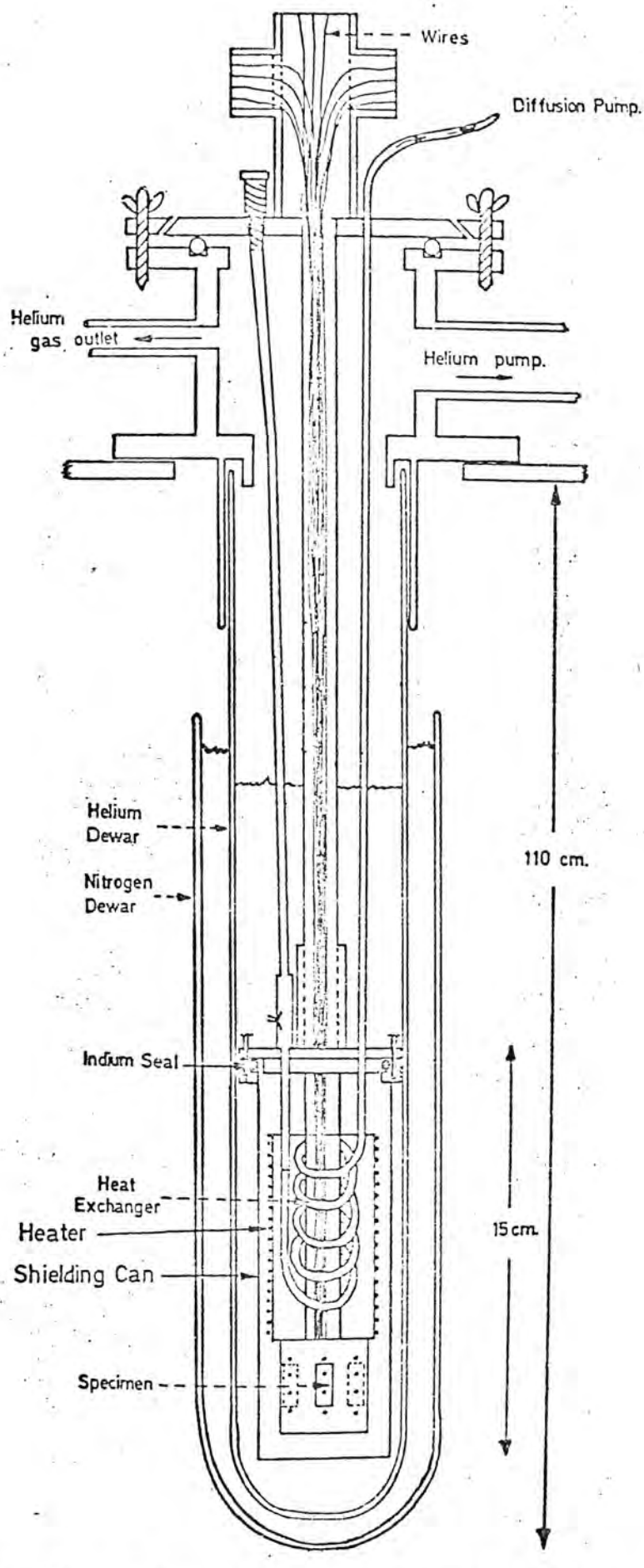

FIG. (7·5) General view of Cryostat for resistivity measurements (after Alltunbas)

the crystal to 300°K at a rate of less than 1.25°K per minute to ensure good thermal equilibrium.

7.2.1 Apparatus for Resistivity Measurements

Fig. (7.5) shows cryostat which was used for resistivity measurements and was made originally by Altunbas (1975). In general it works for resistivity measurements from 1.3°K to 300°K. It is possible to accomodate a maximum of four samples on a copper heat sink to ensure uniform temperature. Each sample has a separate pair of potential leads, whereas by connecting the specimens in series a single pair of current leads can be used. For the present measurements the shielding can was removed so that the specimens were initially immersed in liquid helium. As this evaporated and the level fell the specimen temperature began to rise above 4.2°K and readings were taken at intervals of temperature up to 77°K. To achieve temperature in the range 77-300°K a small heater wound on the outside of the heat exchanger can was used. By suitable current through this any temperature in the range could be obtained. The temperature of the samples was measured using a calibrated Cu - (AuFe) thermocouple for the range of 4.2° - 77° and a calibrated Cu - constantan thermocouple for the range of 77 - 300°K. These were attached to the copper block on which the specimens were mounted.

7.3 Magnetization Measurements

A variety of techniques has been developed and used to measure the magnetization of a specimen, see Bates (1963). Amongst these the vibrating sample magnetometer and Faraday balance magnetometer are very commonly used.

7.3.1 Vibrating Sample Magnetometer

In this method a sample of magnetic material is vibrated in a uniform applied field using a loudspeaker movement. The vibration creates an oscillating magnetic field which induces voltages in a pair of stationary detection coils. Carried on the same vibrating system, but lying outside the magnetic field, a small permanent magnet or alternatively a small coil carrying a current also vibrates inside a similar pair of detection coils. Various arrangements are possible in which the voltages from the two pairs of detection coils may be balanced against each other and the magnetic moment of the sample related to that of the permanent magnet or current carrying coil. By varying the magnetic field it is possible to measure the magnetic moment of the sample as a function of magnetizing field and with, suitable arrangements, temperature. It is also possible to measure magnetization $\underline{M}$ along any crystallographic direction by attaching the sample so as to vibrate in a desired direction. The accuracy of this method can be very high and depends very much on accurate calibration of the apparatus. Foner (1956) measured the magnetic moment of a nickel crystal sphere of 1.2 mm diameter with an accuracy of 0.5%. Danan et al (1968) and Kaul (1969) by using modifications of the Foner-type of vibrating

sample magnetometer have measured the magnetization of Ni with an accuracy of 0.1%. In a similar fashion it is possible to make a magnetometer in which the sample is fixed and the coil will vibrate. This was developed by Smith (1956) and is called the vibrating coil magnetometer. The difficulties connected with this method are that it needs an extremely uniform magnetic field and to allow for departures from this is very difficult as the field nonuniformities are functions of the applied fields.

7.3.2 Faraday Balance Magnetometer.

In this method the magnetization is measured by measuring the magnetic force acting on a specimen when placed in a non-uniform magnetic field. This is not so accurate as the previous method and especially for an anisotropic sample the amount of error may increase, Wolf (1957). However in the course of the present work it was found necessary to measure the value of $\frac{M(T)}{M(0)}$ of some NiV single crystals to be able to compare the variation with temperature of this ratio with corresponding changes in the first anisotropy constant . As the construction of a Faraday balance was in progress in the laboratory it was decided, even though not so accurate as a vibrating sample magnetometer, to use this system for measuring magnetization. The operation and detail of the construction will be discussed in the next sections.

7.3.3 Construction

This was designed and constructed in the laboratory for measurement of the magnetization of samples of some ferromagnetic

powders. The work was to be carried out at room temperature and only changes in saturation and remanence were required. It was decided that it would be worthwhile to use this to measure the variation of magnetization with temperature for the NiV alloys of high vanadium concentration. Reliable measurements for pure Ni were already available from the work of Kaul (1969).

7.3.4 Principle of Operation

A Faraday balance magnetometer uses a balance to measure the amount of force which will be exerted on a sample when it is located in a non-uniform field. This force is proportional to field gradient $\frac{dH}{dZ}$, in which Z is the vertical direction.

$$F_Z = R_Z \frac{dH}{dZ} \qquad (7.1)$$

R_Z is called the dipole moment in the Z - direction, Zijlstra (1967), and is given by:

$$R_Z = m \chi H_Z \qquad (7.2)$$

where m is the mass of the sample and χ is the susceptibility per unit mass, thus equation (7.1) can be written as follows:

$$F_Z = m \chi H_Z \frac{dH_Z}{dZ} \qquad (7.3)$$

In the Faraday balance constructed in the laboratory the weight of the sample is counterbalanced and an electronic balance then measures the magnetic force on the sample. This is proportional to the current I flowing in a bridge circuit associated with the balance. i.e. $F_Z = \frac{I}{A}$ where A is a constant for the system. Then from equation (7.3),

$$\chi = -\frac{I}{Am H_Z} \left(\frac{dH_Z}{dZ} \right)^{-1} \qquad (7.4)$$

If the sample lies at a fixed point in a constant field the gradient will be constant and so equation (7.4) can be written as follows:

$$\chi = \frac{I}{mH_Z} C \qquad (7.5)$$

in which

$$C = \left(A \frac{dH_Z}{dZ} \right)^{-1} \qquad (7.6)$$

Using a suitable sample of known magnetic characteristics it is possible to calculate the constant C. As the magnetization of a sample is equal to χH_Z so equation (7.4) will give the following for M

$$M = \frac{I}{Am} \left(\frac{dH_Z}{dZ} \right)^{-1} = \frac{I}{m} C \qquad (7.7)$$

If the field H_Z is increased it should be possible to measure M as a function of H_Z, but unfortunately (dH_Z/dZ) will also vary and allowance must be made for this. In practice it is found better to use an extra constant gradient coil giving an additional gradient $\frac{dH_Z}{dZ}$ and equation (7.7) may then be written,

$$M = \frac{I'}{mA} \left(\frac{dH_Z}{dZ} + \frac{dH_Z'}{dZ} \right)^{-1} \qquad (7.8)$$

in which I and I' are the balance currents without and with current flowing in the extra gradient coil respectively. It is obvious that by eliminating $\left(\frac{dH_Z}{dZ} \right)$ from equations (7.8) and (7.7) the value of M is given by,

$$M = \frac{I - I'}{m} \left(A \frac{dH_Z'}{dZ} \right)^{-1} = \frac{I - I'}{m} (C) \qquad (7.9)$$

Again by using a suitable sample for which the value of M is known it is possible to find the constant $C = (A \frac{dHz}{dZ})^{-1}$.

7.4 Description of the Apparatus

The apparatus used in general has been made in four main parts.

7.4.1 Solenoid

The magnet used for producing the necessary field was an oil cooled pancake wound solenoid. By passing a constant current from a Brentford Stabilized DC supply through the magnet it was possible to produce a maximum field of 9 kOe. The magnet was mounted on a metal framework and vertical movement was obtained by using an oil-jacked system to any desired height. The magnetic characteristic of the solenoid had been extensively investigated by Mundell (1975) and his calibration curves were used for the present work.

7.4.2 Balance

An electronic microforce balance, Mark 2CT5 from C.I. Electronics Ltd. was used with a measuring head which could be sealed inside a glass envelope in case evacuation was needed. The balance arm, made of aluminium and berylium copper, carries a shutter which lies between a lamp and a pair of silicon photoresistors. A movement coil, free to rotate in the field of a permanent magnet when a current passes through its windings, is fixed exactly at the centre of the arm. This forms a simple servo system which enables the balance arm to be retained at a fixed position. Any movement causes an unbalance in the output currents of the photo resistors, the difference in which is fed back to the movement coil and the balance rotated. The movement produced by this balancing current is directly proportional to the current so that changes in load on the arm are measured as changes in movement coil current.

To facilitate the loading of the balance it was found reasonable to locate the head on a trolley which could move it in a horizontal direction. The pan in which weights should be located to counterbalance the specimen weight is shown in fig (7.6) and the sample could be loaded inside a small quartz bucket. This could then be hung, using a glass fibre or other non-magnetic suspension in a non-magnetic specimen tube made of a copper-nickel alloy. This tube could be fixed to the head of the balance through a vacuum tight seal. The samples used were in the shape of spheres, described in chapter 5, and this was then convenient for the measurements as they could freely rotate inside the bucket until an easy axis [111] of the crystal became aligned with the magnetic field. In this case the applied magnetic field required to saturate the sample was in the order of 4.5 kOe. This was somewhat higher than that expected from demagnetization considerations, the demagnetizing factor of the sphere being taken as $\frac{4}{3}\pi$.

7.4.3 Electrical control cabinet

This is designed to control the change in the current due to unequal illumination on the photoresistors and is connected to the movement coil through a multi-way cable. The complete circuit in this unit is used to amplify the current of the photocells to give zero adjustment and also to provide range switching for different weights. In addition to these there is provision for an output for use with an x-y recorder or to provide feed-back in automatic control applications. Usually this output is connected via a matching circuit to an x-y recorder. This is necessary because the DC output from the balance has some noise due to pan swing, vibration, air currents etc. and

these can be reduced by using the universal matching circuit. This system has three controls.

1) Ratio, to give a suitable selected output to the recorder through a 5000 ohm resistance and a potential divider.

2) Set Gain, to provide a calibration facility for the recorder.

3) Damping, to reduce the noise level measured by the recorder by a variable damping.

The x-y recorder could be used in two ways. In each case the y-deflection was fed from the output of the electrical control cabinet as described above. The x-deflection could either be controlled by a voltage derived from the solenoid current, giving $x \propto H$, or by the e.m.f. from a thermocouple placed close to the sample giving $x = f(T)$. The first arrangement is most suitable for isothermal experiments and the latter for measurements at constant field.

7.4.4 Cryostat

As already mentioned the main reason for using this apparatus was to obtain the variation of $\frac{M(T)}{M(0)}$ with temperature, from 4.2K to room temperature. It was thus necessary to design a cryostat system for this purpose. As was mentioned in section (7.3.4) for M measurements it is necessary to have an extra gradient field and this was obtained by winding a suitable coil on the He - dewar using a mixed acetone - durofix adhesive for rigidity of the coil. The coil was fed from a DC stabilized 24V supply. In addition a vacuum system to provide a good vacuum before flashing with the gas was used. The gas from the liquid He boiling could flow away through an exhaust pipe line attached to the system. The syphon system was a commercial demountable

FIG.(7·6) Schematic arrangement of Faraday Balance Magnetometer Details of vacuum, gas handling and electronic circuit not shown.

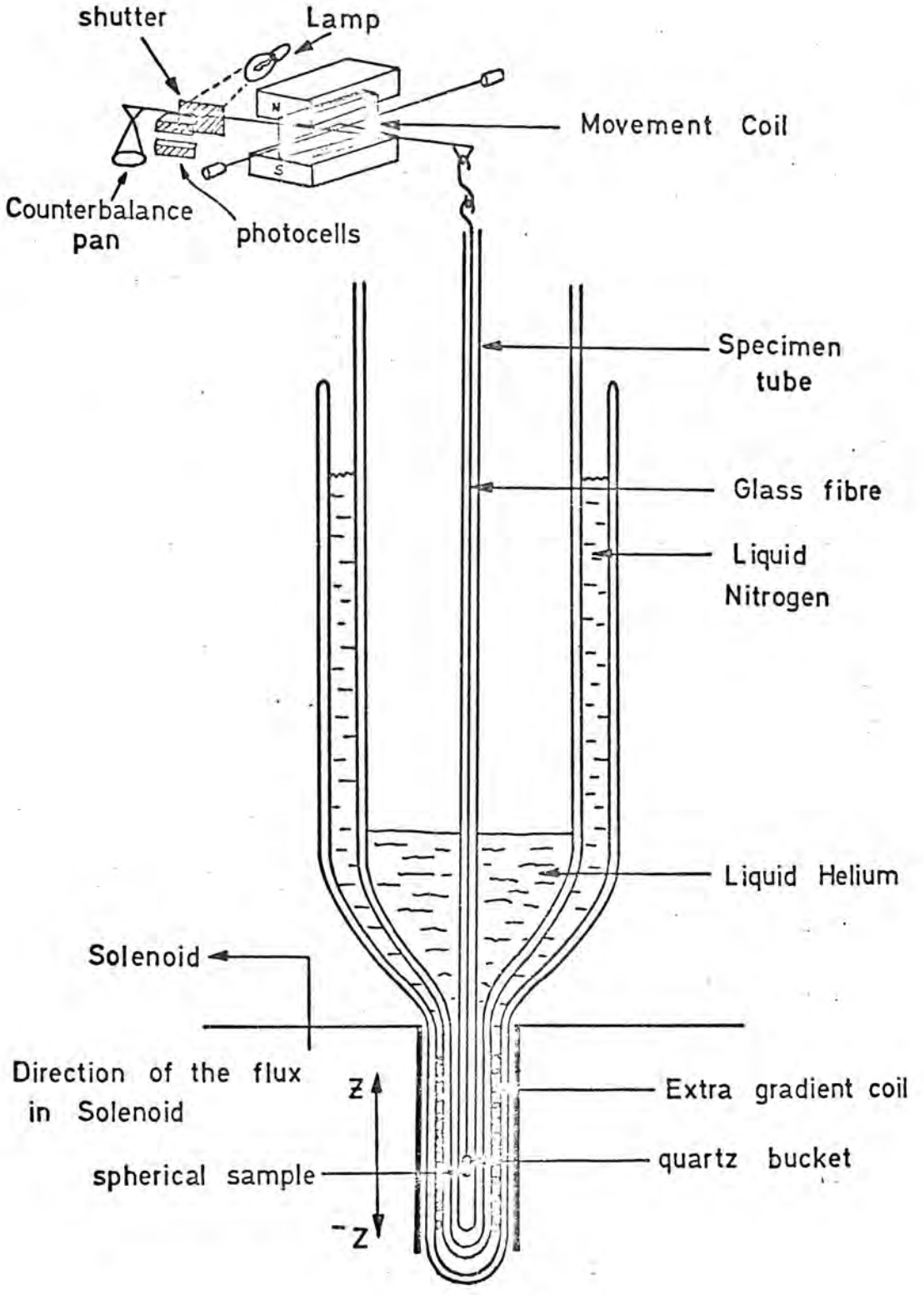

unit supplied by Thor Cryogenics. The temperature was measured using a copper-constantan thermocouple attached to the bottom of the specimen tube which was located in the liquid He dewar Fig. (7.6).

CHAPTER 8

Analysis of the results

In this chapter the analysis of torque, resistivity and magnetization measurements will be discussed.

8.1 Analysis of Torque Measurements:

8.1.1 The Effect of Sample Misorientation

As already mentioned (chapter 6), all the measurements were performed in a (001) plane, in which only the K_1 and K_3 components of magnetocrystalline anisotropy energy were important. A typical torque curve in this plane has been shown in Fig.(8.1), for a sample which had been aligned by X-ray Laue photographs so that the axis of rotation was within $\pm \frac{1}{2}$ degree of a $\langle 100 \rangle$ direction. Errors of orientation greater than this were found to produce noticeable asymmetry in the torques. The influence of the K_3 component was too small to be observed by simple inspectation of the curves. Franse et al (1968) have calculated the influence of angular deviations on the torque curves in all three crystallographic directions for cubic materials. They showed that, for the (001) plane, if the angle between the normal to the (001) plane and the rotation axis of the crystal in the magnetic field is less than 2° the asymmetry produced was within their experimental accuracy. Unfortunately this was not true in our case and a deviation of even 1.5° could give a noticeable difference in the form of the curves. For this reason great care was taken in specimen alignment rather than attempting to apply corrections as

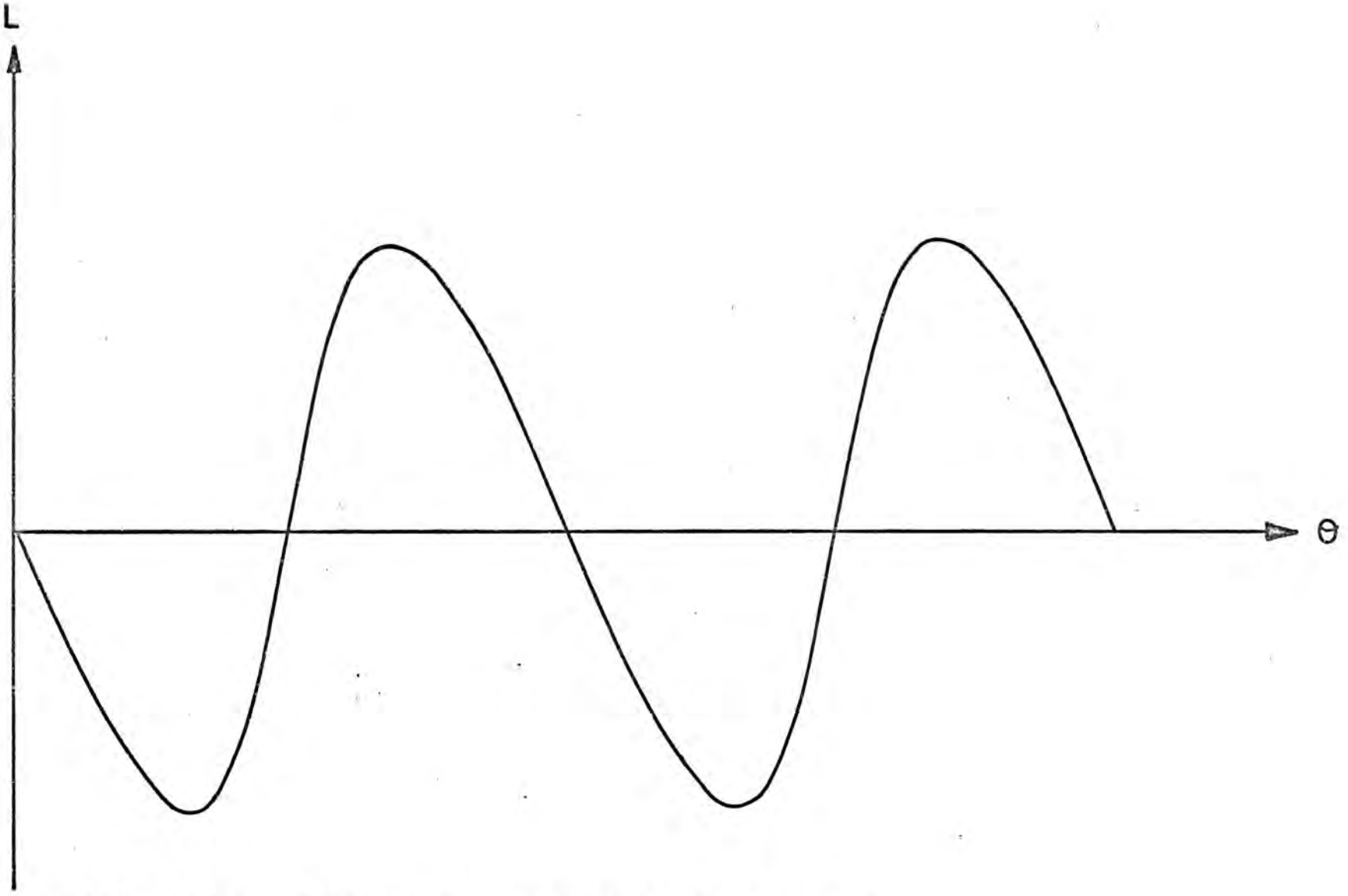

FIG. (8·1) Shows a typical torque curve in (001) plane at 77°K (5N purity Ni)

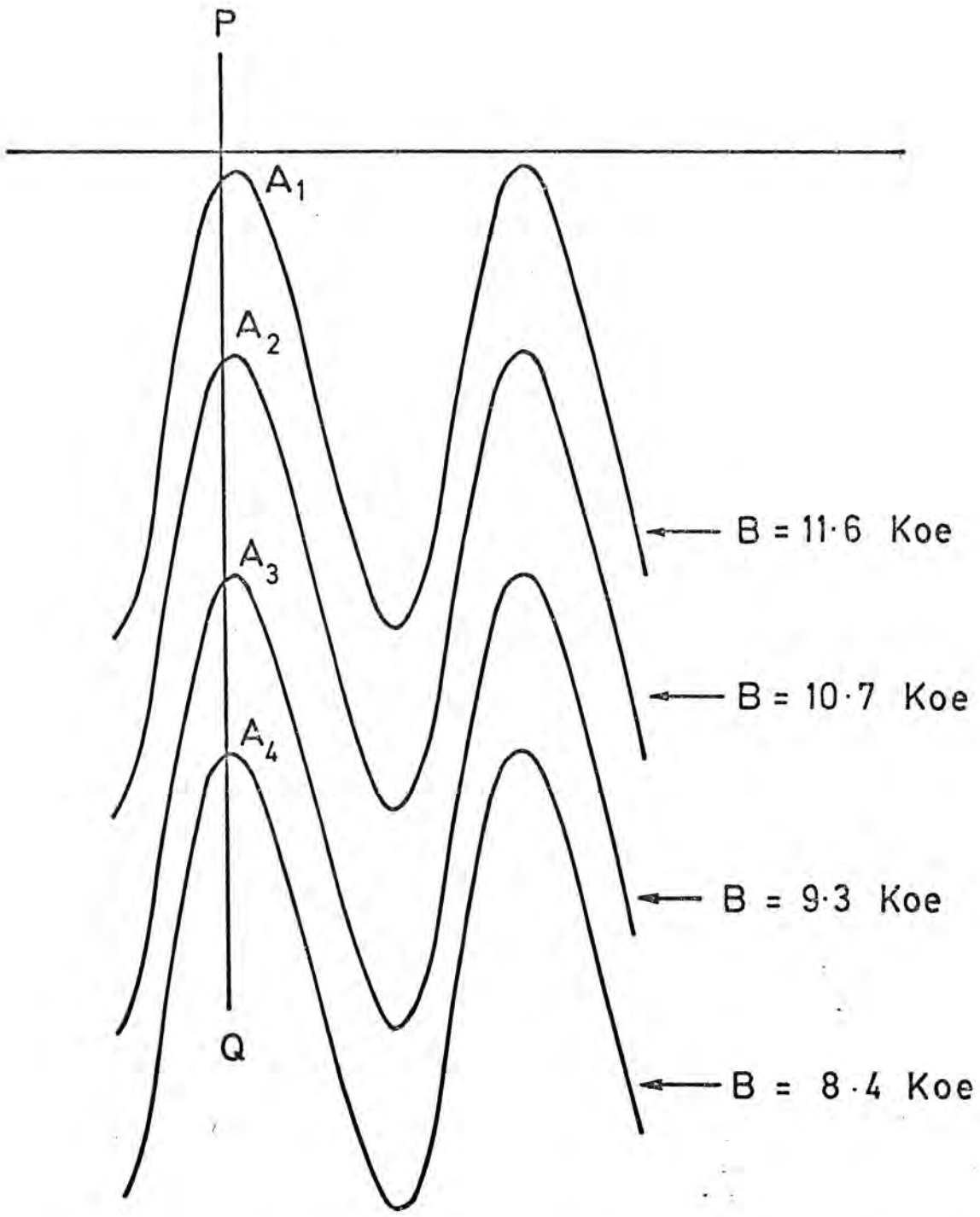

FIG.(8·2) Shows the effect of shear at different fields at 4·2K. This can be seen from the distances of A_1, A_2, A_3, and A_4 from vertical line PQ (NiV containing 5·14 at % V)

suggested by Franse et al.

8.1.2 Shearing Effect

The field at which torque curves were recorded was not enough to align the magnetization vector M in the crystal parallel to the field. This is due to the applied field being inadequate to overcome the torque on M due to the variation of anisotropy energy with angle except when H is close to an easy direction. This can be easily seen from a comparison of curves at high and low fields for a typical sample Fig. (8.2). The shearing is much more pronounced for the lower field curve. Similarly, curves for a given field and sample show more shearing at low temperatures where the magnocrystalline anisotropy energy is greater. It is obvious that angular deviation between external field and the magnetization has a zero value when the field is in the easy direction (torque is zero) and has a maximum value in the hard direction (torque is maximum). A detailed explanation and several methods of shearing effect correction has been given by Welford (1974).

8.1.3 Correction for shear

It was found convenient to use a graticule for correction. For this purpose torque curves were plotted on an x-y recorder in such a way that a rotation of 180° corresponded to 18 cm. along the x - deflection. This permitted the use of an ordinary graticule in which one degree of rotation corresponded to one milimeter of the graticule. The inclination of the graticule was found such that the points on one cycle of the curve, M and N, had a two fold symmetry with respect to the graticule line PQ which passes exactly through the highest point of the maximum

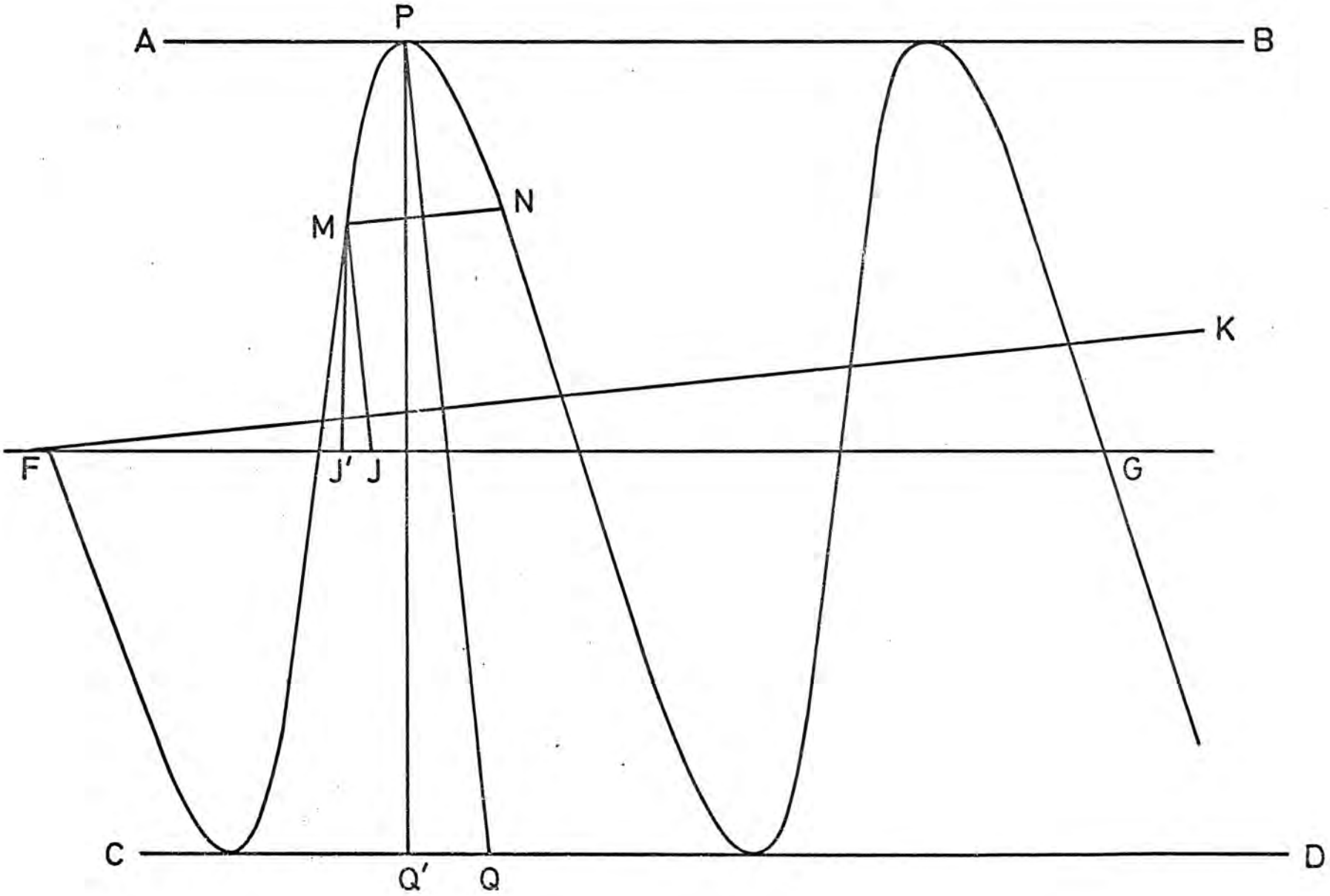

FIG. (8·3) Reading With An Inclined Graticule.

or the lowest point of the minimum of the cycle (Fig.8.3). Then the reading of the ordinate of each point on the curve was the distance MJ between that point and the line FG passing through the curve. The corresponding angle was read at point J. The line FG should firstly be parallel to the lines AB and CD joining maxima and minima of the curve and secondly should have equal distances from them. However since the angle of shear was never greater than about 6° it was found to be more convenient to measure MJ than MJ', the error so introduced being less than 0.6% and well within the overall accuracy of measurement. This procedure was adopted whenever a full Fourier analysis required a series of torque and angle values. In all other cases the distance PQ' was measured on the torque curve and used in the calculation of K_1 or $(K_1 + \frac{K_3}{4})$. These ordinates and their corresponding angles were taken as corrected readings for the construction of an unsheared curve. They formed the data that was supplied to the computer.

8.1.4 Calculation of the $(K_1 + \frac{K_3}{4})$ coefficient

As already mentioned the torque in the (001) plane can be written as follows

$$L_{(001)} = -\left(\frac{K_1}{2} + \frac{K_3}{8}\right) \sin 4\theta + \frac{K_3}{16} \sin 8\theta \qquad (8.1)$$

The effect of $\frac{K_3}{16}$ is so small that in a torque curve such as Fig. (8.1) it would hardly be observed. It is obvious that at $\theta = 22.5^\circ$ the effect of the $\frac{K_3}{16}$ component is zero and (8.1) will reduce to

$$L_{(001)} = -\left(\frac{K_1}{2} + \frac{K_3}{8}\right) \qquad (8.2)$$

This infact is the amplitude of the torque curves in the (001) plane. To measure this quantity it was found more convenient to measure the vertical distance between two lines joining maxima and minima of these curves; this distance of course is proportional to the value of $(K_1 + \frac{K_3}{4})$. As mentioned in the previous section this value of $(K_1 + \frac{K_3}{4})$ is exactly corrected for shear and so this procedure was followed for most of the measurements. However, for the pure Ni and 0.98% NiV alloy a few curves at low temperatures were subjected to a full Fourier analysis involving 32 points in 180°, to obtain values of K_3 which would be used with the above results for the calculation of K_1.

8.1.5 Calculation of K_3 coefficient.

The effect of $\frac{K_3}{16}$ in equation (8.1) is too small to be measured in a simple way. Aubert (1968) by using extrapolation methods found a negative value for K_3, which had never been measured before for nickel. Franse (1969) by using extrapolation methods and a cubic harmonic description of torque curves found the same sign for K_3. Contrary to these results Tokunag et al (1972) found a positive value of K_3, using Fourier analysis. In the present work a least squares regression programme, described in Appendix (1), was used and the values of K_3 found to be negative. The errors from these determinations were somewhat greater than those of Franse's results. This may be due to the fact that Franse used a field of 18.1 kOe compared with 11 kOe in the present work. This would give curves which required a smaller shearing correction and have less error in

making this. Hofmann et al (1970) used only 6.78 kOe and did not attempt to estimate K_3, but used Franse's values for pure nickel. Values of K_3's for some temperatures have been given in table (8.1) in which Franse's values are also shown for comparison.

As can be seen from table (8.1) the errors on K_3 in the case of 5N and 4N materials are quite large so it was decided to combine these two results with Franse's results using the following statistical procedure to decrease the errors.

1) Values of K_3 obtained on 5N material by Franse and on both 5N and 4N material in the present investigation were plotted against temperature, the confidence intervals of each measurement being indicated.

2) A smooth curve was drawn by eye to pass through all the confidence intervals. It was noticed that the magnitude of the error also appeared to follow a smooth curve falling as the temperature rose.

3) The observations were split into four groups and a pooled error estimate (R.M.S.) applicable at the mean temperature of the group was calculated.

4) A weighted mean square deviation from the drawn curve was calculated using the pooled standard deviation estimates as weights.

5) A new error estimate could then be made for each of the group mean values, equal to the group weight multiplied by the square root of the weighted mean square deviation for all eleven

FIG. (8·4) Temperature Dependence of K_3 Before Statistical Treatment.

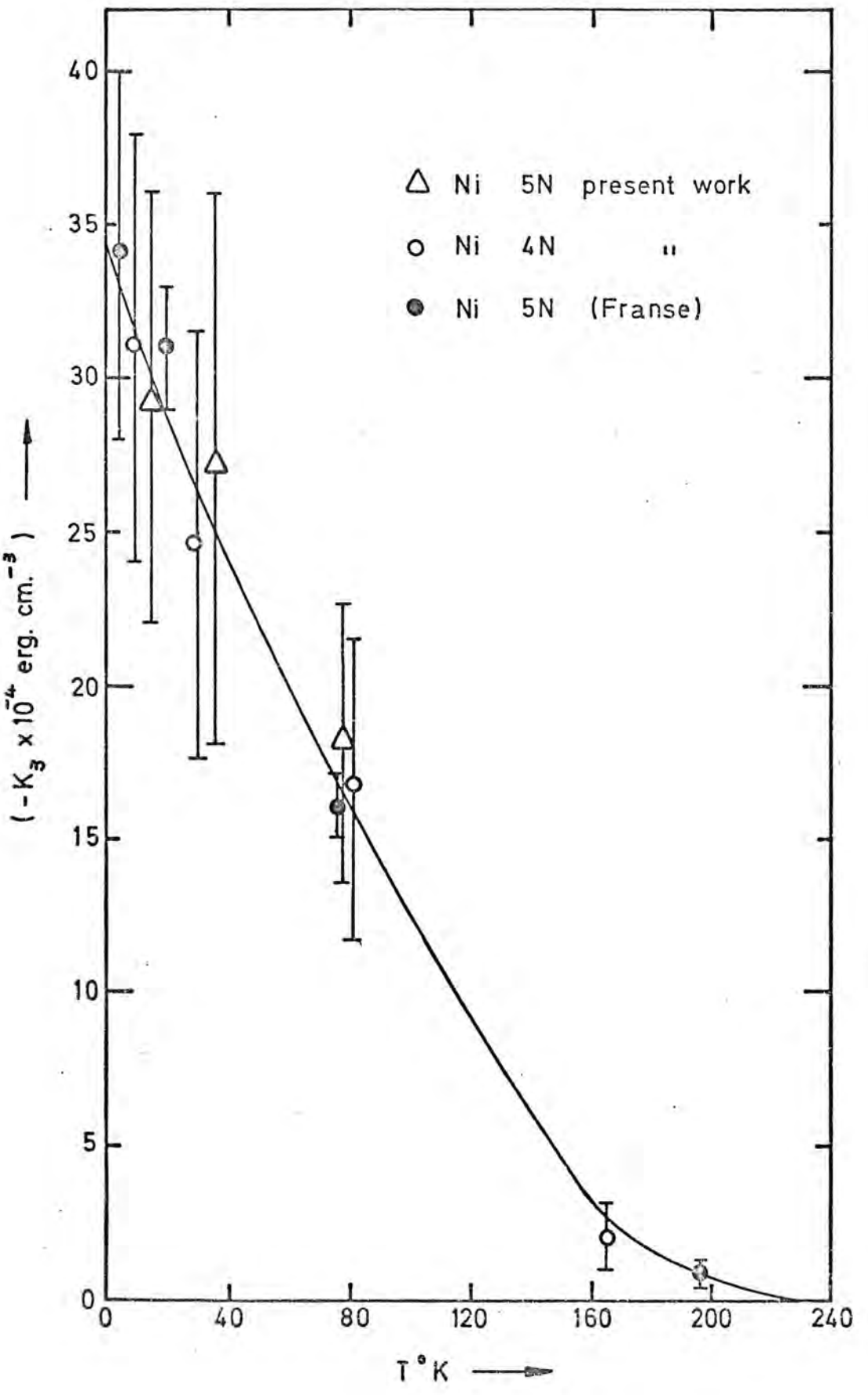

FIG.(8·5) Temperature Dependence of K_3 of Pure Ni.

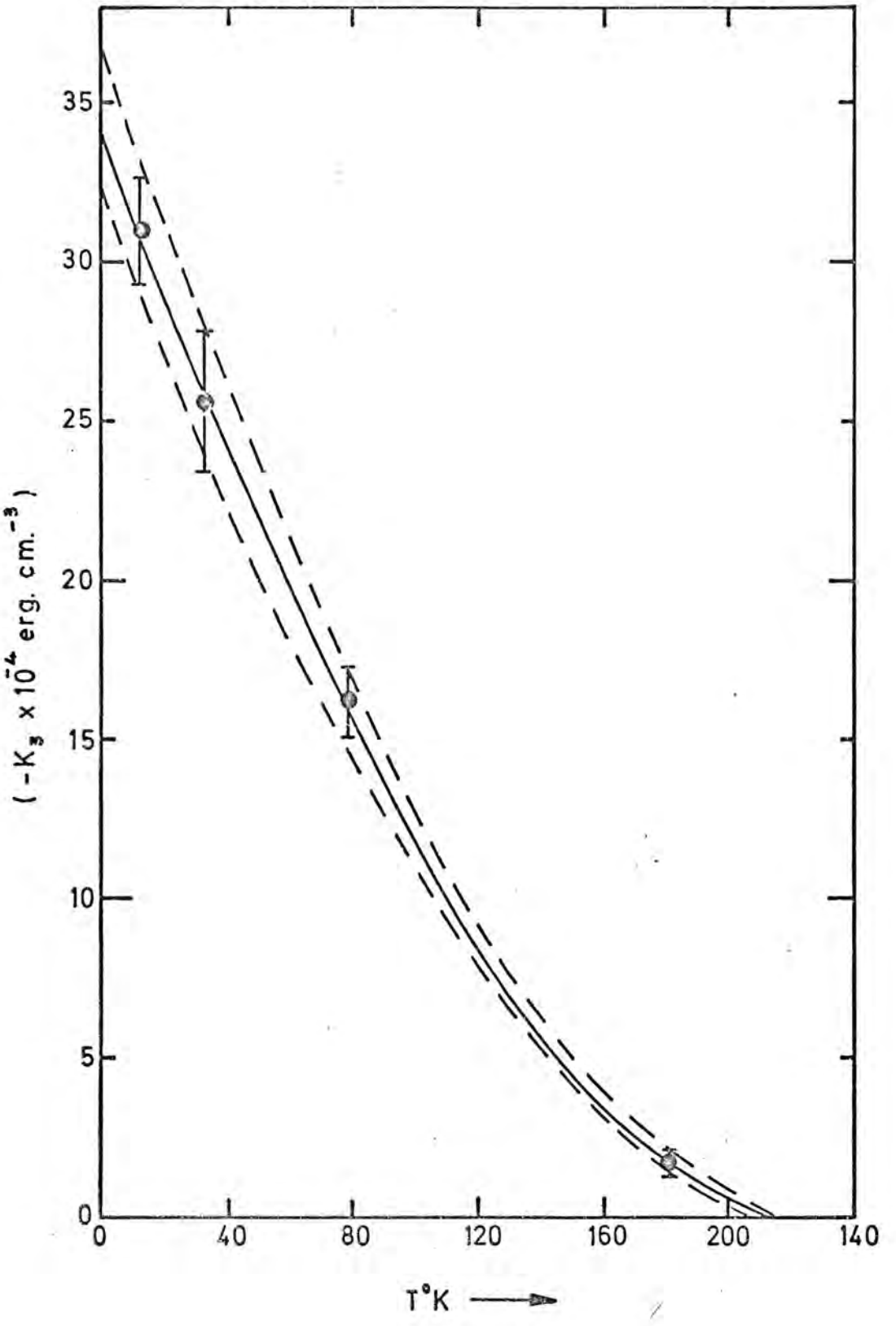

points.

6) Finally when the revised confidence intervals were erected at the group mean T values, smooth curves were drawn through the upper points and lower points respectively to give a confidence level for the curve. This procedure is shown in table (8.1) and the initial and final results are displayed in fig.(8.4) and (8.5) respectively.

Table (8.1) The Procedure of Statistical Treatment.

Group	T_i °K	$(-K_3 \pm \sigma_i) \times 10^{-4}$ (erg/cm^{-3})	$\bar{\sigma}_i$ for each group	$\rho_i = \frac{\bar{\sigma}_i}{\sigma_i(\text{LASW})}$	$-K_3 \times 10^{-4}$ estimate erg/cm^{-3}	NO	Author
1	4.2	34.0 ± 6.0			33	1	FRANSE
	10	30.9 ± 7.4			31.5	2	present work
	16	29.2 ± 7.3	6.071	6.784	30	3	"
	20	31.0 ± 2.0			29	4	FRANSE
2	37	27.5 ± 9.6	8.541	9.543	25	5	present work
	29	24.5 ± 7.3			26.5	6	"
3	77	16.4 ± 1.0			17	7	FRANSE
	81	16.7 ± 5.3	4.034	4.507	16	8	present work
	77	19.0 ± 4.5			17	9	"
4	195	1.0 ± 2.0	.895	1.000	1	10	FRANSE
	164	1.8 ± 1.3			2.2	11	present work.

FIG.(8·6) Temperature Dependence of K_3 of Ni-V Containing 0·98 at % V .

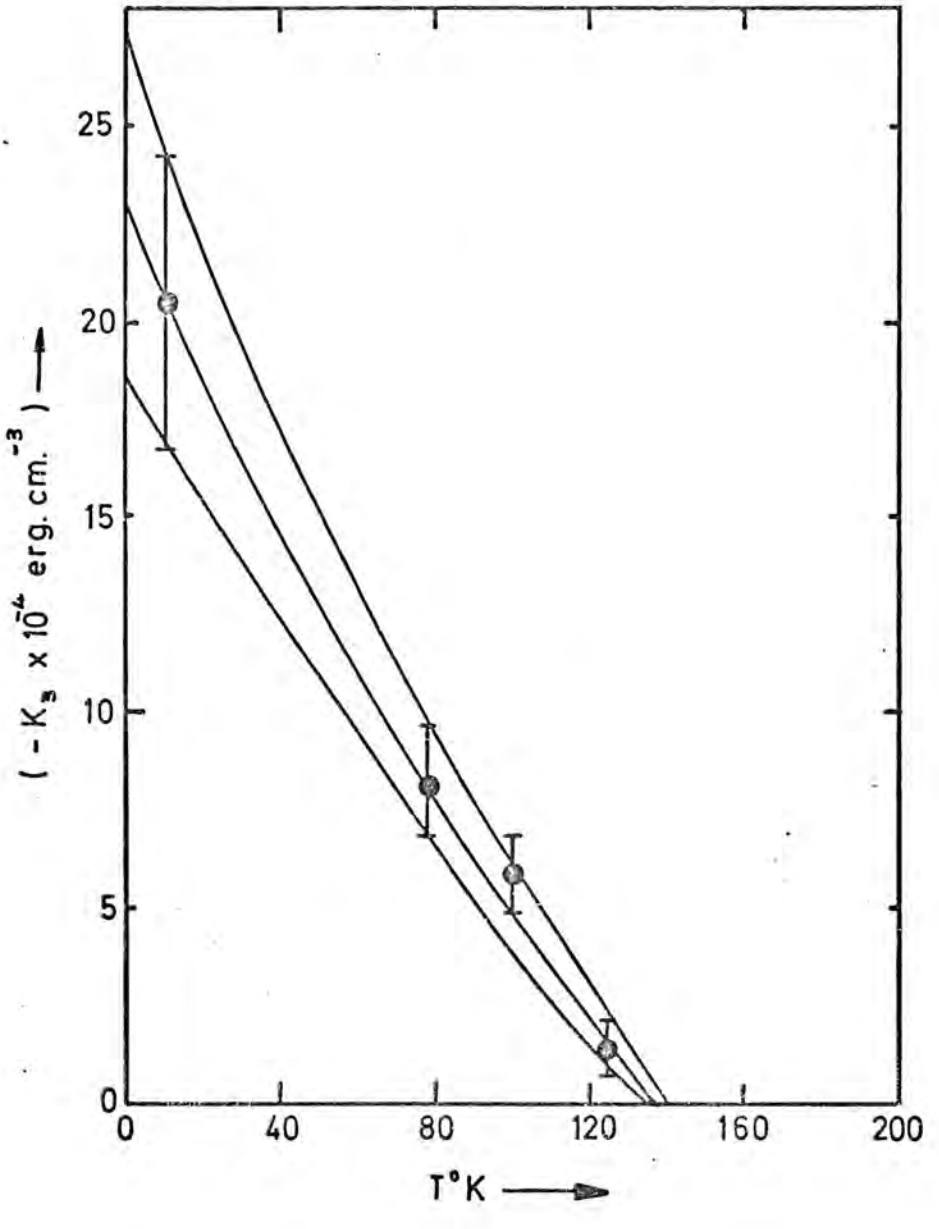

This procedure will give much reduced errors for pure nickel results as follows

Table (8.2) Values of K_3 for pure Ni

Group	$T^{o}K$	$-(K_3 \pm \sigma_{K_3}) \times 10^{-4}$ erg cm^{-3}
1	12.6	31.4 ± 1.6
2	33.0	25.6 ± 2.3
3	78.3	16.2 ± 1.1
4	179.5	1.50 ± 0.24

These values were then used to calculate values of K_1 from the amplitudes of torque curves as described in section (8.1.4). The corresponding values of K_1 and their standard deviations at some temperatures are shown in table (8.3).

For the 0.98 at % NiV alloy it was not possible to follow a similar procedure since only one set of measurement of K_3 was available. These are shown in Fig. (8.6) and their values as used for correction of K_1 with their corresponding error have been given in table (8.3).

Table (8.3) Values of K_1 and K_3 for pure Ni and NiV alloys containing 0.98 at % V. The values of Franse's results on pure Ni are also given.

SPECIMEN	T°K	$(-K_1 - \frac{K_3}{4}) \times 10^{-4}$ erg cm^{-3}	$-K_3 \times 10^{-4}$ erg cm^{-3}	$-K_1 \times 10^{-4}$ erg cm^{-3}	Author
99.999% (Ni)	296		0 ± 0.1	5.7 ± 0.1	FRANSE (1968)
	195		1.0 ± 0.4	24.8 ± 0.8	"
	77		16.4 ± 1.0	84.5 ± 1.0	"
	20		31.0 ± 2.0	116.5 ± 1.0	"
	4.2		34.0 ± 6.0	121.7 ± 1.0	"
99.999% (Ni)	77	88.1 ± 1.0	17.0 ± 1.0	83.9 ± 1.1	present work
	37	114.5 ± 1.0	25.0 ± 2.0	108.2 ± 1.1	"
	16	120.0 ± 1.0	30.0 ± 2.2	112.53 ± 1.12	"
99.99% (Ni)	64	36.6 ± 0.2	2.5 ± 0.4	36.0 ± 0.2	"
	81	83.0 ± 0.8	15.8 ± 1.2	79.0 ± 0.9	"
	29	112.0 ± 0.8	25.0 ± 2.1	105.7 ± 1.0	"
	10	119.0 ± 0.9	32.0 ± 2.2	111.0 ± 1.0	"
0.98 at % V	124	39.2 ± 0.3	4.3 ± 0.8	38.1 ± 0.4	"
	100	47.9 ± 0.6	5.0 ± 1.0	46.7 ± 0.6	"
	77	57.9 ± 0.6	8.3 ± 1.2	55.8 ± 0.7	"
	10	75.4 ± 0.6	20.5 ± 3.5	70.3 ± 1.1	"

Corrections for measurements below 12 K could only be applied by extrapolating the values of K_3 shown in table (8.2). Values of K_1 and K_3 at 4.2° K obtained by this method were $(-116.7 \pm 1.1) \times 10^4$ erg cm^{-3} and $(-32.8 \pm 2.2) \times 10^4$ erg cm^{-3} respectively compared with values due to Franse of $(-121.7 \pm 1.0) \times 10^4$ erg cm^{-3} and $(-34 \pm 6) \times 10^4$ erg cm^{-3}, all being measured on 5N purity material.

8.1.6 Estimate of Errors (Anisotropy results)

The errors mentioned in table (8.3) have different sources which can be summarised as follows

1 - Error due to the shear of the torque curves and in reading the curves.

This error as mentioned can be reduced by using the procedure in section (8.1.3) and the reading of the curves for measuring $(K_1 + \frac{K_3}{4})$ can have ± 1 mm error which with other errors has been shown in table (8.3).

2- Errors in the calibration of the torque magnetometer. This has also been included in table (8.3) and was fully described in chapter (7).

3 - Errors in the (x-y) recorder calibration.
A Philips x-y recorder type PM 8120 with 0.25% error of full scale deflection was used.

4 - Errors in measuring the volume of the samples.
These were calculated using the data from table (5.1), and were comparatively small of the order of .15%.

5 - Errors in the measurement of temperatures.

On the whole temperature range the accuracy of measurement was about $\pm 1^{\circ}$ K.

8.2 Analysis of Resistivity Measurements

The resistivity measurements were carried out by the D.C. method and so the resistivity is equal to

$$\rho = (R_S \quad \frac{V}{V_S}) \left(\frac{a\ b}{\ell} \right) = (P)\ (Q) \qquad (8.3)$$

In which a and b are the width and thickness of the sample respectively, ℓ is the separation of the potential leads, R_S is a standard resistance (one ohm) in series with the specimen, V_S and V are the voltages across R_S and the potential leads respectively. The errors due to this measurement will be as follows.

8.2.1 Random Error

As can be seen from figs. (9.6) and (9.7) the measured points are only slightly scattered about a smooth curve showing that the effects of random error are small. As all random errors contributed to the scatter of points it has not been considered necessary to show error bars on typical measurements, the scatter being an indication of their effects.

8.2.2 Systematic Error

This can arise from the following sources.

i) Errors in Q.

The measurement of dimensions and estimation of errors were described and the results tabulated in table (5.3). In table (8.4) the value and the error of Q in equation (8.3) has been

given from which it can be seen that any error due to this cause is of the order of $\pm$ 1%.

ii) Errors in P.

These are also small, because the value of R_S was 1.0000 $\pm$ 0.0001 and the values of V and V_S were measured by a Solartron type A200 digital voltmeter with 2 microvolts resolution and in any case only ratios of these voltages are involved.

iii) Errors due to positioning of electrodes on sample

It has been shown by Stephens et al (1971) that Equation (8.3) is an approximation valid if $\frac{a}{2} \sim b \lesssim d \ll \ell$ in the following more general expression

$$\rho = P\ Q\ F = P\ Q \left[1 - \frac{2}{\pi}\left(\frac{d}{2\ell}\exp\left(\frac{-2\pi d}{a}\right) + \frac{b}{\ell}\exp\left(\frac{-\pi d}{b}\right)\right)\right] \quad (8.4)$$

In which a, b, P, Q and ℓ are those described and shown in equation (8.3) and d is the separation of neighbouring current and potential leads. Values of F were calculated for some representative specimens and are tabulated in table (8.4). It can be seen that in all cases F is very close to unity.

iv) Errors due to the temperature reading.

Temperature was measured using suitable thermocouples in different ranges as described in chapter (7) and using the previously mentioned digital voltmeter. Checks on the calibration of the thermocouples used were made at 77K and 4.2° K. The maximum error in reading temperature could not exceed $\pm$ 1°K. In table (8.4) only results for four typical samples are given. Samples in the first three rows are of particular importance for the results in chapter (9). It can be seen that the principal source of error is in the measurement of sample size Q.

Table (8.4) Different sources of errors in resistivity measurements.

Sample	F	P(ohms)	Q (m m)
4N PURE Ni	1.00037	1.0000 ± .0001	0.286 ± 0.002
0.98 at % V	0.999998	1.0000 ± .0001	0.299 ± 0.005
1.02 at % Mo	0.999999	1.0000 ± .0001	0.286 ± 0.002
6.72 at % V	1.0017	1.0000 ± .0001	0.211 ± 0.003

8.3 Analysis of Magnetization Measurements

A value of 55.01 ± 0.05 e.m.u./gram for the saturation magnetization of nickel at 290K from Aubert (1968) was used for calibration of the apparatus. The value of $(I - I')$ in equation (7.9) at this temperature, using a Ni sample of 4N purity and of mass 418 mg, corresponded to a deflection of 58 ± 2 mm on the x-y recorder. This error was mainly due to the vibration of the apparatus. From this figure a value for C of 792 ± 27 e.m.u./volt was obtained, equation (7.9). This then was used for the measurement of M for other samples and at different temperatures. As in calculating the value of C the main error ± 3.4% was due to the reading of $(I - I')$, so in making measurements on another sample a further error of the order of ± 3.4% will be obtained. Combining these, a total error on M of about ± 5% will result. No attempt was made to include errors due to the mass of the samples, x-y recorder calibration or the error of ± 0.1% from Aubert's

result, as these were quite small compared with the above errors. For a similar reason, and also because of the minute change of M with temperature, the error due to the temperature reading was also ignored.

It would have been possible to reduce the effects of vibration by increasing the balance damping. Unfortunately this also had the effect of increasing the balance response time. Measurements of M were being taken as the apparatus warmed up from 77K and further increase of response time would have prevented the balance from following the changes in magnetization at a sufficiently rapid rate. Further attention to this problem would be worthwhile. The mass of the spherical samples used in determing of M have been given in table (8.5)

Sample	Ni (99.99)	0.98 at % V	2.71 at % V	3.92 at % V	5.14 at % V	6.72 at % V
mass $\pm$ 0.5 mg	418 mg	220 mg	850 mg	575 mg	505 mg	390 mg

Table (8.5) Mass of the Spherical Samples

CHAPTER 9

Results

In this chapter the results of magnetocrystalline anisotropy, resistivity and magnetization measurements will be described.

9.1.1 K_1 results

The values of K_1 as measured and tabulated in chapter (8) with the other results for 2.71, 3.92, 5.14, and 6.72 at % Ni V alloys for a series of reasonably spaced temperatures are given in table (9.1) and they are shown in figures (9.1) and (9.2). In the case of Ni V alloys of concentration greater than 0.98 at % V the K_3 correction was found to be unnecessary.

9.1.2 Calculation of n using $K_1(T)$ values.

Values of $K_1(T)$ read at various temperatures from the smoothed curves of Figures (9.1) and (9.2) were then used for calculating n in a similar expression to equation (4. 6) as follows.

$$K_1\ (T,C) = K_1(0,C)\ \exp\ (-\ \frac{T}{T_o})^n \qquad (9.1)$$

where $K_1\ (0,C)$ is an extrapolated value of anisotropy constant at OK and T_o is a constant. For convenience the value of T_o was chosen to be 100 K and using a very simple programme (Appendix 2) the values of $K_1(T)$ from 4.2 K to room temperature were fed into the computer to find the value of n. This was

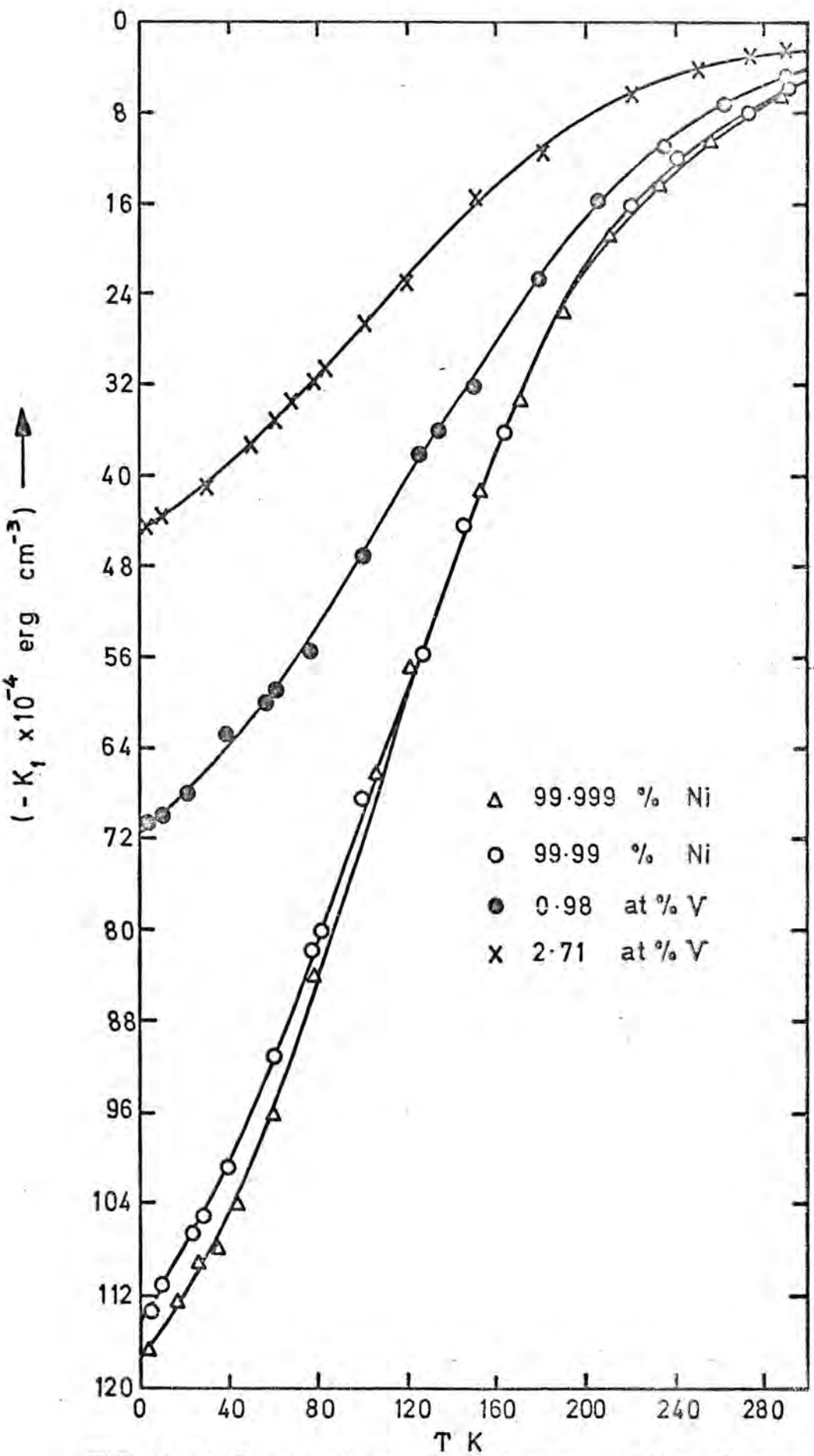

FIG. (9·1) Temperature dependence of the first anisotropy constant of Ni and Ni V crystals.

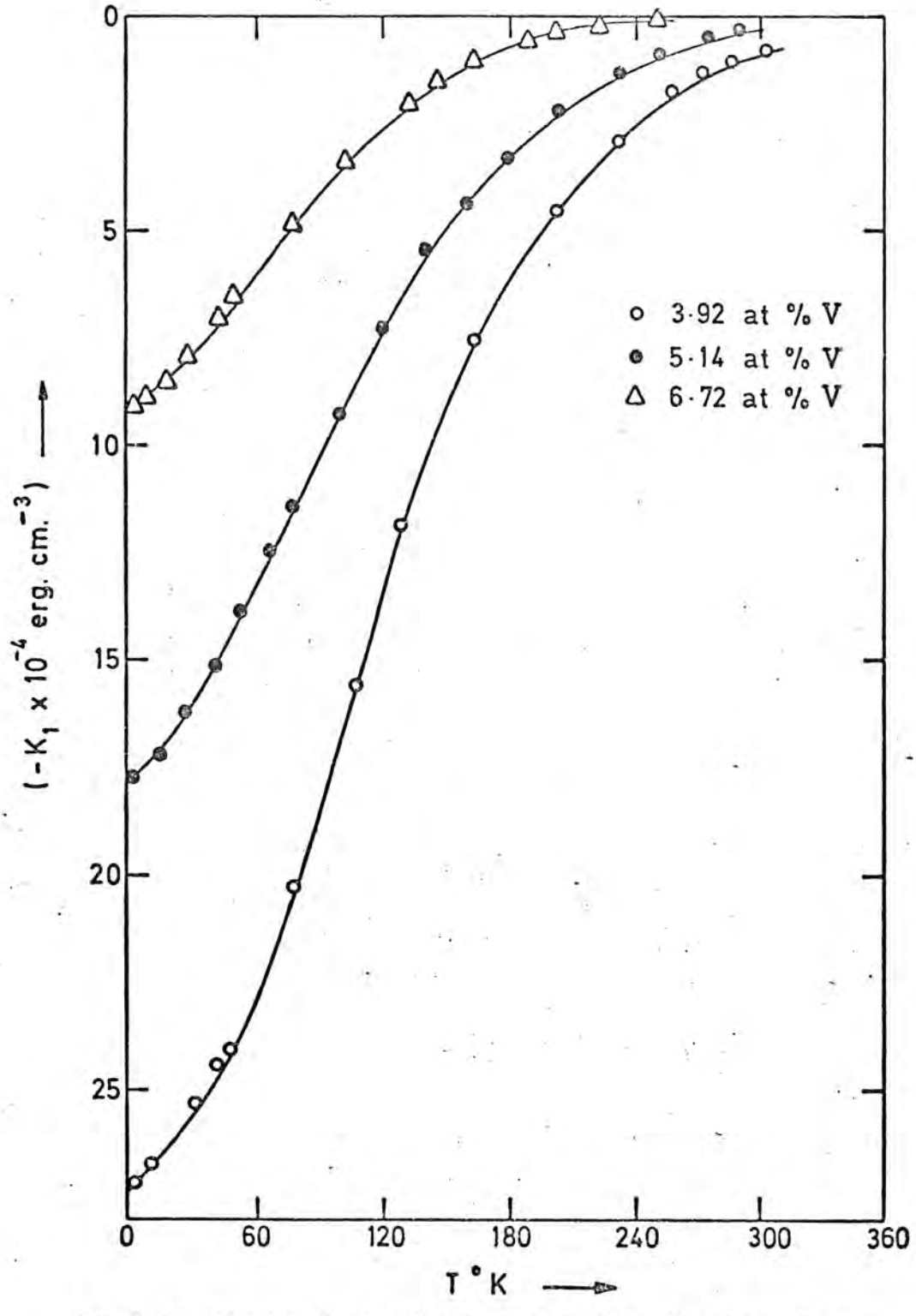

FIG. (9·2) Temperature Dependence of the first Anisotropy Constant of NiV Crystals.

99.999% (Ni)	T^{o} K	4.2	16	26	37	45	60	77	105	121
	$-K_1 \times 10^{-4}$ erg cm^{-3}	116.7	112.5	109.2	108.2	104.4	96.3	83.9	66.4	56.8
99.99% (Ni)	T^{o} K	4.2	10	24	29	40	60	77	81	100
	$-K_1 \times 10^{-4}$ erg cm^{-3}	113.5	111.0	106.3	105.7	101.5	91.3	82.0	79.0	68.0
0.98 at % V	T^{o} K	4.2	10	21	40	57	61	77	100	124
	$-K_1 \times 10^{-4}$ erg cm^{-3}	71.3	70.3	68.2	62.9	60.0	59.1	55.8	46.7	38.1
2.71 at % V	T^{o} K	4.2	10	30	49	60	67	77	82	100
	$-K_1 \times 10^{-4}$ erg cm^{-3}	44.6	43.8	40.9	37.4	35.1	33.5	31.8	30.8	26.7
3.92 at % V	T^{o} K	4.2	12	32	42	41	49	77	107	129
	$-K_1 \times 10^{-4}$ erg cm^{-3}	27.2	26.8	25.3	24.4	24.6	24.2	20.2	15.5	11.84
5.14 at % V	T^{o} K	4.2	17	27	41	53	67	77	100	120
	$-K_1 \times 10^{-4}$ erg cm^{-3}	17.7	17.3	16.2	15.1	13.9	12.4	11.4	9.2	7.3
6.72 at % V	T^{o} K	4.2	10	19	28	42	50	77	103	133
	$-K_1 \times 10^{-4}$ erg cm^{-3}	9.0	8.9	8.4	7.9	7.0	6.4	4.7	3.3	1.8

Table (9.1) The values of K_1 for Ni and NiV alloys at different temperatures.

99.999% (Ni)	T^{o} K	151	171	190	233	256	273	289
	$-K_1 \times 10^{-4}$ erg cm^{-3}	41.6	33.2	25.9	15	10.5	8.25	6.5
99.99% (Ni)	T^{o} K	127	146	164	221	242	273	293
	$-K_1 \times 10^{-4}$ erg cm^{-3}	56.6	44.5	36.0	16.0	12.0	8.2	5.8
0.98 at % V	T^{o} K	133	150	179	206	235	262	290
	$-K_1 \times 10^{-4}$ erg cm^{-3}	37.2	32.3	22.6	15.6	10.8	7.2	4.6
2.71 at % V	T^{o} K	120	150	180	220	250	273	290
	$-K_1 \times 10^{-4}$ erg cm^{-3}	23.1	15.4	12.0	6.75	4.3	2.9	2.4
3.92 at % V	T^{o} K	164	203	233	258	273	287	303
	$-K_1 \times 10^{-4}$ erg cm^{-3}	7.6	4.5	2.9	1.7	1.3	1.1	0.9
5.14 at % V	T^{o} K	140	160	180	204	250	275	290
	$-K_1 \times 10^{-4}$ erg cm^{-3}	5.4	4.4	3.3	2.1	1.0	0.5	0.3
6.72 at % V	T^{o} K	146	163	185	202	223	252	
	$-K_1 \times 10^{-4}$ erg cm^{-3}	1.4	1.0	0.5	0.3	0.2	0.15	

Table (9.1) -continued-

found to be more convenient if equation (9.1) be written as follows.

$$\text{Ln Ln}\left[\frac{K_1(0,C)}{K_1(T,C)}\right] = n \text{ Ln}\left[\frac{T}{100}\right] + \text{constant} \quad (9.2)$$

The values of n from this programme are shown in table (9.2), and the average value of n for each sample to obey equation (9.1) found to be 1.49 ± 0.02 in good agreement with the results for Ni Mo alloys of Hausmann et al (1971).

Table (9.2) Different values of n in equation (9.1) for different Ni and NiV alloys

Sample	5N(Ni)	4N(Ni)	0.98%V	2.71%V	3.92%V	5.14%V	6.72%V
n	1.47	1.43	1.46	1.47	1.51	1.49	1.63

9.1.3 Results from equation (9.1)

Using n = 1.5, as a good approximation with the value of 1.49 in the previous section, values of Ln K_1 (T,C) against T^n were plotted, using equation (9.1) in the following form.

$$\text{Ln}\left[K_1(T,C)/1000\right] = \text{Ln}\left[K_1(0,C)/1000\right] - \left[\frac{T}{100}\right]^{1.5} \quad (9.3)$$

where the factor 1000 has been chosen only for convenience in drawing the graphs. A least squares programme (Appendix 3) was written to give the best line passing through the available points. In the case of 6.72 at % V alloy only the data from 4.2 to 210 K were used, this was due to the fact, that for this sample, measurements of K_1(T,C) for higher temperatures were

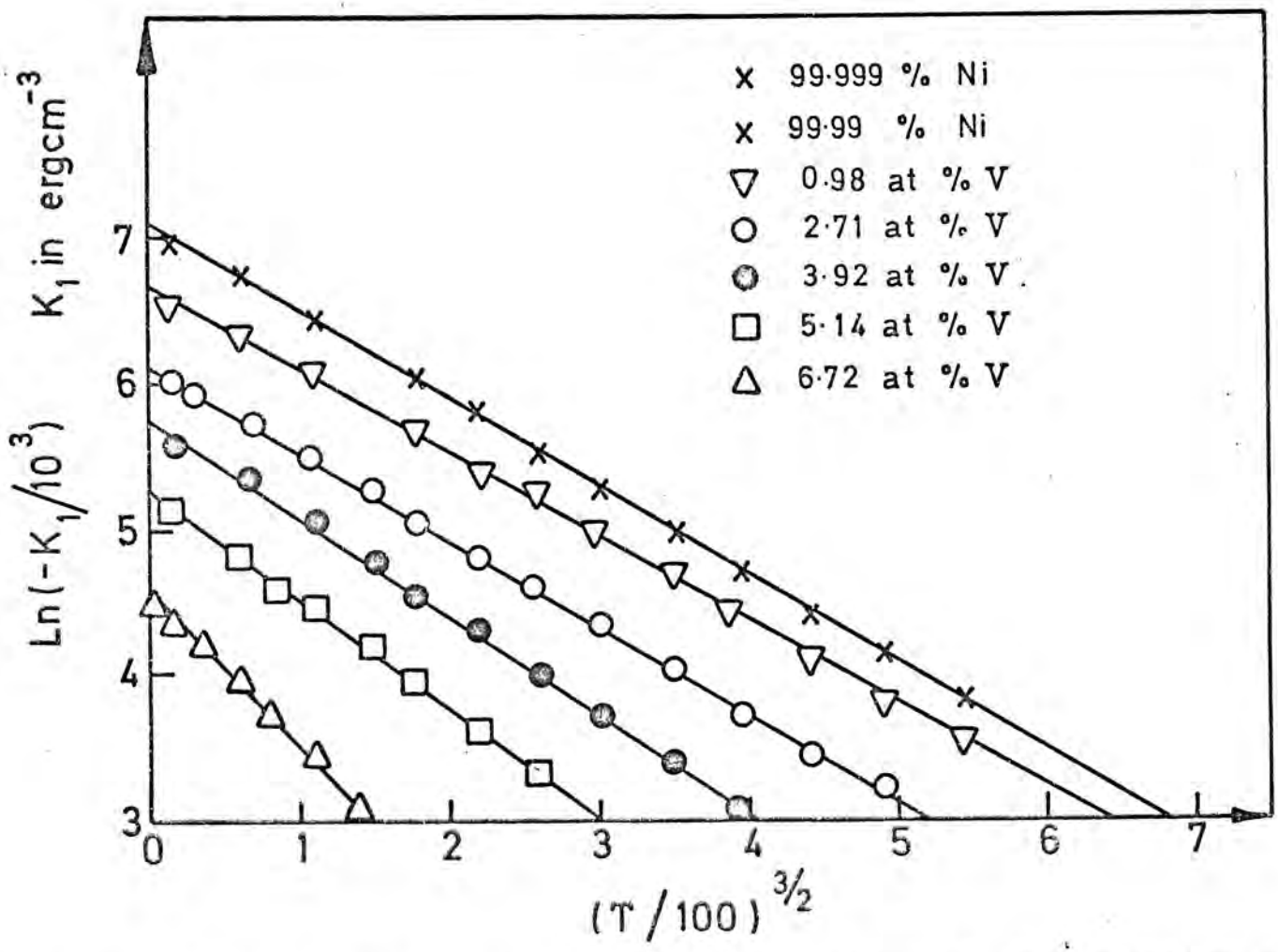

FIG. (9·3) TEMPERATURE AND CONCENTRATION DEPENDENCE OF LnK_1 IN NiV ALLOYS.

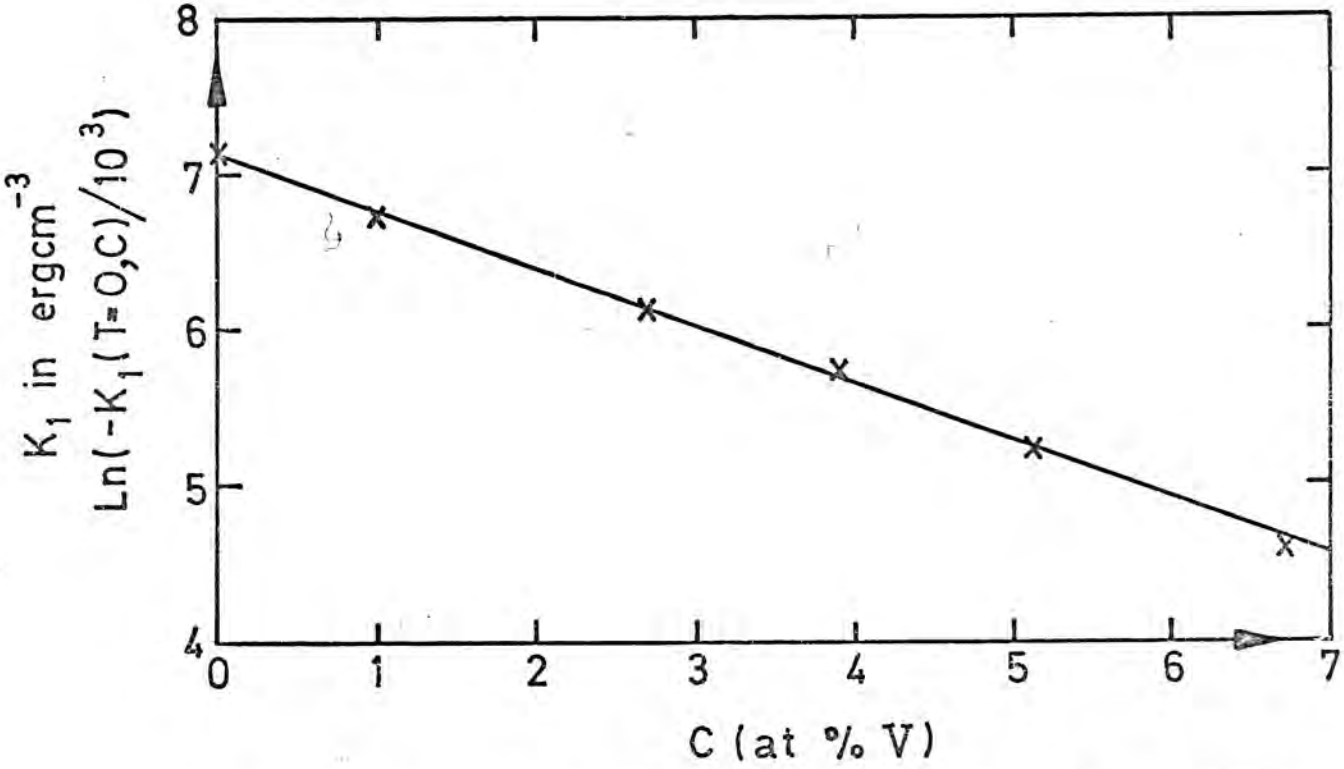

FIG. (9.4) DEPENDENCE OF LnK_1 ON THE CONCENTRATION OF V IN NiV ALLOYS AT T = 0°K

too small to give a reliable result. Figure (9.3) shows values of Ln $(K_1 (T,C)/_{1000})$ plotted against $(T/_{100})^{1.5}$. The differences in the results in the case of 5N and 4N purity Ni samples are too small to be shown (Fig. (9.3)). For a similar reason no attempt has been made to show the error bars on these graphs. As can be seen from fig. (9.3) the values for each sample lie close to a straight line which can be extrapolated to give values of Ln $(K_1(0,C)/_{1000})$.

9.1.4 Calculation of α in equation (4.11) for NiV alloys

As already mentioned, Hausmann and Wolf (1971), by assuming that it is possible to separate the reciprocal mean free path of the conduction electrons in Ni-rich binary alloys into temperature and concentration dependent components, derived an expression for the first anisotropy constant, at low temperature T and small concentration C of the second element, as follows.

$$K_1^{\underline{Ni}Me}(T,C) = K_1^{Ni}(T) \exp(-\alpha C) \qquad (9.4)$$

where α is a constant for a particular metal Me.
This expression at T = 0 can be written as follows

$$K_1^{\underline{Ni}Me}(0,C) = K_1^{Ni}(0) \exp(-\alpha C) \qquad (9.5)$$

or
$$\mathrm{Ln}\left[K_1^{\underline{Ni}Me}(0,C)/_{1000}\right] = \mathrm{Ln}\left[K_1^{Ni}(0)/_{1000}\right] - \alpha C \qquad (9.6)$$

In which $K_1^{Ni}(0)$ is the value of K_1 for pure Ni at T = 0 and $K_1^{\underline{Ni}Me}(0,C)$ are the values of $K_1(T,C)$ at T = 0. The values of $\mathrm{Ln}\left[K_1(0,C)/_{1000}\right]$ obtained from the data shown in fig (9.3) are shown in fig. (9.4) plotted against concentration C. This

shows a linear graph from which a value of α may be obtained. In the case of the NiV results the value of α was found to be 0.36 (at %)$^{-1}$, which can be compared with the results of Kortekaas et al (1972) for Cu, Co and Fe alloyed with nickel. This will be discussed in section (9.4).

9.1.5 Calculation of α for NiMo alloys

Hausmann and Wolf (1971) by using available results from Hofmann obtained similar results for NiMo samples to those in fig (9.4). It was considered desirable, for comparison with other available results for α, to calculate the value of α for Mo in nickel. The only available source of results to do this was fig.(3) from Hausmann and Wolf's paper (1971). Using the data from this figure the value of α was found to be 0.42 (at %)$^{-1}$.

9.1.6 Variation of $K_{1V}(T)$ with temperature

As was mentioned in chapter (4) Hausmann and Wolf (1971) suggested that K_{1V} is temperature dependent in the following way when the temperature is well below the Curie temperature,

$$K_{1V}(T) = K_1(T) \left[\frac{M(0)}{M(T)} \right]^{10} \qquad (9.7)$$

In an attempt to investigate whether a similar exponential dependence on temperature is valid for K_{1V} as has been shown to apply for K_1 a series of calculations were performed, using the available results for $K_1(T)$ from the present work and M(T) results from Kaul et al (1969). This was tried for 5N and 4N purity Ni and the values of $K_{1V}(T)$ for a range of temperatures

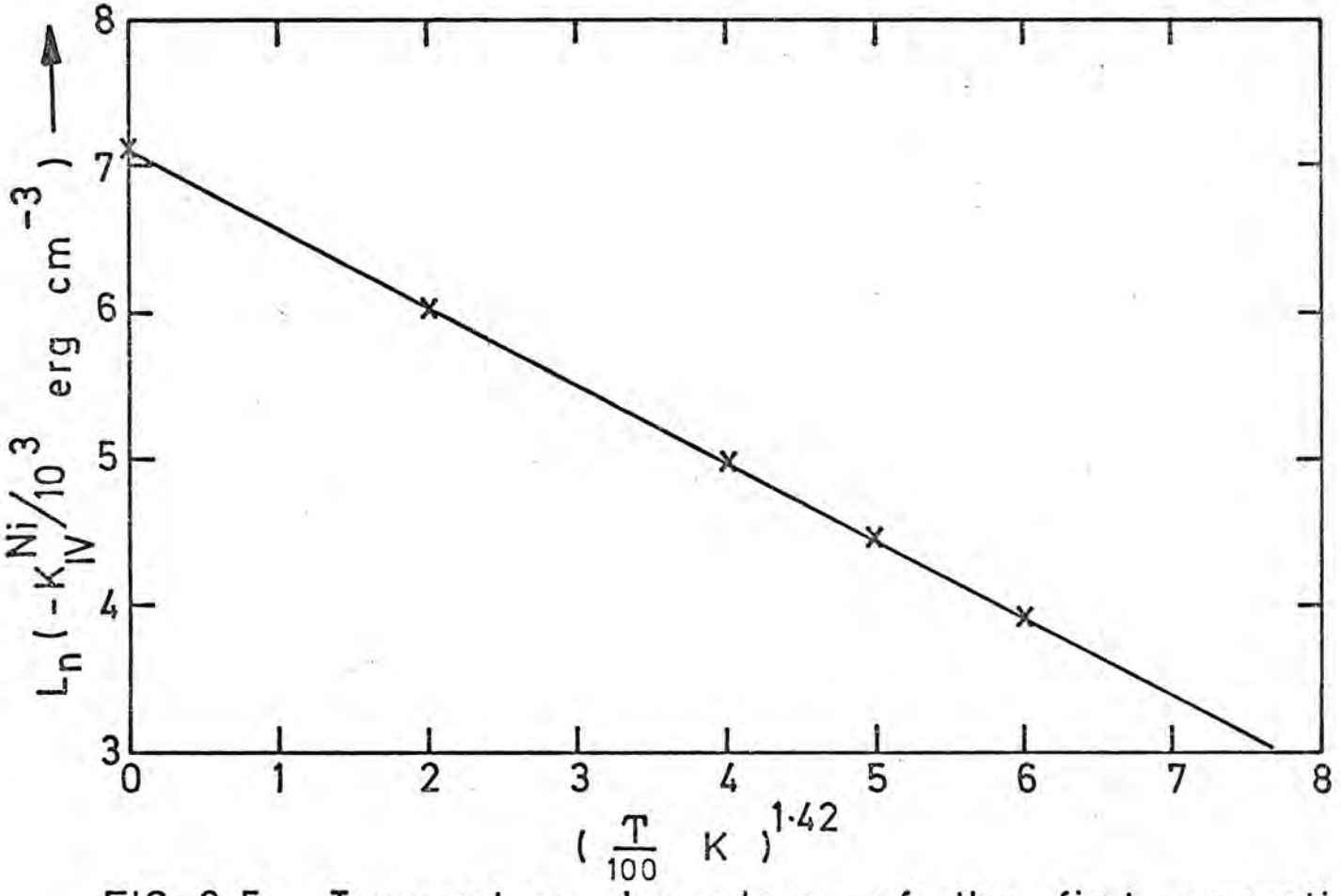

FIG. 9·5 Temperature dependence of the first magnetic anisotropy constant of Ni in the magnon vaccum state.

from 4.2K to room temperature were fed to the computer to give the value of n as mentioned in section (9.1.2). The values obtained from this programme were not exactly 1.5, as obtained by Hausmann and Wolf (1971), and instead the values of 1.417 ± 0.020 and 1.421 ± 0.020 were found respectively for 5N and 4N purity Ni samples which gives an average of n = 1.42 instead of n = 1.5 as found for $K_1(T)$. Then by using an exponential form of function the values of $Ln\left[-K_{1V}^{Ni}/10^3\right]$ were plotted against $\left[T/100\right]^{1.42}$ for both 4N and 5N purity Ni crystals and the results have been shown in fig.(9.5). It seems from this figure that the variation of the first anisotropy constant of nickel in the magnon vacuum state follows the same sort of law which was suggested by Hausmann (1970) and found to apply to $K_1(T)$. Also it should be noticed that the value of n = 1.42 found for $K_{1V}(T)$ is different from n = 1.5 which was used by Hausmann and Wolf (1971) for the same purpose. This would be expected because the values of $K_{1V}(T)$ are at all temperatures higher than the values of $K_1(T)$; when the temperature is raised the difference increases and if the variation is capable of being represented by an exponential law then the values of n must be smaller. This can be seen from the values of $K_1(T)$ and $K_{1V}(T)$ for some temperatures in table (9.3).

	T^o K	10	30	50	70	90	130
4N Ni	$-K_1(T)\times10^{-4}$	111.7	105.8	97.5	87.3	74.6	52.2
	$-K_{1V}(T)\times10^{-4}$	111.9	106.9	100.1	91.2	79.8	59.6
5N Ni	$-K_1(T)\times10^{-4}$	114.7	109.0	101.7	91.5	75.6	53.2
	$-K_{1V}(T)\times10^{-4}$	114.9	110.0	104.4	95.8	80.9	60.7

Table (9.3) The values of $K_{1V}(T)$ and $K_1(T)$ in erg cm^{-3} for Ni crystals of two grades of purity.

FIG. (9·6) Temperature Variation of Resistivity of Ni and NiV Alloys.

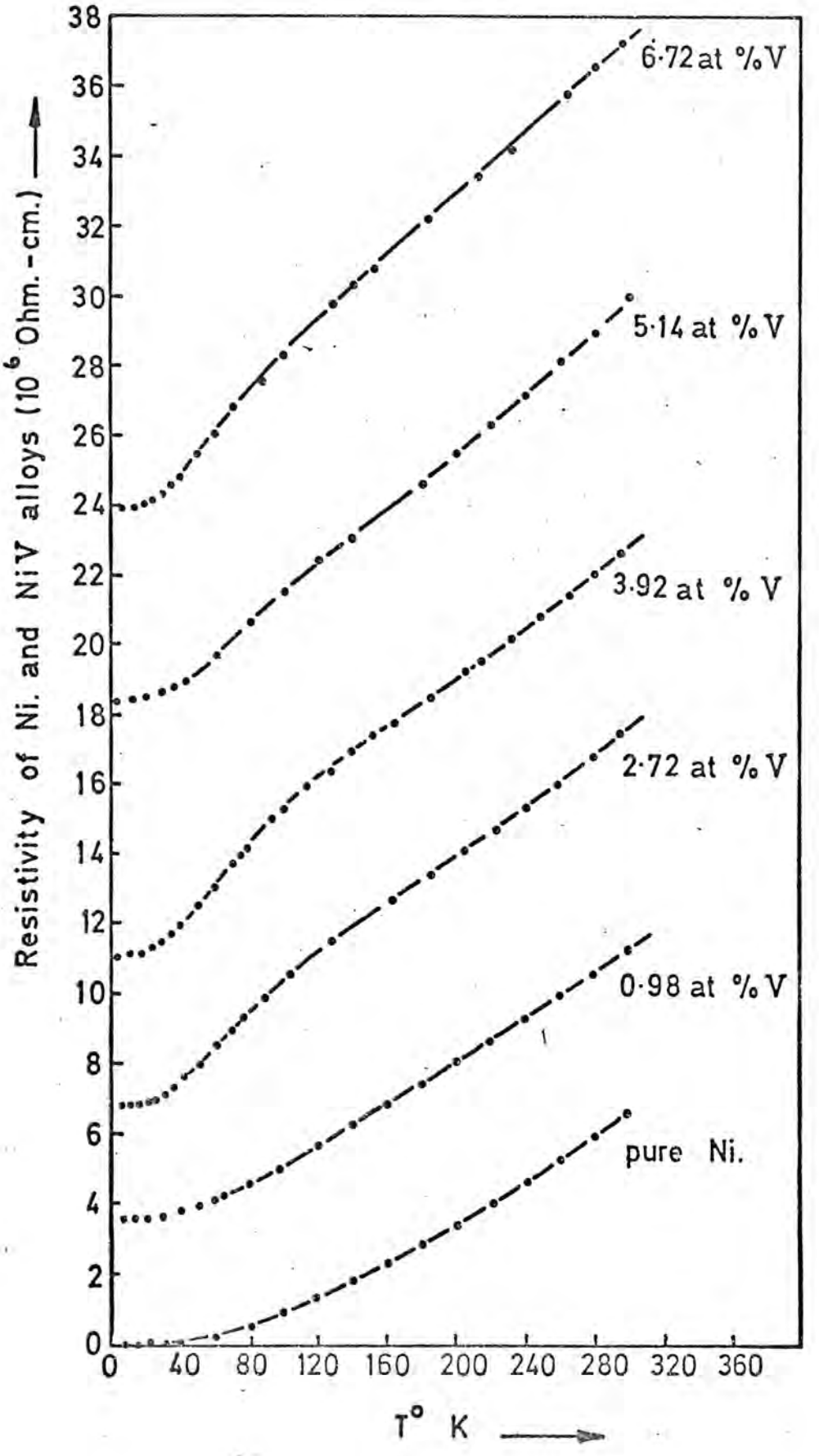

	T^{o} K	170	210	250	270	290
4N Ni	$-K_1(T)\times10^{-4}$	32.6	18.3	10.6	8.0	6.0
	$-K_{1V}(T)\times10^{-4}$	40.3	25.1	16.6	13.8	11.4
5N Ni	$-K_1(T)\times10^{-4}$	33.0	18.7	10.8	8.4	6.3
	$-K_{1V}(T)\times10^{-4}$	40.8	25.6	16.9	14.5	11.9

Table (9.3) - continued-

The values of $K_{1V}(T)$ and $K_1(T)$ in erg cm^{-3} for Ni crystals of two grades of purity.

9.2 Resistivity Results

9.2.1 Resistivity measurement from 4.2K to room temperature

The resistivity of each sample was measured from 4.2K to 300K. The results have been plotted in Fig. (9.6) from which it can be seen that the random error is small. In the case of pure nickel and the 0.98 at % V sample the curves showed the usual temperature variation of a typical metal whereas for the rest of the samples it can be seen that there is an anomalous effect about 120K. The values of ρ_o and some values of $\rho(T)$ are given in table (9.4). For the sample compositions which show the anomalous behaviour the validity of the ρ_o values and others below 120K may be in some doubt; the cause of the anomaly is not understood. As the main interest of this work is to test the validity of the hypothesis, suggested by Hausmann (1970) and discussed in chapter (4), it was found to be more acceptable not to concentrate on the elucidationof the anomaly. However, it is of interest to record that, the resistivity of a NiV sample containing 12.5 at % V and made from the same material was measured

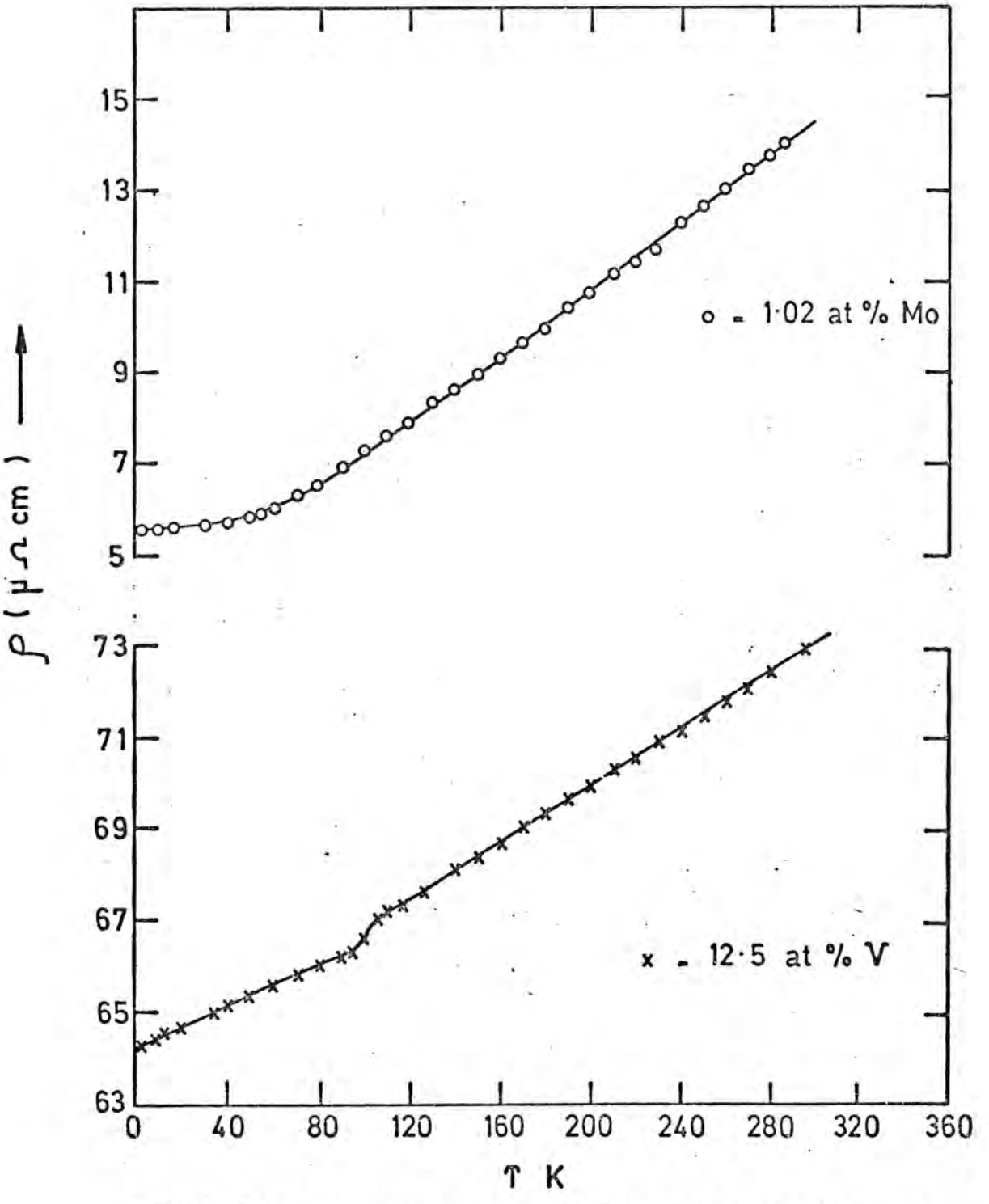

FIG.(9·7) Temperature variation of resistivity of 1 at % Ni Mo and 12·5 at % Ni V alloys.

from 4.2K to room temperature and the results are plotted against temperature in fig. (9.7). For an alloy of this composition the Curie temperature is well below room temperature. As can be seen from fig. (9.7) the previous anomaly which as shown in fig. (9.6) has completely vanished and instead there is a discontinuity of slope at about 105K, which shows the well known change of slope of a Curie temperature anomaly. This result can be important, because it suggests that the mentioned anomaly at about 120K can not be seen when the alloy is paramagnetic at this temperature. The slope of the results for the 12.5 at % V alloy in the ferromagnetic part is less than in the paramagnetic part in agreement with Gautier et al (1972). However the anomaly noticed in the present work in the ferromagnetic part was not mentioned by Gautier or other investigators e.g. Arajs (1964).

9.2.2 Resistivity of NiMo containing 1.02 at % Mo

As mentioned in chapter (4) Franse et al (1973) have proposed a relation between α and residual resistivity ρ_o. Since in section (9.1.5) the value of α could easily be obtained from anisotropy measurements of NiMo alloys, it was decided to measure the resistivity of NiMo containing 1.02 at % Mo to get the $\rho_o(\downarrow)$ and $\rho_o(\uparrow)$ mentioned in chapter (4). The results of such measurements have been plotted in fig.(9.7) and some typical values of resistivity at various temperature has been given in table (9.4). As can be seen from fig. (9.7) the anomalous effect mentioned in section (9.2.1) can not be observed on such a curve.

5N (Ni)	T	4.2	20	37	45	55	77	98	127
	$\rho \times 10^6$ ΩCm	0.023	0.034	0.080	0.113	0.159	0.460	0.885	1.54
4N (Ni)	T	4.2	16	30	43	60	77	118	153
	$\rho \times 10^6$ ΩCm	0.081	0.094	0.121	0.162	0.351	0.553	1.32	2.24
0.98 at % V	T	4.2	25	40	50	65	77	100	130
	$\rho \times 10^6$ ΩCm	3.72	3.72	3.84	4.08	4.23	4.50	5.16	5.97
2.71 at % V	T	4.2	20	33	43	60	77	118	140
	$\rho \times 10^6$ ΩCm	6.86	6.99	7.29	7.68	8.55	9.24	11.0	11.9
3.92 at % V	T	4.2	20	35	45	60	77	98	140
	$\rho \times 10^6$ ΩCm	11.2	11.3	11.7	12.3	13.1	14.1	15.3	16.9
5.14 at % V	T	4.2	19	30	50	65	77	100	130
	$\rho \times 10^6$ ΩCm	18.4	18.5	18.6	19.3	19.7	20.4	21.5	22.7
6.72 at % V	T	4.2	17	25	45	60	77	98	127
	$\rho \times 10^6$ ΩCm	24.0	24.1	24.2	25.2	26.1	27.1	28.3	29.8
12.5 at % V	T	4.2	11	30	45	60	77	95	100
	$\rho \times 10^6$ ΩCm	64.3	64.4	64.8	65.2	65.5	65.9	66.3	66.6
1.02 at % Mo	T	4.2	20	34	45	60	77	95	125
	$\rho \times 10^6$ ΩCm	5.60	5.61	5.67	5.81	6.01	6.41	7.13	8.13

Table (9.4) Values of ρ for Ni and NiV alloys at different temperatures

5 (Ni)	T	163	195	223	249	273	296
	$\rho \times 10^6$ ΩCm	2.43	3.31	4.13	4.97	5.81	6.56
4 (Ni)	T	175	195	231	257	273	296
	$\rho \times 10^6$ ΩCm	2.81	3.37	4.45	5.26	5.83	6.58
0.98 at % V	T	150	180	210	240	270	290
	$\rho \times 10^6$ ΩCm	6.60	7.47	8.37	9.33	10.3	11.0
2.71 at % V	T	175	205	223	249	273	296
	$\rho \times 10^6$ ΩCm	13.1	14.1	14.8	15.7	16.6	17.5
3.92 at % V	T	175	205	231	249	273	296
	$\rho \times 10^6$ ΩCm	18.2	19.2	20.2	20.9	21.8	22.7
5.14 at % V	T	160	190	220	250	270	290
	$\rho \times 10^6$ ΩCm	23.9	25.1	26.3	27.6	28.6	29.6
6.72 at % V	T	153	175	231	257	273	296
	$\rho \times 10^6$ ΩCm	30.8	31.8	34.2	35.3	36.2	37.3
12.5 at % V	T	105	110	130	190	250	280
	$\rho \times 10^6$ ΩCm	67.0	67.2	67.8	69.6	71.5	72.5
1.02 at % Mo	T	150	180	210	240	270	293
	$\rho \times 10^6$ ΩCm	9.02	9.97	11.2	12.3	13.5	14.0

Table (9.4) -continued-

9.3 Combination of the Resistivity and Anisotropy results to check the validity of Hausmann's hypothesis

As mentioned in chapter (4) the anisotropy and resistivity for small concentrations can be expressed as follows.

$$K_1^{\underline{Ni}Me} = K_1^{Ni} \left(1 - \alpha_{Me} C_{Me}\right) \qquad (9.8)$$

$$\rho^{\underline{Ni}Me} = \rho^{Ni} \left(1 + \beta_{Me} C_{Me}\right) \qquad (9.9)$$

Using the following equation

$$\frac{1}{K_1^{Ni}} \frac{dK_1^{\underline{Ni}Me}}{dT} = \frac{1}{K_1^{Ni}} \frac{dK_1^{\underline{Ni}Me}}{d\rho^{\underline{Ni}Me}} \frac{d\rho^{\underline{Ni}Me}}{dT} \qquad (9.10)$$

and writing equation (9.8) as follows

$$K_1^{\underline{Ni}Me} = K_1^{Ni} \left[1 - \alpha_{Me} \frac{\rho^{\underline{Ni}Me} - \rho^{Ni}}{\rho^{Ni} \beta_{Me}} \right] \qquad (9.11)$$

Hausmann arrived at the following expression which relates anisotropy measurements to resistivity results,

$$\frac{1}{K_1^{Ni}} \frac{dK_1^{\underline{Ni}Me}}{dT} = -\frac{\alpha_{Me}}{\beta_{Me}} \frac{1}{\rho^{Ni}} \frac{d\rho^{\underline{Ni}Me}}{dT} \qquad (9.12)$$

in which $\alpha = \dfrac{K_1^{Ni} - K_1^{\underline{Ni}Me}}{K_1^{Ni} C_{Me}}$. However it is better to use equation (9.4) instead of equation (9.8) in the derivation of a similar expression. Equation (9.8) is an approximate form of equation (9.4) which is valid when $\alpha_{Me} C_{Me}$ is small. Using the exponential form the same result is found for the right hand side of equation (9.12), but the left hand side is

different. For this derivation equation (9.10) should be written as follows.

$$\frac{1}{K_1^{\underline{NiMe}}}\frac{dK_1^{\underline{NiMe}}}{dT} = \frac{1}{K_1^{\underline{NiMe}}}\frac{dK_1^{\underline{NiMe}}}{d\rho^{\underline{NiMe}}}\frac{d\rho^{\underline{NiMe}}}{dT} \qquad (9.13)$$

and using equation (9.9) equation (9.4) can be written

$$K_1^{\underline{NiMe}} = K_1^{Ni}\exp\left[-\alpha_{Me}\frac{\rho^{\underline{NiMe}} - \rho^{Ni}}{\rho^{Ni}\beta_{Me}}\right] \qquad (9.14)$$

ans so by simple algebra

$$\frac{dK_1^{\underline{NiMe}}}{d\rho^{\underline{NiMe}}} = \frac{-\alpha_{Me}}{\beta_{Me}}\left[\frac{1}{\rho^{Ni}}\right]K_1^{\underline{NiMe}} \qquad (9.15)$$

and so using equation (9.15) equation (9.13) can be written as follows

$$\frac{1}{K_1^{\underline{NiMe}}}\frac{dK_1^{\underline{NiMe}}}{dT} = \frac{-\alpha_{Me}}{\beta_{Me}}\frac{1}{\rho^{Ni}}\frac{d\rho^{\underline{NiMe}}}{dT} \qquad (9.16)$$

in which $\alpha = \frac{1}{C_{Me}}\,\mathrm{Ln}\,\frac{K_1^{Ni}(T)}{K_1^{\underline{NiMe}}(T,C)}$. It has been pointed out e.g. Elliott and Gibson (1974) p.313, that Equation (9.9) is not strictly applicable to alloys and that a more adequate expression takes the form

$$\rho^{\underline{NiMe}} = \rho^{Ni}\left[1 + \beta(C - C^2)\right] \qquad (9.17)$$

By similar calculations the corresponding equation to (9.16) has the following form.

$$\frac{1}{K_1^{NiMe}}\frac{dK_1^{\underline{NiMe}}}{dT} = \frac{-\alpha_{Me}}{\beta_{Me}\rho^{Ni}}(F)\frac{d\rho^{\underline{NiMe}}}{dT} \qquad (9.18)$$

	T K	10	30	50	70	90	110	130	150	170	190	210	230	250
0.98 at % V	(R.H.S.)x10^{-1}		1.6	4.7	5.2	6.9	7.2	6.9	6.6	6.0	7.1	7.0	7.4	7.5
	(L.H.S.)		6.3	8.3	11.3	15.3	20.3	28.5	35.3	48.3	62.8	69	69.4	72
2.71 at % V	(R.H.S.)		13.3	15.5	15.7	14.7	12.8	9.5	9.4	9.1	9.15	9.1	8.9	9.5
	(L.H.S.)		11.8	14.4	18.6	23.7	25.5	28.3	37.9	33.8	42.8	44.1	42.1	35
3.92 at % V	(R.H.S.)		12	17.4	17.7	13.9	14.9	10.5	9.0	9.0	8.9	9.4	9.3	9.3
	(L.H.S.)		8.1	12.2	16.4	22.7	29.2	34.1	35.8	34.4	35.0	38.3	40.3	42.5
5.14 at % V	(R.H.S.)	1.4	5.5	9.4	13.0	13.0	11.2	10.4	9.6	8.9	8.8	9.3	9.1	9.6
	(L.H.S.)	7.9	14.4	17.8	22.4	25.3	29.0	31.4	32.4	35.0	39.0	41.0	44.0	46.2
6.72 at % V	(R.H.S.)	2.8	9.7	17.3	16.5	14.2	12.7	11.0	10.6	9.9	9.7			
	(L.H.S.)	9.8	19.7	23.7	29.5	31.0	35.8	38.6	49.2	51.7	5.20			

Table (9.5) The values of right hand side and left hand side of equation (9.16) if both sides be divided by α. The unit of each side is at % K^{-1}.

in which an additional factor F appears where

$$F = \left[1 - 4\left(\frac{\rho^{\underline{Ni}Me} - \rho^{Ni}}{\beta_{Me}\,\rho^{Ni}}\right)\right]^{-1/2} \qquad (9.19)$$

The effect of this factor on the right hand side of equation (9.18) is small and so not important. e.g. F for T = 50K for NiV alloy containing 0.98 at % V is about 1.020 and so the value of right hand side for this temperature will increase from 28 x 10^{-4} to 28.56 x 10^{-4} $(deg)^{-1}$ which is not very different in comparison with other variations. This is not surprising since the alloys used had low concentrations of V. The results obtained for some typical temperatures for different samples have been given in table (9.5), in which right hand side (r.h.s.) and left hand side (l.h.s.) of equation (9.16) has been compared. The values in table (9.5) are divided by α in order to compare anisotropy results with resistivity measurements.

The values of $\frac{d\rho}{dT}$ and $\frac{dK}{dT}$ have been measured from the experimental curves and the values of α and β have been calculated from the measured values of $K_1(T)$ and $\rho(T)$ respectively.

9.4 Calculation of $\rho_o(\uparrow)$ and $\rho_o(\downarrow)$ for 1 at % NiV and NiMo alloys

In chapter (4) it was described how the values of $\rho_o(\uparrow)$ and $\rho_o(\downarrow)$, minority and majority resistivities can be calculated from the following two equations

$$\rho_o = \frac{\rho_o(\uparrow)\rho_o(\downarrow)}{\rho_o(\uparrow) + \rho_o(\downarrow)} \qquad (9.20)$$

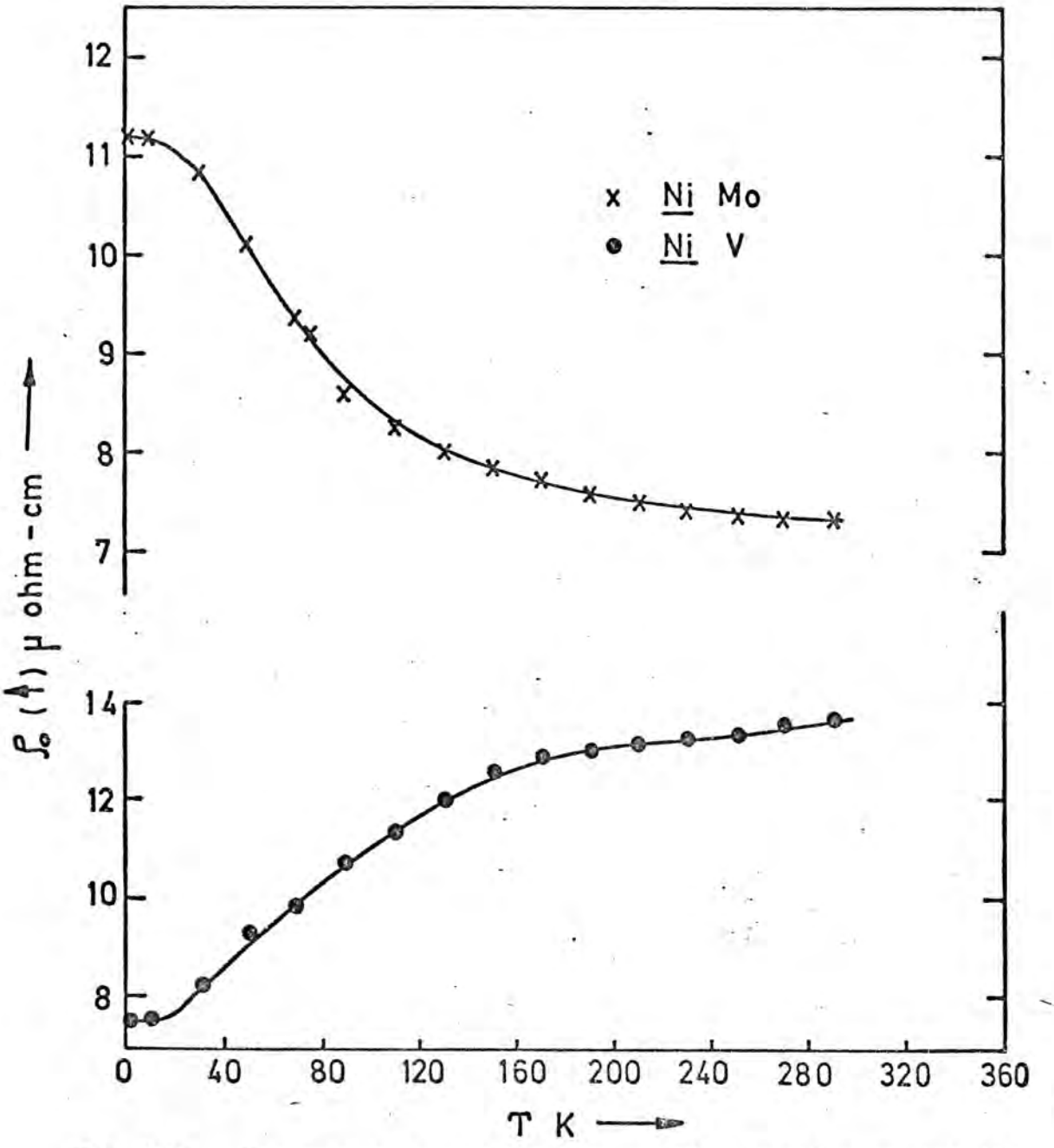

FIG. 9·8 Temperature dependance of minority resistivity $\rho_{\downarrow}(\uparrow)$ for 1 at % V and Mo in Ni V and Ni Mo alloys.

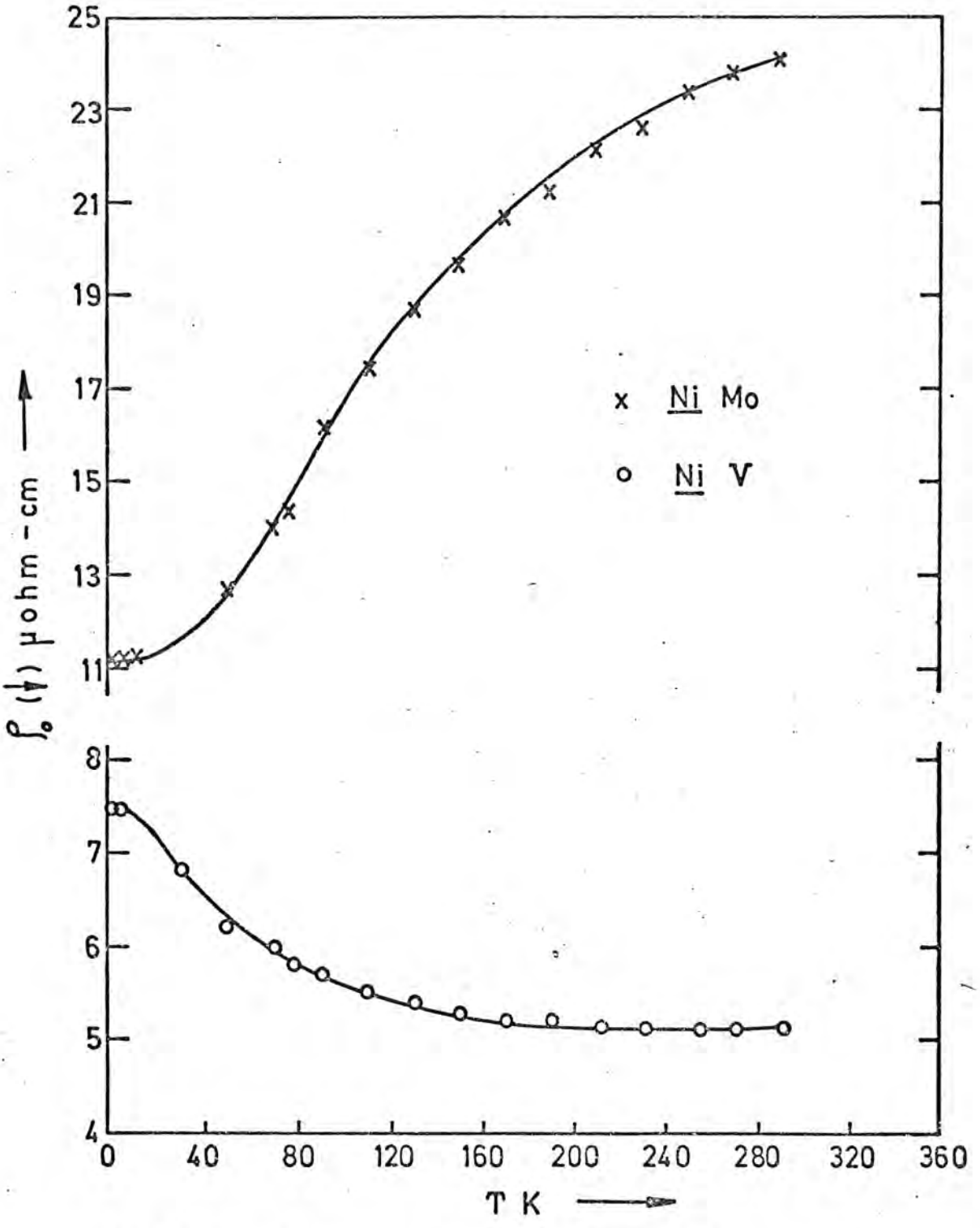

FIG. 9·9 Temperature dependance of majority resistivity for 1 at % V and Mo in Ni V and Ni Mo alloys.

$$\frac{\Delta}{\rho_0} = \frac{\left[\rho_0(\uparrow) - \rho_0(\downarrow)\right]^2}{4\rho_0(\uparrow)\rho_0(\downarrow)} \qquad (9.21)$$

in which the values of Δ and ρ_0, described in chapter (4), can be calculated from experimental resistivity results on pure nickel and corresponding alloys. From these two equations the following results will obtain for $\rho_0(\uparrow)$ and $\rho_0(\downarrow)$.

$$\rho_0(\downarrow) \text{ OR } \rho_0(\uparrow) = 2\left[(\rho_0 + \Delta) \pm \sqrt{\Delta(\rho_0 + \Delta)}\right] \qquad (9.22)$$

From measurements on NiV and NiMo alloys of approximately 1 at % V and Mo content the values of $\rho_0(\uparrow)$ and $\rho_0(\downarrow)$ have been obtained by the solution of these equations (9.22). Farrell and Greig suggest that in the evaluation of Δ room temperature values of ρ_m should be employed since at this temperature spin mixing is dominant. In an attempt to test the validity of this suggestion a series of evaluations were carried out using ρ_m values at various temperatures. The results of these computations are shown in Figures (9.8) and (9.9) where it can be seen that for the NiV alloys the variation of $\rho_0(\uparrow)$ and $\rho_0(\downarrow)$ are small above a temperature of about 180K. The results for the NiMo alloys do not, however, show saturation at so low a temperature, the ρ_0/T graphs showing an appreciable gradient even at 300K. Values for NiV may be considered reasonably well founded while those for NiMo alloys are probably slightly less reliable. The $\rho_0(\uparrow)$ value for NiV alloy is $(13.7 \pm 0.5) \times 10^{-6}$ ohm cm. while that for NiMo alloy is 7.3×10^{-6} ohm cm. which is not likely to be more than about 0.3×10^{-6} ohm cm. greater than an ultimate saturation value. These and corresponding $\rho_0(\downarrow)$

values along with values given by Franse et al (1973) are given in table (9.6) along with values of α from anisotropy measurement on a range of Ni based alloys. The choice of which solution to equations (9.22) to associate with $f_o^{\uparrow}$ for Mo has been made on the same basis as suggested by Farrell and Greig (1968). This is justified by the similarity of the outer electron structure between Mo($4d^5$, 5s) and Cr($3d^5$ 4s).

9.5 Magnetization Results and their connection with the Anisotropy Measurements.

The values of M, using a value of (792 ± 27) e.m.u./volt for the calibration of the system, were obtained from 77K to room temperature. These are shown in Fig.(9.10) with smoothed curves drawn through them. The changes in M for the pure Ni and low vanadium concentration samples over this temperature range were only of the order of the experimental uncertainty, but that for 3.92%, 5.14% and 6.72% vanadium content showed a reasonable degree of variation. Values of M read from the smoothed curves for some temperatures have been given in table (9.7).

Using a function of the form $M(T) = M(0)\ (1-AT^{1.5})$, Weiss (1937), and taking values of M(T) between 77K and 170K from the smoothed curves a mean value of M(0) was calculated. The error on the calculations of these mean values of M(0) was very much less than 5%. However, the values of M(4.2) were measured for 5.14% and 6.72% vanadium content alloys. These are shown in Fig. (9.10) and within experimental error agree with the results for the above extrapolation. The values of Ln(M(T)/M(0)) for 3.92%, 5.14% and 6.72% vanadium content alloys were calculated and were compared with corresponding values of

Table (9.6) values of α_i ,(at %)$^{-1}$, ρ_0 , $\rho_0(\uparrow)$ and $\rho_0(\downarrow)$,($\mu\Omega$cm)

Alloy	α_i	ρ_0		$\rho_0(\uparrow)$		$\rho_0(\downarrow)$	
Ni - Pd	0.01[x]	0.15[+]		0.30[+]		0.30[+]	
Ni - Cu	0.11[x]	0.77[+]		3.6[+]		0.98[+]	
Ni - Co	0.25[x]	0.14[+]	0.15[*]	2.0[+]	4.5[*]	0.15[+]	0.15[*]
Ni - V	0.36	3.72	4.2[+]	13.7	14.1[+]	5.1	6.0[+]
Ni - Fe	0.37[x]	0.39[+]	0.33[*]	3.3[+]	7.0[*]	0.45[+]	0.35[*]
Ni - Mo	0.42	5.6		7.3		24	
Ni - Cr	0.45[x]	4.8[+]	4.9[*]	5.8[+]	7.0[*]	28[+]	16[*]
Ni - Ti		3.3[+]		12.3[+]		4.5[+]	
Ni - Mn		0.79[+]		5.07[+]		0.935[+]	

* Measurements Fert and Campbell (1971)

x Measurements Fransе et al (1973)

\+ Measurements Farrell and Greig (1968)

present work unmarked.

FIG.(9·10) The variation of saturation magnetization with respect to temperature.

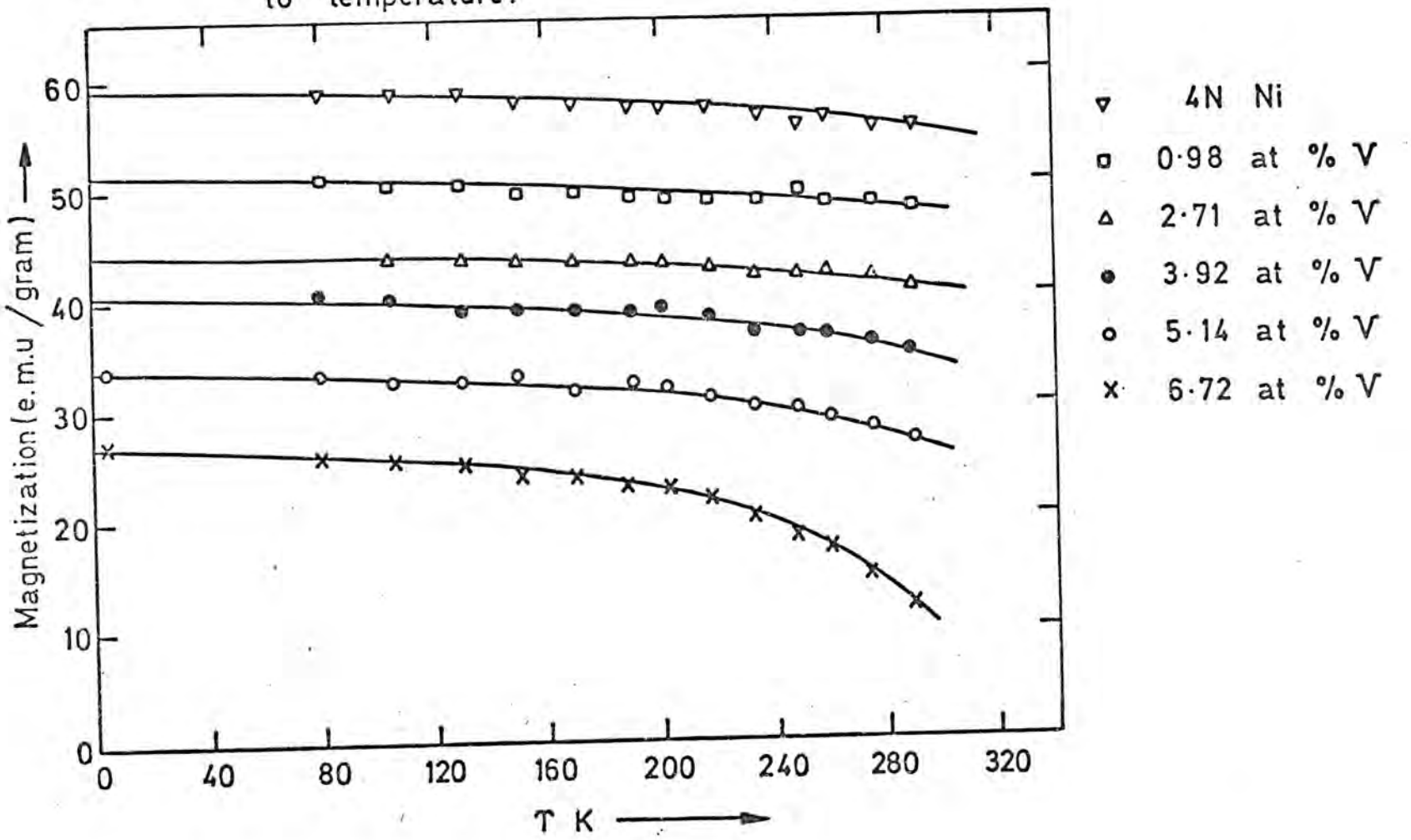

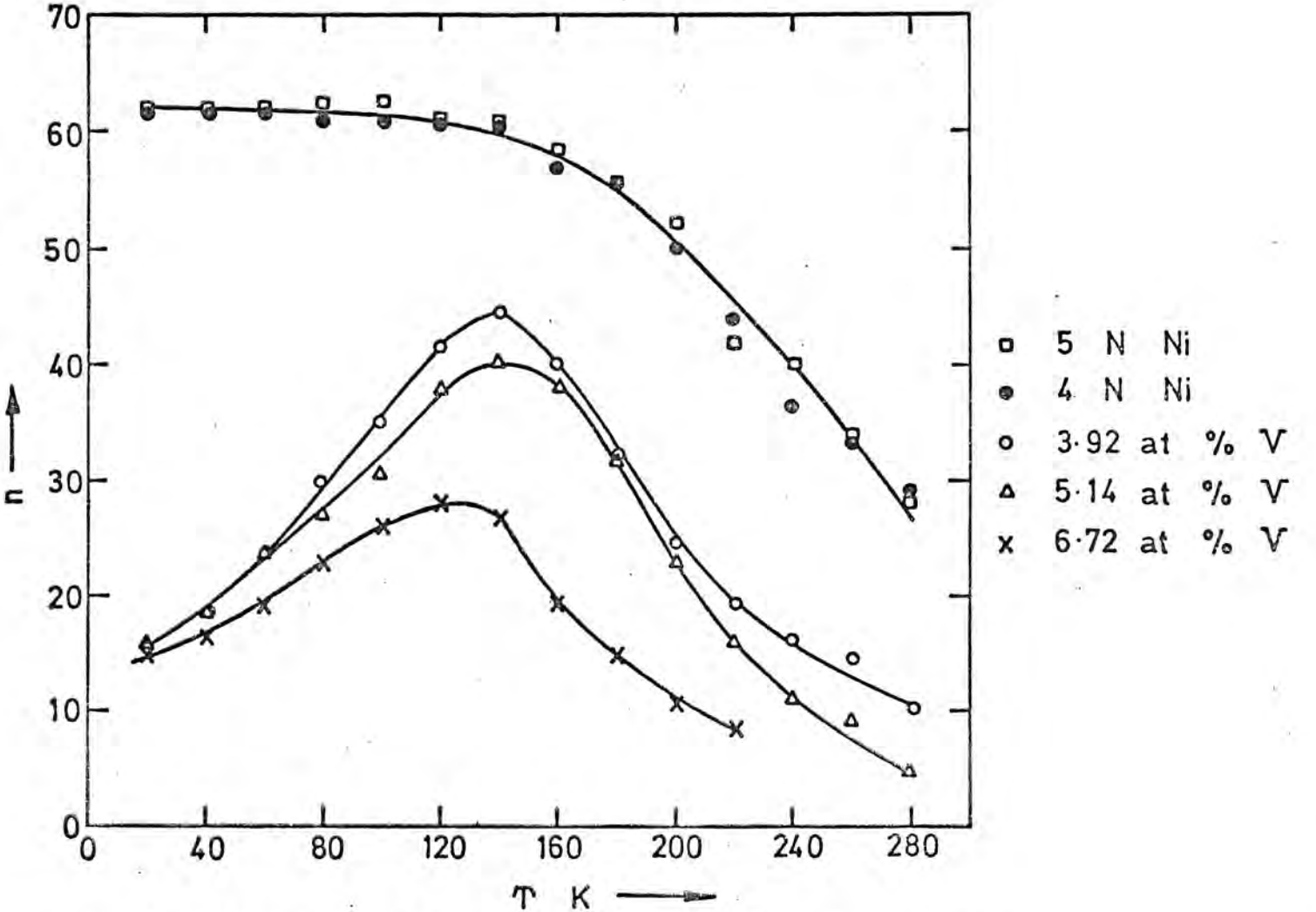

FIG.(9·11) Values of exponents n as a function of temperature for pure Ni and three NiV alloys.

$\mathrm{Ln}(K_1(T)/K_1(0))$ from anisotropy measurements. These were plotted and a smooth curve passed through them. To investigate what sort of relation is obeyed between reduced anisotropy and reduced magnetization a set of calculations was performed to evaluate n assuming a simple power relation of the form:

$$\frac{K_1(T)}{K_1(0)} = \left[\frac{M(T)}{M(0)}\right]^n$$

As in this relation the value of n is temperature dependent it was decided to evaluate n from the following relation

$$n = \partial \mathrm{Ln}(K_1(T)/K_1(0))/\ \partial \mathrm{Ln}(M(T)/M(0))$$

This value could then be obtained by measurement of the slopes of the above curves at particular temperatures. The results of this evaluation has been shown in fig.(9.11). To show the difference between the variation of n from the above and those of 5N and 4N pure Ni a set of calculations was performed, using the measured results on M from Kaul et al. (1969). These combined with anisotropy results from the present work to give the variation of n with respect to temperature, using the same procedure as used for NiV alloys. The results of these determinations have also been shown in fig. (9.11) for comparison.

Material	TK	0	10	30	50	70	90
6.72 at % V	M(e.m.u./gram)	26.75	26.70	26.40	26.20	25.90	25.70
5.14 at % V	M(e.m.u./gram)	33.63	33.60	33.50	33.35	33.20	32.90
3.92 at % V	M(e.m.u./gram)	40.37	40.3	40.25	40.15	40.00	39.80

Material	TK	110	130	150	170	190
6.72 at % V	M(e.m.u./gram)	25.40	25.00	24.55	23.90	23.11
5.14 at % V	M(e.m.u./gram)	32.70	32.50	32.25	32.00	31.70
3.92 at % V	M(e.m.u./gram)	39.60	39.35	39.10	38.80	38.50

Material	TK	210	230	250	270	290
6.72 at % V	M(e.m.u./gram)	22.00	20.50	18.40	15.55	12.70
5.14 at % V	M(e.m.u./gram)	31.20	30.50	29.70	28.50	27.00
3.92 at % V	M(e.m.u./gram)	38.10	37.40	36.40	35.80	34.50

Table (9.7) Values of M for some NiV crystals at different temperatures. The results for pure Ni have been tabulated by Kaul et al. (1969).

CHAPTER 10

Discussion

10.1 The mean free path of the conduction electrons and the first anisotropy constant of Ni

In chapter (4) some ideas of how the mean free path of the conduction electrons and the magnetocrystalline anisotropy can be related were reviewed. In this section by using the fact that the mean free path of the conduction electrons is temperature and concentration dependent $\lambda(T, C_i)$ some of the results given in chapter (9) will be discussed. As already mentioned Hausmann and Wolf (1971) suggested that the following formula for low temperatures T and small concentration C_i can be obtained using an argument based on the similarity of the effects of temperature and concentration on the mean free path of the electrons.

$$K_1^{NiMe}(T, C_i) = K_1^{Ni}(T) \exp(-\sum \alpha_i C_i) \qquad (10.1)$$

The term containing $\alpha_i C_i$ in which α_i is a constant is due to the fact that the mean free path of conduction electrons is proportional to C_i^{-1}. It should be noticed that the temperature dependence of the mean free path is also included in the term $K_1^{Ni}(T)$ in this formula. For a series of measurements on Ni and Ni V alloys this formula was examined and a good agreement with this suggestion was obtained Fig.(9.3). Comparing the present results and those obtained for NiMo and NiCu, Williams and Bozorth (1939), alloys shows that the factorization of the temperature and the concentration dependence of the first anisotropy constant of Ni alloys is consist-

ent with the suggestion that the variation of the mean free path of the conduction electrons is an important factor controlling measured values of anisotropy constants. Also from the measurements on Ni Mo it can be seen that there is a good similarity between the present measurements and those performed by Hausmann and Wolf (1971). Looking back at the results for NiV alloys shown in Figs. (9.3) and (9.4) and the results for Ni Mo alloys shown in Figs. (2) and (3) from Hausmann and Wolf's paper it can be seen that the effect of temperature T on the first anisotropy constant K_1 (T) of Ni is the same as the effect of concentration C_i on this constant. Comparing these two sets of results also suggests that the variation of Ln (K_1(T)) with respect to the temperatures obeys the same law in the form of $(\frac{T}{100})^{1.5}$. It is well known that increase of impurity concentration or increase of temperature both lead to a reduction of electron mean free paths in metals. Also from the present measurements and the results of Hausmann and Wolf increase in concentration or in temperature will each effect the first anisotropy constant in the same way. This gives a basis for the belief that there should be a relation between the electron mean free path $\lambda(T, C_i)$ and the first anisotropy constant K_1 (T, C_i) of Ni. The mechanism by which the temperature is thought to affect anisotropy has been described by several investigators and was reviewed in chapter (3). Also the effect of impurity concentration on anisotropy may be due at least in part to conduction electron spin deviations produced by scattering by impurity atoms. However, at this stage it is not intended to discuss further a possible mechanism for the effect of

impurity concentration, but merely to draw attention to the evidence for similarity of effects of concentration and temperature. Further attention will be given to the question of a mechanism after the resistivity results have been discussed in section (10.4).

10.2 Magnon Vacuum State Anisotropy Constant.

Another interesting concept discussed by Hausmann (1970) and used to describe the anomalous temperature dependence of K_1 of Ni is the idea of the energy of the electrons in the state of vacuum of magnons E_V which consists of an isotropic part and an anisotropic part as follows:

$$E_V = E_V^{\,i} + E_V^{\,a} \qquad (10.2)$$

The anisotropic part E_V can be expressed using equation (1.9) and neglecting higher order terms, as,

$$E_V^{\,a} = V(- MH + K_{1V} (S - \tfrac{1}{5})) \qquad (10.3)$$

in which M, H and V are magnetization, external field and the volume of the sample respectively. K_{1V} represents the first anisotropy in the magnon vacuum state in a cubic crystal and can be related to the first anisotropy constant and the magnetization as follows:

$$K_1 (T) = K_{1V} (1- 10 \frac{M(0)-M(T)}{M(0)}) \qquad (10.4)$$

where in this general form of M^{10} law K_{1V} is temperature independent. This simple power law is not however obeyed for M and equation (10.4) would therefore imply that K_{1V} must itself be temperature dependent. In section (9.1.6) the

results of an investigation of this were presented and it was found that a similar behaviour to that of K_1 occurred, fig (1) of Hausmann and Wolf's paper, and the results were plotted in Fig. (9.5). It is difficult to see how K_{1V} should be a function of temperature relating as it does to a defined state. However, it is only a simple concept if the 10th power law is true and equation (10.4) represents the effect of temperature as a separate factor. It should be noticed that equation (10.4) is derived by omitting higher order terms in the anisotropy expression. It may be that the inclusion of these would yield a more realistic expression which would be satisfactory for Ni as well as the other ferromagnetic transition metals.

10.3 The validity of Hausmann's Hypothesis

A comparison of the values of right hand side (R.H.S.) and left hand side (L.H.S.) derived from equation (9.16) and given in table (9.5) seems to be not in a good agreement with the suggestions of Hausmann (1970). As can be seen from this table, even though a more realistic formula for representing the temperature variation of the first anisotropy constant was used, there is not good agreement. It was also shown that a more sophisticated formula for resistivity has a very small effect on the results, Elliot and Gibson (1974). Another important point is that in this work a series of measurements was performed to check this hypothesis over a large range of temperatures, see table (9.5). It seems from this table that there is a better comparison at low temperatures

than high temperatures. This may be due to the fact that equation (9.4) which was used for the expression of $K_1(T,C_i)$ was an approximate equation which was suitable for low temperatures and small concentrations. Where this is no longer a reasonable approximation the expression can also be corrected by the use of measurements of the magnetizations of these crystals. This leads to the same equation as (9.16), but the value of α_i is different and is given by:

$$\alpha_i = \frac{1}{C_i} \quad \mathrm{Ln}\left[\frac{K_1^{Ni}}{K_1^{\underline{Ni}Me}}\right] + A \qquad (10.5)$$

in which an extra term A is equal to

$$A = \frac{1}{C_i} \quad \mathrm{Ln}\left[\frac{M^{\underline{Ni}Me}(T,C_i)\; M^{Ni}(0)}{M^{\underline{Ni}Me}(0,C_i) M^{Ni}(T)}\right]^{10} \qquad (10.6)$$

As at any particular temperature the ratio of $M^{\underline{Ni}Me}(T,C_i)/M^{NiMe}(0,C_i)$ is always smaller than $M^{Ni}(T)/M^{Ni}(0)$ so term in square brackets in equation 10.6 is less than one and hence the value of A in equation (10.6) is negative. Using equation (10.5) this leads to values of α_i smaller than those obtained in calculating the values of (L.H.S.) and (R.H.S.). From table (9.5) it is obvious that only in the case of the 2.71 at % V sample at 30 and 50K and the 3.92 at % V sample at 30, 50 and 70K is this applicable. For all other compositions and temperatures the effect of the correction is to make the disagreement worse. It seems from this discussion that the equation suggested by Hausmann is not generally valid and the agreement found by him using only room temperature results for NiFe and NiCo is not a sufficient support for the accuracy

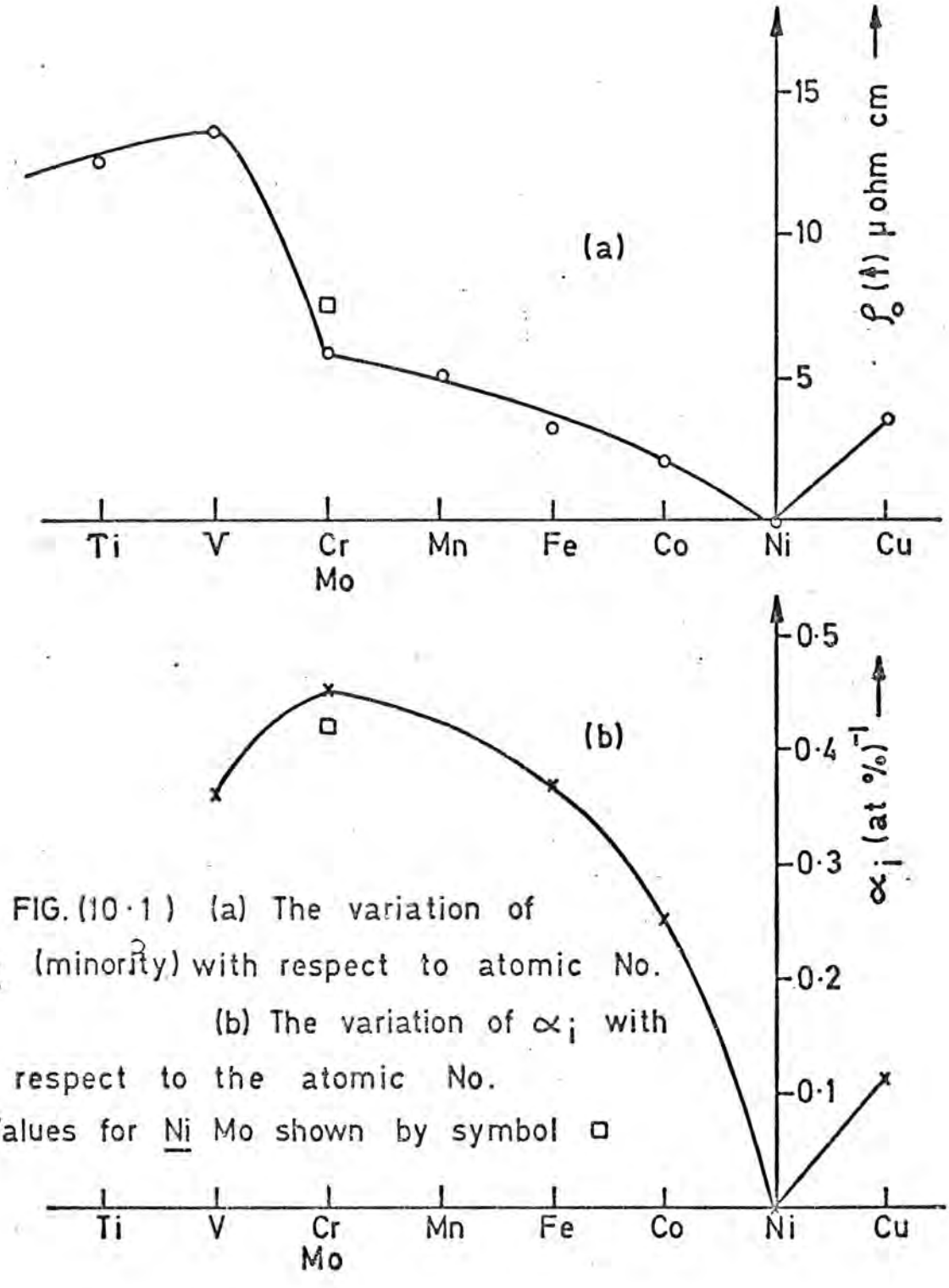

FIG. (10·1) (a) The variation of ρ_0 (minority) with respect to atomic No.
(b) The variation of α_i with respect to the atomic No.
Values for Ni Mo shown by symbol □

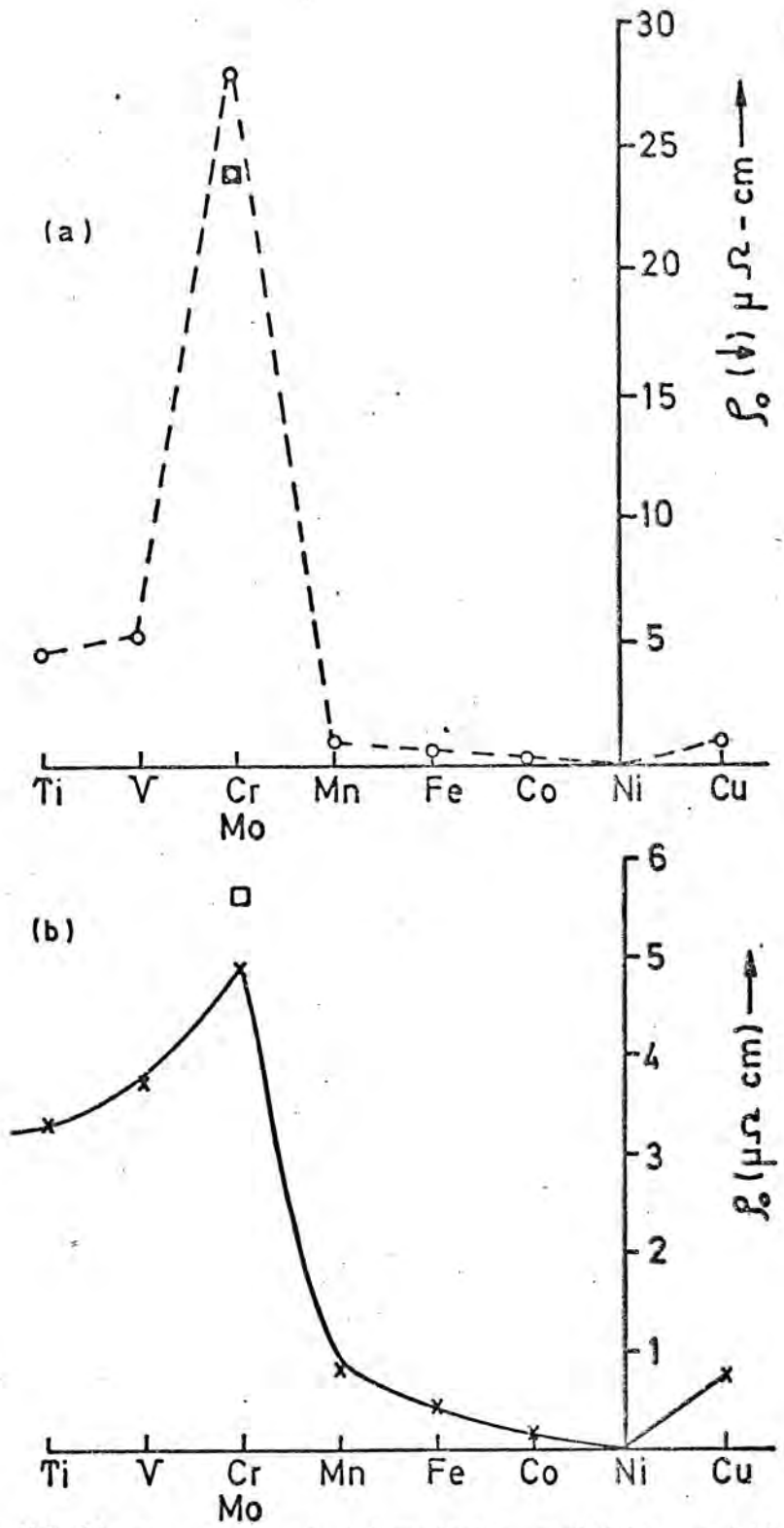

FIG. (10·2) Variation of (a) majority resistivity $\rho_0(\downarrow)$ and (b) total resistivity ρ_0 for 1 at % content of Me in Ni Me alloys. The values for Ni Mo are shown by symbol □

of the equation. It is perhaps not too surprising that the equation should be found to be inadequate. It is based on empirical expressions for anisotropy and resistivity and it does not include the consideration of any mechanism to connect variations of one with those of the other. A more adequate treatment must await the development of this aspect of theory and some suggestions about the way in which this might be done are made in section (10.4).

10.4 Minority Spin Resistivity and Magnetic Anisotropy

The values of ρ_o, ρ_o ($\uparrow$), ρ_o ($\downarrow$) and α_i tabulated in table (9.6) have been plotted against the atomic number for 1% impurities in nickel in figures (10.1) and (10.2). As can be seen in the results of ρ_o the variation is quite smooth from Cu to Mn and after that there is a sudden change to higher values in the case of Cr, V and Ti. The effect has been discussed by Friedel (1958, 1963) in the following way:

As Cu, Co, Fe and Mn have nuclear charges which differ from those of the matrix Ni they might be expected to produce a perturbation to subtract a bound state from the full half of the d band and move it towards higher energies. In the case of these elements however, it would appear that the change in energy produced was not enough to move the state through the Fermi level, but when the impurity element is further away in atomic number from the matrix element Ni this difference between nuclear charges would be sufficiently high to achieve this. In the series Cr, V and Ti in which the difference in Z is equal to -4, -5 and -6 respectively the perturbation is quite

large and so the bound state will pass through the Fermi level. This state will then empty itself into the other half of the d - band with opposite spin direction see Fig. (10.3). Owing to the degeneracy of the d - band it may accommodate the maximum value of 5 electrons per atom in it. As the spins of these electrons are in the opposite direction so the net charge in μ would be $10\,\mu_B$ in this process. In the case of Cr which has an anomalously high moment the d^5 state has only partially been emptied and this can in turn be due to the broadening of the d^5 level into a virtual level, through resonance with the conduction band. That is why in Figure (10.2), a large resistivity for Cr can be seen.

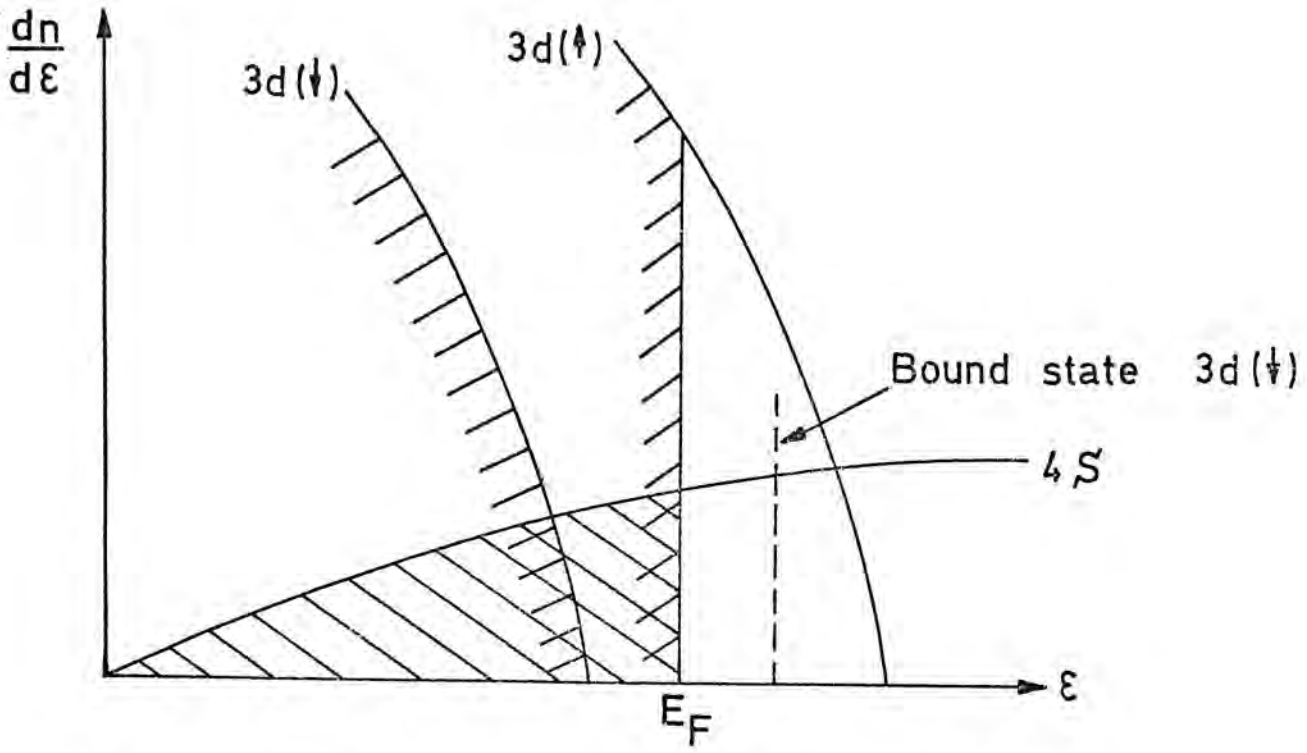

Fig. (10.3) Illustration of Virtual bound state (after Friedel).

The same mechanism may apply in the case of ρ_o resistivity of V and Ti as has been shown in Fig. (10.2).

In the case of the α_i values the change is not so sharp, even though at Cr a maximum in α_i is observed. Looking back to the curve for $\rho_o(\uparrow)$ Fig. (10.1) it is seen that the sharp rise appears between Cr and V. This is a consequence of following Farrell and Grieg (1968) in deciding on the identification of the components $\rho_o(\uparrow)$ and $\rho_o(\downarrow)$ of ρ_o . In the solution of equations (9.20) and (9.21) it is not possible to distinguish the components which appear merely as two solutions of the equations. Farrell and Greig (1968) chose to associate the larger solution with the ρ_o ($\uparrow$) (minority) component for Cu, Co, Fe, Mn, V and Ti, but took the smaller solution for ρ_o ($\uparrow$) in the case of Cr. This choice was based on their knowledge of the relevant band shapes and positions of the bound state and supported by the results of some thermopower measurements. They suggest that in the case of Cr the bound state is derived from the 3d ($\downarrow$) band and that it lies above the Fermi level. However, in the case of V and Ti they claim that the bound state is derived from the 3d ($\uparrow$) band and since it lies well above the Fermi level has a smaller influence on resistivity than that in Cr. It is not clear why this should be so and the possibility of V and Ti behaving in a similar way to Cr, as indeed was suggested by Friedel, is worth examining. This involves interchanging the values for ρ_o ($\uparrow$) and $\rho_o(\downarrow)$ shown in table (9.6) in the case of V and T_i. The results of this change is shown in Fig. (10.4) where it can be seen that the α_i and ρ_o ($\uparrow$) curves are of closely similar form.

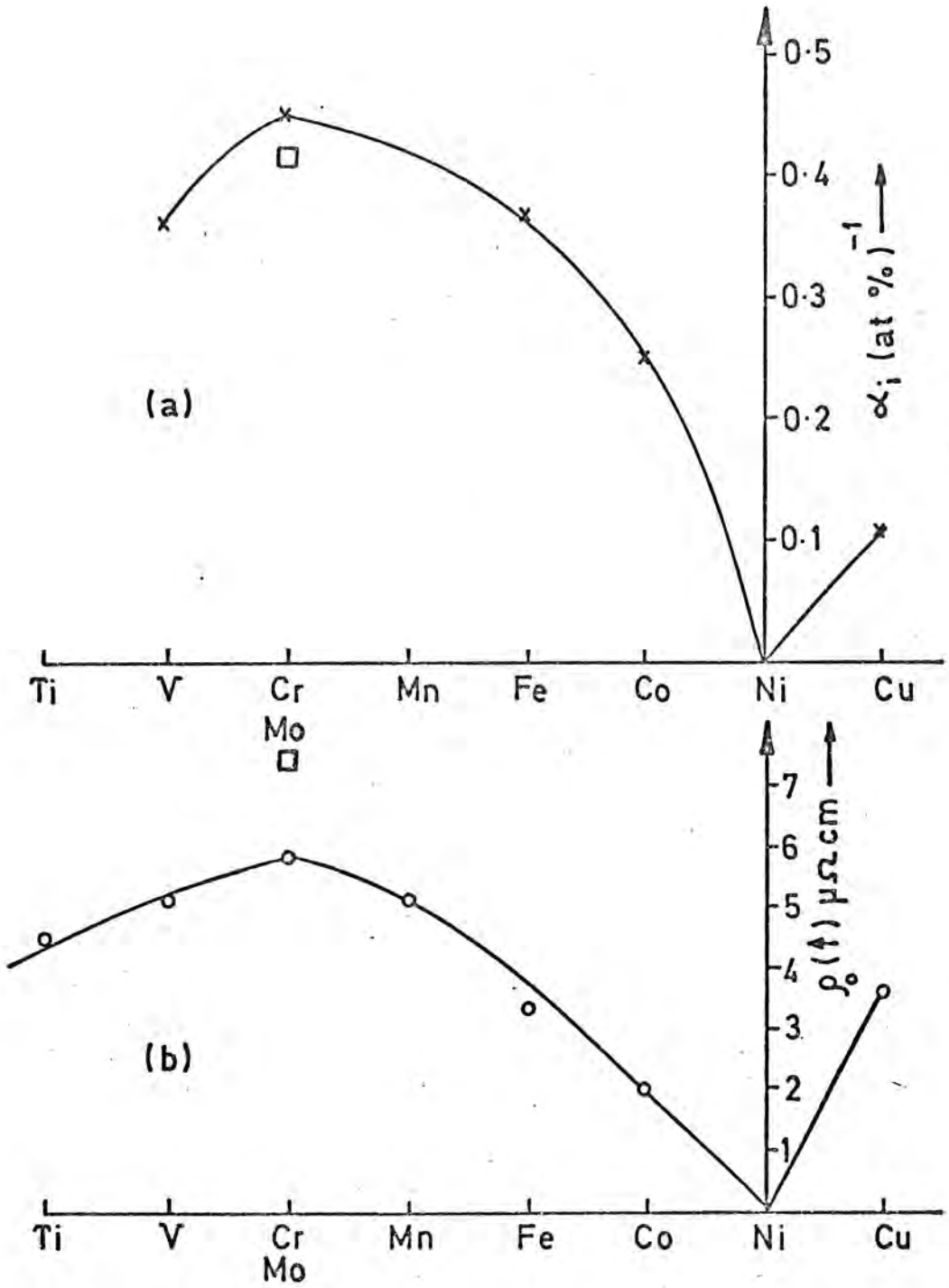

FIG.(10·4) (a) The variation of α_i respect to atomic No. (b) The variation of ρ_o (minority) with respect to atomic No. Values for Ni Mo shown by symbol □

If this is followed the results give a good degree of support to the suggestions of Fransе et al (1973) as discussed in chapter (4). It would bring into agreement the resistivity measurements and the ideas of Furey (1967) on the origin of the magnetic anisotropy of Ni.

10.5 Discussion of Magnetization Measurements

The main purpose of present work was to investigate the anomalous temperature dependence of the first magnetocrystalline anisotropy constant of Ni which differs from other ferromagnetic transition metals which obey an ordinary M^{10}- law. This has been discussed in terms of effects due to changes in the mean free path of the conduction electrons and corresponding changes in electrical resistivity, but it was also considered worthwhile to measure the magnetization of some NiV crystals to see what kind of law would be applicable to them. The results of this investigation have already been shown in fig.(9.11). It can be seen from this, that the values of n for these alloys are definitely less than those of pure Ni and as the concentration is increased the values of n is decreased. Another interesting result is that the value of n passes through a maximum and at very low temperatures tends towards a value between 10 and 15, the variation in the value of n showing a maximum at about 130K and then falling again with rising temperature. It is not particularly surprising since the 10th power law is not expected to hold for temperatures which are more than a fairly small fraction of the Curie temperature. The values of n for 5N and 4N pure Ni do not show such a peak and seem to remain constant at low temperatures with a value of slightly over 60. There

is no real indication of a tendency to fall at low temperatures as in the alloys. Clearly further investigation is required for the 0.98% and 2.71% vanadium content alloys so that reliable values of n may be calculated for these. It should then be possible to observe how the low temperature values of n vary with composition and for what composition the peak begins to develop. Whether there is a relation between these peaks and those, which were observed at about 120K in the resistivity measurements on these alloys and are discussed in chapter (9), is worthy of further investigation. In the case of pure Ni no peak is found and the resistivity/temperature curve shows no anomaly. Should such a connection be found it would give a further link between anisotropy and resistivity variations.

10.6 Conclusions

The aim of the present work was primarily to investigate the anomalous temperature dependence of the first anisotropy constant of Ni and to test further suggestions which were given by several investigators, chapter (4), to relate anomaly to the mean free path of the conduction electrons.

The results on the first magnetocrystalline anisotropy constant of Ni and NiV alloys gave a good support for such a connection and showed that the work of Hausmann and Wolf (1971) is also applicable for NiV alloys. Also the calculations on the magnon vacuum state constant K_{IV} showed a similar result to Hausmann and Wolf's but with a different value of n. Further the combination of anisotropy results with resistivity measurements indicates, if the changes in identification of ρ_o ($\uparrow$) and ρ_o ($\downarrow$) can be justified, that a mechanism may exist which can

explain the link between the first magnetocrystalline anisotropy constant of Ni and the mean free path of the conduction electrons. This in fact is in line with the theory of anisotropy of Furey (1967), which has recently received further theoretical support from Kondorsky (1974). According to this the main contributions to the anisotropy energy of Ni arise from scattering processes in the 3d minority energy states which are close to the Fermi level near the point X in the Brillouin Zone. In their treatment of the resistivities of dilute Ni alloys Farrell et al. (1968) and Fert et al. (1971) have also shown the values of ρ_o (min) to be determined to a large extent by the scattering of the minority spin conduction electrons in the minority 3d energy states. This means that an interpretation based on this type of band theory approach may be the correct one.

The anisotropy and resistivity measurements have also been used to test the general validity of Hausmann's relation between the variation of the first magnetocrystalline anisotropy constant K_1 and the resistivity ρ with temperature. These indicate that the relation is not generally valid and it would perhaps be rather surprising if it were considering the various factors involved in variation of K_1 and ρ over a large temperature range. This conclusion does not, however, throw any light on the principal mechanism for variation of these quantities.

An investigation of the variation of the first anisotropy constant with magnetization has indicated that at low temperatures the results for the more concentrated NiV alloys follow a power law with n approaching 10 in contrast to pure Ni. It was also found that the value of n varies with temperature and, in the temperature range of interest, is always less than the value

for pure Ni. A particularly interesting observation is that n passes through a peak about 120 - 130K. It may not be merely coincidence that this peak occurs at a temperature close to that at which anomalies were found in the resistivity/temperature curves of NiV of higher vanadium content than 1 at %. This may be due to oxygen contamination or to some more fundamental effect, but this has not been established from the present work.

10.7 Suggestions

It is clear that although the present work has enabled some conclusions to be drawn there is still room for further investigation of a number of aspects. The following appear to be useful lines for further development.

1) Looking back at the results obtained in fig. (10.3) for α values suggests that further anisotropy measurements on Ni Mn and Ni Ti alloys are needed in order to check whether the values of α corresponding to Ni Mn and Ni Ti will lie on the curve of fig.(10.3) or not.

2) Considering figs. (10.1) and (10.3) for minority spin resistivity suggests that a further investigation, both theoretical and experimental, would be valuable to decide whether the choice of spin-minority and spin-majority resistivities adopted by Farrell and Grieg (1968) in the case of V and Ti is right. If the suggestion that the spin-minority resistivity in the case of V is the smaller component (as also supported by Fert and Campbell (1971)) then it may be that the same applies in the case of Ti as suggested in section (10.4). This requires further study, but if it is found to be correct gives good support for

the proposal of Fransе et al. (1973).

3) As there are several ways to change the mean free path of the conduction electrons it would be very interesting and strongly to be recommended to carry out experiments in which the mean free path is charged by irradiation (e.g. using neutrons) in a pure Ni crystal. The effect of irradiation can then be examined by measurements on both resistivity ρ and the first anisotropy constant K_1. These then can be compared with the values obtained for these two quantities before irradiation. It would be desirable to give a series of doses of radiation to the samples and to measure K_1 and ρ after each measured dose. The results on 5N purity Ni for both resistivity and anisotropy from 4.2K to room temperature which are recorded in tables (9.1) and (9.4) can be used as a standard comparison. Recent work by Allia et al. (1974) has shown that there is a large change in anisotropy when Ni crystals are bombarded by neutrons in the presence of a magnetic field. It is difficult to interpret their results unless information is available on the changes in anisotropy produced by irradiation in the absence of a field and this is another good reason for carrying out the measurements suggested above.

Hausmann et al. (1971) have studied the effect of ordering on the first magnetic anisotropy constant and resistivity of Ni_3Fe crystals and have found a strong correlation between the changes in these two quantities indicating a common mechanism. It would be interesting to make similar measurements on NiV and and other dilute Ni alloys.

4) By using a more sensitive magnetometer, e.g. a vibrating sample magnetometer, a series of magnetization measurements on NiV and Ni Mo alloy, for which experimental measurements of the first anisotropy constant K_1 are available, should be made in order to find the effect of inclusion of the term in square brackets in equation (4.10) which was neglected at low temperatures and small concentrations. This should provide a method of obtaining more reliable values of the coefficient .

Improvement in the accuracy of measurement of M(T) would enable a better test to be made of how the first anisotropy constant $K_1(C,T)$ for these alloys varies with magnetization M(T). This was tried only for the NiV alloys with higher vanadium content and the results are shown in Fig. (9.11). The results could be used to determine the value of n in a power law for lower vanadium concentrations. It would be interesting to know whether the value of n shows a similar variation with temperature passing through a peak or tends towards the curve for pure Ni as the vanadium content decreases. Also it is possible by the relation of $K(T) = K_{IV}(T)\ (M(T)/M(0))^{10}$ to find how the value of $K_{IV}(T)$ for these alloys varies with respect to temperature.

5) Further consideration should be given to the effect of including the higher order terms in the derivation of the tenth power law following Hausmann's method (section 10.3).

6) Experiments on resistivity and anisotropy could usefully be performed with the samples under uniform pressures. The effect of pressure on the anisotropy of Ni and Fe has been studied by Franse (1969) and a review of the effects on the resistivity of

some methods has been given by Meaden (1966). Interpretation of the results might, however, be rather difficult owing to the changes in band structure that would undoubtedly take place under pressure.

ACKNOWLEDGMENTS

I am first grateful to my supervisor, Dr. W.D. Corner, who has guided me with his most helpful encouragement from the beginning till the end of this work. I would also like to thank Professor G.D. Rochester and Professor A.W. Wolfendale for accepting me to learn at this department and for their continuous interest in my progress. I am also indebted to the authorities of Isfahan University, Iran, for the grant which enabled me to work on this problem. I have also been greatly helped by suggestions from Dr. B.K. Tanner and other members of the solid state group and am grateful for help with the magnetization and resistivity measurements from P. Mundell and from M. Altunbas respectively. The work has also been greatly assisted by the technical staff of the department and in particular by Mr. K.G. Moulson, Mr. J. Scott and the staff of the workshop.

A great deal of help in developing suitable computer programmes was received from Mr. M. O'cllaghan . The use of some specimen preparation facilities in the Department of Applied Physics and Electronics has been most valuable. I have been grateful also for help by Mr. T. Brown (University of Cambridge) in the growing of crystals by the Czochralski technique and by Mr. W.T. Davison (University of Newcastle-upon-Tyne) for the analysis of all samples.

In conclusion I should like to thank the staff of the University library for their helpfulness on numerous occasions, Mrs. J. Lincoln for typing the manuscript and Mrs. E.M. Johnston for preparing many of the diagrams.

REFERENCES

Akulov, N. (1936) Z. Phys., 100, 197.

Alberts, H.L., Alberts, L. (1971) Journal de Physique, Supplement to Vol. 32, C_1-110.

Aldenkamp, A.A., Marks, C.O., Zjilstra, H. (1960) Rev.Sci.Instr., 31, 544.

Allia, P. and Soardo, G.P. (1974) 20th Conference on Magnetism and Magnetic Materials, San Francisco.

Altunbas, M. (1975) Ph.D. Thesis, Durham Univ., Unpublished, England.

Arajs, S., Chessin, H., Colvin, R.V. (1964) Phys. Stat. Sol., 7, 1009.

Argyle, B.E., Charap, S.H., Pugh, E.W. (1963) Phys. Rev., 132, 2051.

Aubert, G. (1968) J. App. Phys., 39, 504.

Aubert, G., Escudier, P. (1971) Journal de Physique, Supplement to Vol. 32, C_1-543.

Bates,L.F. (1963) Modern Magnetism, Cambridge University Press,

Bly, P.H. (1967) Ph.D. Thesis, Durham Univ., England.

Bozorth, R.M. (1937) J. Appl. Phys., 8, 575.

Bozorth, R.M., Walker, J.G. (1953) Phys. Rev., 89, 624.

Bozorth, R.M., Williams, H.J. (1941) Phys. Rev., 59, 828.

Brailsford, F. (1966) Physical Principles of Magnetism, Van-Nostrand, London.

Brenner, R. (1957) Phys. Rev., 107, 1539.

Bridgman, P.W. (1925) Proc. Am. Acad. Arts Sci., 60, 303.

Brooks, H. (1940) Phys., Rev., 58, 909

Brukhatov, N.L. Kirensky, L.V. (1937) Phys. Z. S.U., 12, 602.

Callen, E., Callen, H.B. (1960) J. Phys. Chem. Solids, 16, 310.

Callen, E., Callen, H.B. (1965) Phys. Rev., 139, A455.

Callen, H.B., Callen, E. (1966) J. Phys. Chem. Solids, 27, 1271.

Carr, W.J., J.R. (1958) J. Appl. Phys., 29, 436.

Carr, W.J., J.R. (1957) Phys. Rev., 108, 1158.

Chikazumi, S. (1964) Physics of Magnetism, John Wiley, New York.

Connolly, J.W.D. (1967) Phys. Rev., 159, 415.

Corner, W.D., Roe, W.C., Taylor, K.N.R. (1962) Proc. Phys. Soc.80 927.

Danan, H., Herr, A., Meyer, A.J.P. (1968) J. Appl. Phys., 39, 669.

Elliott, R.J., Gibson, A.F. (1974) An Introduction to Solid State Physics and its Applications, The Macmillan Press Ltd.

Farrell, T., Greig, D. (1968) J. Phys. C. (Proc. Phys. Soc.), 1, 1359.

Fert, A., Campbell, I.A. (1971) Journal de Physique, Supplement to Vol. 32, C1-46.

Fletcher, G.C. (1954) Proc. Phys. Soc., 67, 505.

Fletcher, G.C. (1952) Proc. Phys. Soc. A, 65, 192.

Foner, S. (1956) Rev. Sci. Inst., 27, 548.

Franse, J.J.M., de Vries, G., Kortekaas, T.F.M. (1973) Proc. Intern. Conf. on Magnetism, Moscow.

Franse, J.J.M. (1971) Journal de Physique, Supplement to Vol.32, C_1-186.

Franse, J.J.M. (1969) Ph.D. Thesis, Amsterdam Univ., Amsterdam, Holland.

Franse, J.J.M., De Vries, G. (1968) Physica, 39, 477.

Friedel, J. (1958) Nuovo Cim. (Suppl.2), 7, 287.

Friedel, J. (1963) Metallic Solid Solutions, Edited by Friedel, J., Guiner, A., Benjamin, W.A., Inc., New York, pp.XIX-1.

Furey, W.N. (1967) Ph.D. Thesis, Harvard Univ., Cambridge.

Gautier, F., Loegel, B. (1972) Sol. Stat. Commu., 11, 1205.

Glen, J.W. (1955) Advances in Phys., 4, 381-478.

Gray, W.J., Spedding, F.H. (1969) Rev. Sci. Inst., 40, 1427.

Hansen, M. (1958) Constitution of Binary Alloys., Mc.Graw Hill Book Company, Inc. pp.1055.

Hausmann, K., Hofmann, U., Wolf, M. (1971) Phys. Stat. Sol. (A), 6, 161.

Hausmann, K., Wolf, M., Mulle, H. (1971) Phys. Stat. Sol. (B), 45, K99.

Hausmann, K. (1970) Phys. Stat. Sol., 38, 809.

Hausmann, K., Wolf, M. (1971) Journal de Physique, Supplement to Vol. 32, C1-539.

Heisenberg, W. (1928) Z. Physik, 49, 619.

Hodges, L., Herenreich, H., Lang, N.D. (1966) Phys. Rev., 152, 505.

Hofmann, U., Bernardt, M., Hausmann, K., Wolf, M., To be published.

Hofmann, U., Private Communication.

Hofmann, U., Handstein, A., Hausmann, K. (1970) Phys. Stat. Sol., 40, K81.

Hopkins, E.N., Peterson, D.T., Baker, H.H. (1965) Proc. of 19th AEC Metallography Group Meeting, Oak Bridge, Tennessee, on a Universal Electropolishing Method.

Hume-Rothery, W. (1961) Phil. Mag., 6, 769.

Iwata, N., Kadena, Y. (1965) J. Phys. Soc. Japan, 20, 1541.

Kaul, R., Thompson, E.D. (1969) J. App. Phys., 40, 1383.

Keffer, F., Oguchi, T. (1960) Phys. Rev., 117, 718.

Keffer, F. (1966) Encyclopedia of Phys., Vol. 18/2.

Keffer, F. (1955) Phys. Rev., 100, 1692.

Kittel, C. (1949) Phys. Rev., 76, 743.

Kittel, C. (1948) Phys. Rev., 73, 155.

Kittel, C. (1949) Rev. Mod. Phys., 21, 541.

Kondorský, E.I., Straube, E. (1973) Sov. Phys. Jetp., 36, 188.

Kondorsky, E.I. (1974) IEEE Transactions on Magnetic Vol.Mag-10, 132.

Kortekaas, T.F.M., Boer, H., Franse, J.J.M. (1972) Phys. Lett., 38A, 145.

Krause, D., Ludwig, B., Patz, U. (1969) Z. Angew Phys., 26, 77.

Martin, B.R. (1971) Statistics for Physicists, Academic Press, London, New York, Chap.8, pp.85.

Mason, W.P. (1954) Phys. Rev., 96, 302.

Mattheiss, L.F. (1964) Phys. Rev., 134A, 970.

Mattis, D.C. (1965) The Theory of Magnetism, Harper and Row Publishers, New York.

Meaden, G.T. (1965) Electrical Resistance of Metals, Plenum.

Mori, Nobuo. (1969) J. Phys. Soc. Japan, 27, 307.

Morrish, A.H. (1965) Physical Principles of Magnetism, John Wiley, New York.

Mundel, P. (1975) Ph.D. Thesis, Durham Univ., England.

Okamoto, T., Kadena, Y., Iwata, N. (1967) J. Sci. Hiroshima Univ., 33, 11.

Pearson, W.B., Hume-Rothery, W. (1951-52) J. Inst. Metals, 80, 641.

Penoyer, R.F. (1959) Rev. Sci. Instr., 30, 711.

Popkova, E.G., Predvoditelev, A.A. (1974) Sov. Phys. Crystallogr., 18, 647.

Rhyne, J.J., Clark, A.E. (1967) J. Appl. Phys., 38, 1379.

Roe, W.C. (1961) Ph.D. Thesis, Durham Univ., England.

Simpson, P.G. (1960) Induction Heating Coil Systems and Design, Mc.Graw-Hill Book Co.

Slater, J.C., Mann, J.B., Wilson, J.M., Wood, J.H. (1969) Phys. Rev., 184, 672.

Slater, J.C. (1968) J. Appl. Phys., 39, 761.

Slater, J.C. (1936) Phys. Rev., 49, 537.

Slater, J.C. (1936) Phys. Rev. 49, 931.

Slater, J.C. (1930) Phys. Rev., 36, 57.

Slonczewski, J.C. (1962) J. Phys. Soc. Japan, 17, Supplement B-I, 34.

Smith, D.O. (1956) Rev. Sci. Instr., 27, 261.

Stoner, E.C. (1938) Proc. Roy. Soc. (London), A165, 372.

Stoner, E.C. (1938) Phil. Mag., 25, 899.

Tajima, K. (1971) J. Phys. Soc. Japan, 31, 441.

Tokunaga, T., Fujiwara, H., Tatsumoto, E. (1972) J. Phys. Soc. Japan, 33, 1719.

Van Vleck, J.H. (1959) J. Phys. Radium, 20, 124.

Van Vleck, J.H. (1937) Phys.Rev., 52, 1178.

Vonsovsky, S.V. (1946) J. Phys. (USSR), 10, 468.

Walker, J.W., Williams, H.J., Bozorth, R.M. (1949) Rev. Sci. Instr., 20, 947.

Weiss, P. (1937) Extr. Actes VII Cong. Int. Froid, 1, 508.

Weiss, P. (1907) J. Phys., 6, 667.

Welford, J. (1974) Ph.D. Thesis, Durham Univ., England.

Williams, H.J. Bozorth, R.M. (1939) Phys. Rev., 55, 673.

Wolf, W.P. (1957) J. Appl. Phys., 28, 780.

Zener, C. (1951) Phys. Rev., 81, 440.

Zener, C. (1951) Phys. Rev., 83, 299.

Zener, C. (1954) Phys. Rev., 96, 1335.

Zijlstra, H. (1967) Experimental Methods in Magnetism, Vol.IX, North Holland Publishing Co., Amsterdam.

Yamashita, J., Fukuchi, M., Wakoh, S. (1963) J. Phys. Soc. Japan, 18, 999.

Yang, J.J. (1971) Ph.D. Thesis, University of California, Los Angeles.

Yang, T.T., Yang, J.J., Robinson, L.B. (1973) Solid State Communications, 13, 53.

APPENDIX 1

Programme used for evaluation of K_3

Equation (8.1) can be written as follows:

$$Y_i = A \sin 4(\theta_i + D) + B \sin 8(\theta_i + D) + E_i \quad , i = 1,\ldots n \quad (A1)$$

in which subscript i describes a particular torque reading out of the set of n such readings in a 180° rotation, D is an unknown systematic error in the measurement of angle and the E_1, E_2,...., E_n are n independent normal deviations with mean zero and variance σ^2. These equations are conveniently summarized in the matrix form of equations as follows:

$$Y = X\beta + E$$

where

$$Y = \begin{vmatrix} Y_1 \\ Y_2 \\ \vdots \\ Y_{n-1} \\ Y_n \end{vmatrix} , \quad X = \begin{vmatrix} \sin 4(\theta_1+D) & \sin 8(\theta_1+D) \\ \vdots & \vdots \\ \sin 4(\theta_n+D) & \sin 8(\theta_n+D) \end{vmatrix} , \quad \beta = \begin{vmatrix} A \\ B \end{vmatrix} , \quad E = \begin{vmatrix} E_1 \\ E_2 \\ \vdots \\ E_n \end{vmatrix}$$

Then, for each fixed D, the value of β that minimises the error sum of squares

$$S = (Y - X\beta)^T (Y - X\beta)$$

is given by

$$\hat{\beta} = (X^T X)^{-1} X^T Y$$

where T denotes transposition of a matrix. See for example Martin (1971).

It is also well known that

$$E(\hat{\beta}) = E$$

$$\text{variance } (\hat{\beta}) = E(\hat{\beta}-\beta)(\hat{\beta}-\beta)^T = \sigma^2 (X^T X)^{-1}$$

and the minimised sum of squares is

$$(n-2)\,\hat{\sigma}^2 = (Y - X\beta)^T (Y - X\beta)$$

The factor (n-2) occurs since in this problem there are only two degrees of freedom.

Now, the most probable estimate of D may be obtained by minimising σ^2 with respect to D. However, since we are interested in obtaining the most efficient estimate of B we choose to minimise variance B with respect to D. This was carried out by a direct search procedure followed by a binary chop to locate the minimum. This procedure was used and the programme called (Regress) has been given below.

```
1 regress
     1            COMMON Y(50),THE(50),XA(50),XB(50)
     2            READ (5,101) N
     3            DO 1 I=1,N
     4          1 READ(5,100) Y(I)
     5        100 FORMAT(F6.2)
     6            DO 2 I=1,N
     7          2 READ(5,102) THE(I)
     8        102 FORMAT(F6.2)
     9        101 FORMAT(I2)
    10            DO 3 I=1,N
    11          3 THE(I)=THE(I)/57.29578
  11.6            DEL=.0001
    12            D=0.0
    13            CALL REG(N,BETA,BETB,A,B,C,D)
    14            V=C
    15            D=D+DEL
    16         11 CALL REG(N,BETA,BETB,A,B,C,D)
    17            VNU=C
    18            IF(VNU.GT.V) GOTO 10
  18.5            V=VNU
    19            D=D+DEL
    20            GOTO 11
    21         10 DUP=D
    22            D=D-DEL
    23         13 CALL REG(N,BETA,BETB,A,B,C,D)
    24            VNL=C
    25            IF(VNL.GT.V) GOTO 12
  25.5            V=VNL
    26            D=D-DEL
    27            GOTO 13
    28         12 DLO=D
    29         16 D=0.5*(DUP+DLO)
    30            CALL REG(N,BETA,BETB,A,B,C,D)
    31            IF(VNU-C.GT.VNL-C) GOTO 14
    32            DLO=D
    33         17 IF(ABS(DUP-DLO).LT.0.00001) GOTO 15
    34            GOTO 16
    35         14 DUP=D
    36            GOTO 17
  36.5         15 CONTINUE
    37            WRITE(6,108)
    38            WRITE(6,105) BETA,A
    39            WRITE(6,106) BETB,C
  39.5            WRITE(6,200) D
  39.6       200 FORMAT(/E20.5)
    40            WRITE(6,107) B
    41        108 FORMAT(/25H 68% CONFIDENCE INTERVALS)
    42        105 FORMAT(/4H A= E13.5,4H +/-E14.5)
    43        106 FORMAT(/4H B= E13.5,4H +/-E14.5)
    44        107 FORMAT(/11HCORRELATION E16.5)
    45            STOP
    46            END
```

```
      SUBROUTINE REG(N,BETA,BETB,A,B,C,D)
      COMMON Y(50), THE(50),XA(50),XB(50)
      DO 3 I=1,N
      XA(I)=SIN(4.0*(THE(I)+D))
    3 XB(I)=SIN(8.0*(THE(I)+D))
      SAA=0.0
      SAB=0.0
      SBB=0.0
      SYA=0.0
      SYB=0.0
      DO 5 I=1,N
      SAA=SAA+XA(I)*XA(I)
      SAB=SAB+XA(I)*XB(I)
      SBB=SBB+XB(I)*XB(I)
      SYA=SYA+XA(I)*Y(I)
    5 SYB=SYB+XB(I)*Y(I)
      DET=SAA*SBB-SAB*SAB
  104 FORMAT(4E15.5)
      A=SBB/DET
      B=-SAB/DET
      C=SAA/DET
      BETA=A*SYA+B*SYB
      BETB=B*SYA+C*SYB
      S=0.0
      DO 6 I=1,N
      Z=Y(I)-BETA*XA(I)-BETB*XB(I)
    6 S=S+Z*Z
      S=S/(N-2)
      A=SQRT(A*S)
      C=SQRT(C*S)
      B=B/(A*C)
      RETURN
      END
END OF FILE
```

APPENDIX 2

Programme used for evaluation of n

Equation (9.1) can be written as follows

$$\text{Ln } K_1 (T,C) = \text{Ln } K_1(0,C) - (T/T_o)^n$$

Then choosing a value of $T_o = 100$ for convenience and again taking logs of both sides the above equation can be written as follows:

$$\text{Ln Ln} \left[K_1(0,C) / K_1(T,C) \right] = n \text{ Ln } (T/100) + \text{constant.}$$

The equation is that of a straight line and the slope of this line gives the value of n. To do this for each value of T the corresponding value of $K_1(T,C)$ was fed into the computer and a least squaresprogramme was written to give the best line through the available points. The programme for calculation of n for a NiV alloy crystal containing of 6.72 at % V has been shown below. In this A = n, X = T, Y = $K_1(T,C)$, $K_1(0,C) = 9.05$, B = constant, X(I) = Ln (T/100) and Y(I) = Ln Ln $\left[K_1(0,C) / K_1(T,C) \right]$.

```
I mandy
     1          DIMENSION X(50),Y(50).
     2          DATA X/4.2,10.,30.,50.,70.,77.,80.,110.,
     3         1130.,150.,170.,190.,210.,230./
     4          DATA Y/0.,.8.95,7.6,6.62,5.3,4.8,4.28,3.16,
     5         1.90,1.32,.815,.51,.305,.153/
     6          K=14
     7          SUMX=0.0
     8          SUMY=0.0
     9          SUMXX=0.0
    10          SUMXY=0.0
    11          DO 10 I=1,K
    12          X(I)=ALOG(X(I)/100.)
    13          Y(I)=ALOG(ALOG(0.05/Y(I)))
    14          SUMX=SUMX+X(I)
    15          SUMY=SUMY+Y(I)
    16          SUMXY=SUMXY+X(I)*Y(I)
    17          SUMYY=SUMYY+Y(I)**2
    18       10 CONTINUE
    19          DENOM=K*SUMYY-SUMY**2
    20          A=(K*SUMXY-SUMX*SUMY)/DENOM
    21          B=(SUMY*SUMYY-SUMY*SUMXY)/DENOM
    22          WRITE(6,1)A,B
    23        1 FORMAT(/20X,'A=',E12.5//20X,'B=',E12.6)
    24          STOP
    25          END
END OF FILE
```

APPENDIX 3

Programme used for equation (9.3)

Using $T_o = 100$ and $n = 1.5$ equation (9.1) will be written as follows:

$$Ln\left[K_1(T,C)\ /1000\right] = Ln\left[K_1(0,C)\ /1000\right] - (T/100)^{1.5}$$

This is a straight line of the form

$$Y(I) = AX(I) + B$$

and a least squares programme was used for the best line to pass through the available results. A typical programme in the case of a NiV alloy with 6.72 at % V has been given below in which $X = (T/100)^{1.5}$ and $Y = Ln\left[K_1(T,C)\ /1000\right]$.

The value of A from this programme gives the slope of this line whereas the value of B gives the best value for $Ln\left[K_1(0,C)/1000\right]$ which was used in section (9.1.4) for calculating the value of α.

```
amod
    1            IMPLICIT REAL*4(A-H,O-Z)
    2            DIMENSION X(40),Y(40)
    3            DATA X/.0086,.032,.134,.353,.585,.676,.854,1.153,1.482,
    4           11.837,2.216,2.619,3.043/
    5            DATA Y/4.5,4.48,4.33,4.2,3.97,3.87,
    6           13.76,3.45,3.,2.6,2.1,1.62,1.1/
    7            K=13
    8            SUMX=0.0
    9            SUMY=0.0
   10            SUMXY=0.0
   11            SUMXX=0.0
   12            SUMXI=0.0
   13            SUMXI=0.0
   14            DO 10 I=1,K
   15            SUMX=SUMX+X(I)
   16            SUMY=SUMY+Y(I)
   17            SUMXY=SUMXY+X(I)*Y(I)
   18            SUMXX=SUMXX+X(I)**2
   19         10 CONTINUE
   20            DENOM=K*SUMXX-SUMX**2
   21            A=(K*SUMXY-SUMX*SUMY)/DENOM
   22            B=(SUMY*SUMXX-SUMX*SUMXY)/DENOM
   23            WRITE(6,1)A,B
   24         1  FORMAT('*'/20X,'A=',E12.6/20X,'B=',E12.6)
   25            END
END OF FILE
```